ARTIFICIAL GROUND FREEZING REFRIGERATION PLANT OPTIMIZATION

A Thesis Submitted to the College of
Graduate Studies and Research
In Partial Fulfillment of the Requirements
For the Degree of Master of Science
In the Department of Mechanical Engineering
University of Saskatchewan
Saskatoon

By

Alex Repski

PERMISSION TO USE

In presenting this thesis in partial fulfilment of the requirements for a Postgraduate degree from the University of Saskatchewan, I agree that the Libraries of this University may make it freely available for inspection. I further agree that permission for copying of this thesis in any manner, in whole or in part, for scholarly purposes may be granted by the professor or professors who supervised my thesis work or, in their absence, by the Head of the Department or the Dean of the College in which my thesis work was done. It is understood that any copying or publication or use of this thesis or parts thereof for financial gain shall not be allowed without my written permission. It is also understood that due recognition shall be given to me and to the University of Saskatchewan in any scholarly use which may be made of any material in my thesis.

DISCLAIMER

The names of certain commercial products were exclusively used to meet the thesis and/or exhibition requirements for the degree of Master of Science at the University of Saskatchewan. Reference in this thesis to any specific commercial products, process, or service by trade name, trademark, manufacturer, or otherwise, does not constitute or imply its endorsement, recommendation, or favoring by the University of Saskatchewan. The views and opinions of the author expressed herein do not state or reflect those of the University of Saskatchewan, and shall not be used for advertising or product endorsement purposes.

Requests for permission to copy or to make other use of material in this thesis in whole or part should be addressed to:

Head of the Department of Mechanical Engineering
University of Saskatchewan
57 Campus Drive
Saskatoon, Saskatchewan, S7N 5A9

ABSTRACT

Artificial ground freezing (AGF) is a process used to strengthen soil and rock by freezing trapped pore water. Freezing is accomplished by pumping calcium chloride brine, chilled to approximately – 30˚C in ammonia refrigeration plants, through heat exchangers drilled into the ground.

A knowledge gap exists in the field of AGF regarding the relationship between the performance of the refrigeration plants and the ground heat removal process. The coupling of these two aspects of AGF requires knowledge of the plant's refrigeration capacity as a function of many factors; the most important of which is the temperature of the brine returning from the freeze pipes. However, refrigeration plant manufacturers do not provide sufficient information about the plant's performance as a function of brine temperature.

Typically, AGF plants are only rated at one operating point due to the impracticality in experimentally rating such large plants and the lack of any standard test methods. Refrigeration system models available in the existing literature do not emulate the compressor control system responsible for preventing compressor overloading. Therefore, the goal of this research is to develop a model that can predict the performance of an AGF refrigeration plant over a range of operating points, using plant specifications that are readily available in the documentation provided by the manufacturer of the plant.

To fill the knowledge gap, a thermodynamic model is developed of an existing 1500 TR AGF plant at Cameco's Cigar Lake mine. The Cigar Lake plant uses flooded shell-and-tube evaporators, two-stage economized twin screw compressors, and air cooled condensers packaged into five refrigeration modules. Each component in the system, including the evaporator, compressor, and condenser, is modeled individually, and then the individual models are combined to calculate the overall system capacity.

The model emulates the behavior of the compressor's slide valves, which are used to limit the plant capacity, limit suction pressure, control intermediate pressure, and control the discharge pressures in the system. In addition, the model accounts for the effects of the oil injection into

the screw compressors, which cools the compressors and seals the spaces between the lobes of the compressor rotors.

The model is validated using operating data from the Cigar Lake plant, which was collected over a period of eight months by plant operators. After calibration, the modeled plant capacities and the temperature of the brine leaving the refrigeration plant are found to be in agreement with the measured capacities and brine temperatures. The overall plant capacity results match measured capacities within ±14%, and the predicted brine temperatures match the measured values leaving the plant within ±5%. The modeled capacities match the measured capacities within the uncertainty in the measured data.

The simulation of the Cigar Lake plant demonstrates that the performance of the plant is highly dependent upon the temperature of the brine returning to the plant. For example, a ±10% change in brine temperature causes a 22% overall change in the capacity of the refrigeration plant. The simulation also demonstrates that, even with the plant's air cooled condensers, changes in the ambient temperature have little effect on the performance of the plant with the existing equipment. Furthermore, the results show that the selected suction pressure of the second compression stage, or intermediate pressure, affects the performance of the refrigeration plant. These findings lead to important plant performance optimization opportunities.

An optimization study using the model demonstrates that, by selecting a lower intermediate temperature than what the existing literature suggests, an improvement in overall refrigeration plant capacity of 3% can be achieved. Additional simulations identify the brine tank, which allows for different brine flow rates to exist on the field and plant side of the tank, as an inefficient component in the system. The brine tank not only cools the brine returning from the field before it is pumped to the refrigeration modules but it allows heat to be transferred between the warm and cold brine. By eliminating the tank, plumbing all of the refrigeration modules in parallel, and installing appropriately sized evaporators, the capacity of the refrigeration plant can be increased by 17%. Further capacity gains can be realized by upgrading the evaporators to increase their capacity.

ACKNOWLEDGMENTS

I would like to express my gratitude to the following people for their help and support with this research project:

- Dr. D.A. Torvi for his supervision, advice, and guidance throughout this research project;
- Dr. J.D. Bugg for his supervision, advice, and guidance throughout this research project;
- Cameco Corporation for their financial support, including their sponsorship of my NSERC IPS scholarship, and for providing me access to the data, equipment, facilities, and personnel in order to complete this research;
- Cameco's Cigar Lake metallurgy department for their assistance in collecting data and equipment specifications, and for their assistance during my visits to the Cigar Lake mine;
- Greg Newman for his supervision, for offering his expertise on artificial ground freezing, and for offering his help and support throughout my research project;
- The Department of Mechanical Engineering and the College of Graduate Studies and Research at the University of Saskatchewan for their support and funding;
- The Natural Sciences and Engineering Research Council of Canada (NSERC) for their support and for funding in the form of an IPS scholarship;
- Startec Refrigeration for providing me the opportunity to visit their shop and for offering their refrigeration expertise;
- My parents, Jeff and Theresa Repski, for their support and encouragement throughout my life and this master's program; and
- My girlfriend, Andreé Morissette, for her support, encouragement, assistance with reviewing this thesis, and for her understanding while I spent many days and nights at my desk.

TABLE OF CONTENTS

LIST OF FIGURES

LIST OF TABLES

NOMENCLATURE

Notation

A	Area (m^2)
C	Capacity rate (kJ/s)
c	Specific heat (kJ/kg)
g	Acceleration due to gravity (9.81 m/s^2)
H	Pump head (m)
h	Enthalpy (kJ/kg)
K	Ratio of specific heats
k	Thermal conductivity (kW/mK)
$\dot{m}$	Mass flow rate (kg/s)
N	Shaft speed (rpm)
P	Pressure (kPa)
Pr	Prandtl number
$\dot{Q}$	Heat transfer rate (kW)
r	Radius (m)
Re	Reynolds number
S	Entropy J/(kgK)
T	Temperature (°C)
U	Overall heat transfer coefficient kW/(m^2K)
u	Velocity (m/s)
V	Volume (m^3)

$\dot{V}$	Volumetric flow rate (m^3/s)
$\dot{W}$	Power (W)
x	Gas Quality

Greek Symbols

β	Evaporator local heat transfer coefficient ratio
ε	Effectiveness
η	Efficiency
ρ	Density (kg/m^3)
μ	Dynamic viscosity ($Pa \cdot s$)
v	Specific volume (m^3/kg)

Subscripts

amb	Ambient
brine	Property of Brine
comp	Compressor
cond	Condensing
D	Discharge
evap	Evaporation
F	Field
GM	Geometric mean
high	High compression stage

i	Isentropic
in	Inlet
int	Intermediate
low	Low compression stage
M	Module
min	Minimum
n	Variable or loop index
out	Outlet
plant	Property of refrigeration plant (tank, modules, and pumps)
R	Ratio
ref	Refrigerant
res	Instrument resolution error
S	Suction
sat	Saturated
f	Saturated Liquid
g	Saturated vapor
stat	Static head
swept	Volume displaced per revolution (m^3/rev)
T	Temperature
Tot	Total head
V	Volumetric
φ	Compressor built in efficiency

Superscripts

i	Inlet
'	Evaporator parameters at new operating point

Abbreviations

AGF	Artificial Ground Freezing
CPIV	Mycom CP4 Compressor Controller
CWC	Catalogue Working Conditions
FC	Flow Controller
FT	Flow Transmitter
IT	Current Transmitter
LC	Level Controller
LIT	Level Indicating Transmitter
LMTD	Log Mean Temperature Difference
PT	Pressure Transmitter
TR	Ton of Refrigeration (1TR = 3.517 kW)
TT	Temperature Transmitter

CHAPTER 1: INTRODUCTION

1.1 Background and Need

Artificial Ground Freezing (AGF) is an engineering tool used to strengthen soil and rock, while also creating an impermeable barrier to groundwater, by freezing trapped pore water. AGF finds many applications worldwide, such as tunneling, groundwater contaminant control, inflow control for underground mine workings, and mine shaft sinking. For example, AGF is being used at the crippled Fukishima power plant to prevent radioactively contaminated water from seeping into the ocean (BBC News, 2014). It has also been used extensively to sink mine shafts required for Potash mining in Saskatchewan (Ostrowski, 1967).

Figure 1-1 illustrates a typical AGF system. As shown in Figure 1-1, the system can be broken into two main subsystems: 1) the calcium chloride brine system, and 2) the ammonia refrigeration system. These two systems are connected by a heat exchanger, also known as the evaporator, which cools the calcium chloride (brine) by evaporating liquid ammonia. The brine is chilled to approximately – 30°C and then pumped to a large tank containing cold and warm brine separated by a baffle with a hole in it. The cold brine from the tank is circulated through borehole heat exchangers (freeze pipes), which remove heat from the ground, forming an ice wall. The warm brine exiting the freeze pipes returns to the tank to be pumped back through the heat exchanger. The ammonia side of the system typically consists of a condenser, two-stage screw compressor, throttling device, and other vessels for compressor intercooling and ammonia storage (some components have been omitted from Figure 1-1 for clarity).

In practice, AGF systems are large and complicated, consisting of multiple pumps, heat exchangers, compressors, condensers, and freeze pipes (Chapman, Harbicht, Newman, & Newman, 2011). By the very nature of geology and hydrogeology, each AGF system is as unique as the ground and the freezing project for which the system is used. Therefore, each AGF project requires careful planning before the project commences.

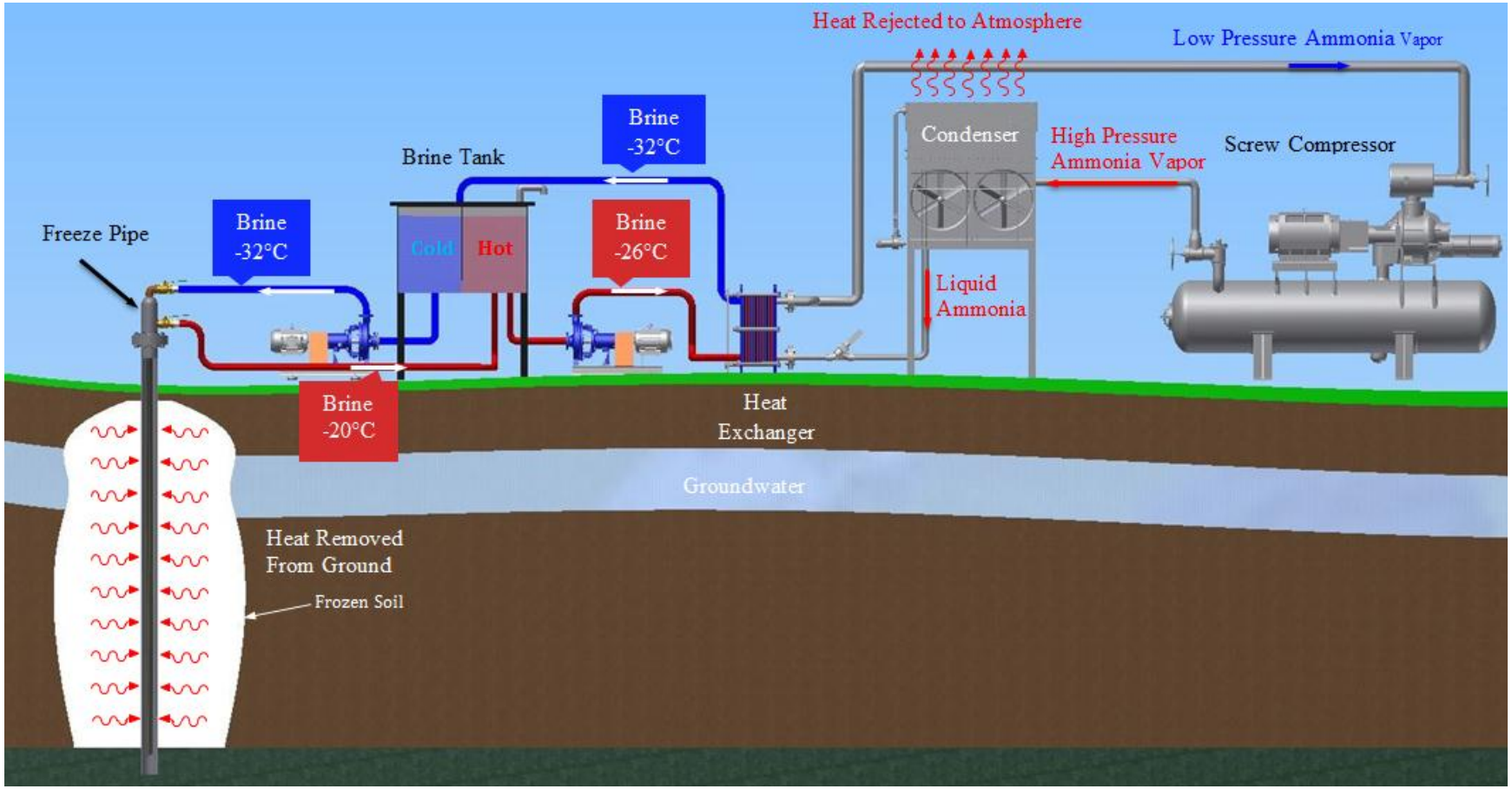

Figure 1-1 Simplified Artificial Ground Freezing System

The most critical step in the planning process is determining the required heat load on the refrigeration plant in order to meet the freezing schedule. Many projects require such a large amount of frozen ground that the rate of heat removal from the brine in the evaporator, or potential heat load, far exceeds the capacity of the largest affordable refrigeration plant. Therefore, the ground is frozen in stages in order to reduce the heat load on the refrigeration plant and to keep the capital cost of the refrigeration plant within the project's budget. This method allows refrigeration plants to be undersized relative to the potential heat load. As a result, the plant will always be operating at maximum capacity, and continually facing new ground heat loads as more freeze pipes are added to the system. This operating philosophy is different than that of most refrigeration systems, which targets a specific output temperature for a space or process fluid. The ASHRAE refrigeration handbook (ASHRAE, 2010) provides details on the operating and design philosophies for typical refrigeration systems.

The staged approach is common on large long-term freezing projects. For example, Cameco's Cigar Lake uranium mine requires the ground to be frozen for the entire life of the mine in order to safely procure the ore. Thus, sections of the ore body are frozen prior to being mined to meet the mine's production schedule.

Every AGF system is custom-built, and typically no testing is carried out to rate the capacity of the plants. As a result, system manufacturers only know the capacity of the plant at one operating point, and neither the engineers planning a freezing project, nor the operators running the plant, have a means of quantifying how the system capacity will change with varying operating conditions. Therefore, developing a method to determine the refrigeration capacity of the system over a range of operating conditions is needed to further understand and improve AGF systems.

1.2 Research Objectives

In the field of AGF, the relationship between the heat removed from the ground and the refrigeration plant performance has long been recognized as a critical aspect in designing and operating AGF systems. In general the freeze plant responds to the ground heat load, and at the same time the ground heat load responds to the refrigeration plant capacity.

Jessberger and Makowski (1981) discuss the importance of the relationship between the rate of heat removal from the ground and the refrigeration plant capacity. Frivik (1982) explores the relationship between the capacity of an AGF plant and the plant's evaporation temperature. He modeled this relationship using a typical compressor capacity versus an evaporation temperature curve. Although this model was effective for generating a simplistic relationship between heat flux and evaporation temperature, it did not provide enough information to allow for accurate predictions of the plant capacity. To determine the capacity of an AGF plant over a wide range of operating conditions, the objectives of this research are:

- to develop a model that can calculate the capacity of the refrigeration plant over the plant's entire operating envelope based on component specifications,
- to use the specifications of an existing refrigeration plant at Cameco's Cigar Lake mine, to develop capacity charts for the Cigar Lake plant using the model,
- to determine how to optimize the capacity of the Cigar Lake plant using existing components, and
- to determine if any components need to be upgraded to maximize the capacity of the refrigeration plant.

1.3 Significance to the Field

This research contributes to the field of AGF a better understanding of the effects of brine temperature on the performance of a refrigeration plant. Current ground freezing modeling relies on trial and error to predict how much refrigeration capacity is available for a particular freezing project. This approach involves assuming a particular brine temperature and checking to see the ground heat load does not exceed plant capacity at the selected brine temperature. The relationship between brine temperature and refrigeration plant performance developed by this research can be coupled with existing finite element models of the ground freezing process to improve the accuracy with which the total freeze time can be predicted. The information provided by the model also provides insight into how the brine distribution systems for AGF should be designed to maximize the performance of the refrigeration plant. In addition, this research will contribute a methodology for modeling twin screw compressors and their control systems under operating conditions where the compressor control system has to reduce the capacity of the refrigeration capacity of the system to prevent overloading.

1.4 Organization of Thesis

The next chapter of this thesis reviews the state of the art in industrial refrigeration systems and how they are modeled. Chapter Three describes the focus of this research, which is the refrigeration plant at Cameco's Cigar Lake mine. Chapter Four describes the development of the equations and algorithms used to develop the models for the plant and its components. The validation of the models using data collected from the Cigar Lake refrigeration plant is presented in Chapter Five. Chapter Six describes the plant performance relationships developed using the model and the sensitivity analysis used to determine what parameters are most important to the performance of the refrigeration plant. The knowledge obtained using the sensitivity analysis is used to optimize the refrigeration plant in Chapter Seven. Finally Chapter Eight presents conclusions and identifies gaps or limitations in the research that require further work.

CHAPTER 2: REVIEW OF THE LITERATURE

This chapter reviews basic refrigeration systems, current practices in industrial refrigeration, current methods used in determining the performance of industrial refrigeration systems, and relevant literature on ground freezing and modeling of industrial refrigeration systems.

2.1 Refrigeration Systems

Refrigeration systems remove heat from bodies or fluids to reduce their temperature to below that of their surroundings. Vapor compression, vapor absorption, air cycle, vapor jet, and thermo-electric refrigeration are several means of accomplishing this (Gosney, 1982).

The vapor compression cycle relies on boiling (evaporating) a refrigerant to remove heat from a body or fluid, and then, rejecting the heat to another body or fluid when the refrigerant condenses. A typical single stage vapor compression cycle is shown on pressure-enthalpy (P-h) coordinates in Figure 2-1.

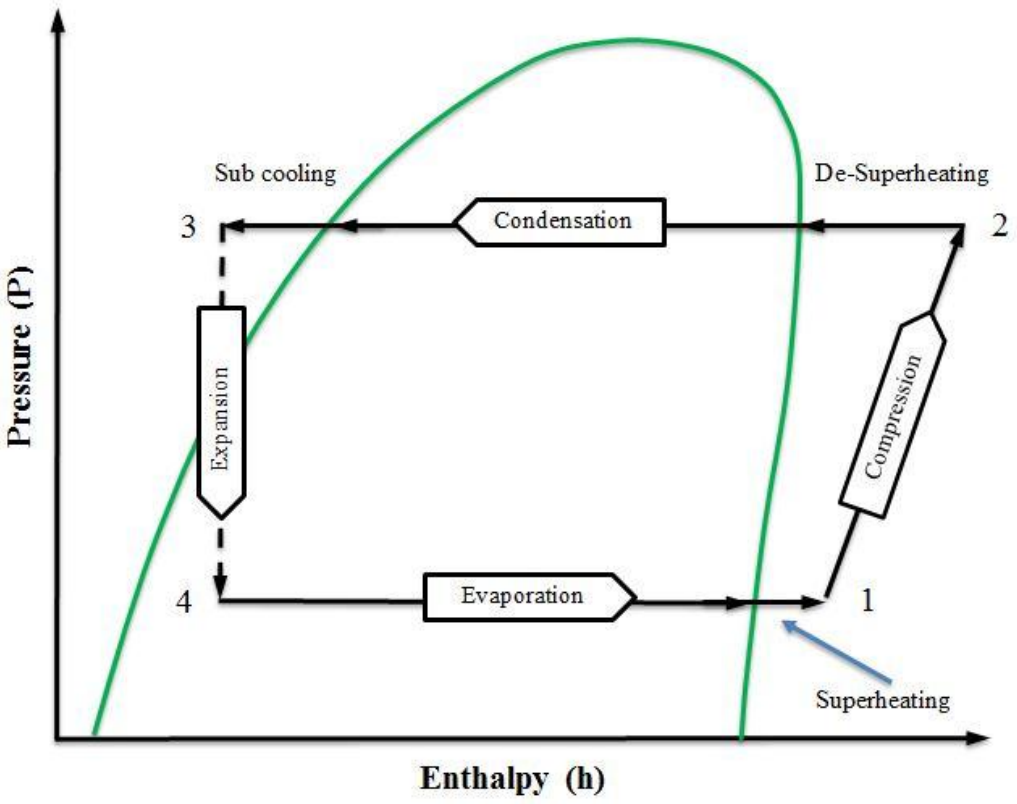

Figure 2-1 Single Stage Vapor Compression Refrigeration Cycle

The cycle uses a heat exchanger (or evaporator) to boil the refrigerant at a low temperature and pressure (process 4-1). In some refrigeration systems, the gas produced in the evaporator may be superheated either in the evaporator or in the refrigerant lines leading to the compressor. The compressor draws refrigerant gas from the evaporator, generating low pressure in the evaporator known as the saturated suction pressure ($P_{sat,s}$). At the same time, in process 1-2, the compressor compresses the gas to the saturated discharge pressure ($P_{sat,D}$). The condenser de-superheats the refrigerant gas, decreasing its temperature from the compressor discharge temperature to the condensing temperature, or saturated discharge temperature ($T_{sat,D}$), and then condenses the refrigerant (process 2-3) by rejecting heat to the surroundings (or another fluid). In some systems, the liquid refrigerant may be subcooled before it leaves the condenser. Finally, in process 3-4, the high pressure liquid refrigerant undergoes a pressure drop through an expansion device, such as orifice or capillary tube.

The working fluids of the system, have suitably low boiling temperatures for refrigeration applications. A few common refrigerants include R-134A, R-22, R-410A, and ammonia. R-134A is commonly used for automotive air conditioners and large chillers. R-22 is commonly used in residential air conditioners and commercial refrigeration equipment. However, because R-22 is a hydrochlorofluorocarbon (HCFC) refrigerant, which is an ozone depleting substance, it is being phased out in favor of HFC based refrigerants, such as R-410A (The Heating, Refrigeration, and Air Conditioning Institute of Canada, N.D.).

2.2 Industrial Refrigeration Systems

2.2.1 Refrigerants

Large industrial refrigeration systems, such as those used in artificial ground freezing systems, hockey rinks, large warehouses, and meat packing plants, often use ammonia (R717) as a refrigerant (ASHRAE, 2010). Ammonia has one of the highest net refrigeration effects of commonly used refrigerants. When used in a standard refrigeration cycle operating between 285 K evaporation temperature and 303 K condensing temperature, ammonia has a net refrigeration effect of 1103.1 kJ/kg, and the net refrigeration effect of R-22 is 105.95 kJ/kg (ASHRAE, 2013). A higher net refrigeration effect means that lower refrigerant mass flow rates are required to obtain the same refrigeration capacity. Furthermore, lower mass flow rates

require smaller refrigerant lines, smaller expansion valves, and compressors with smaller swept volume rates which reduce the initial cost of the refrigeration system. Ammonia can also be considered an environmentally friendly refrigerant because it has an ozone depletion potential (ODP) of 0. In addition, ammonia is not a greenhouse gas with a global warming potential (GWP) of less than 1 (ASHRAE, 2013). As a point of comparison, a chlorofluorocarbon (CFC) based refrigerant such as R-12, has an ODP of 1 and a GWP of 10,900 (ASHRAE, 2013). Although ammonia is environmentally friendly and very efficient, it is toxic at concentrations between 35 and 50 mg/kg. In addition ammonia is flammable and can explode at concentrations of 16 to 25% by weight (ASHRAE,2010).

2.2.2 Multistage Refrigeration

The refrigeration cycle used in industrial systems is governed by the required temperature of the space or fluid being cooled. With ammonia as a refrigerant, evaporation temperatures below -25°C typically need a two-stage system because single-stage systems become inefficient and uneconomical (ASHRAE, 2010). Similarly, evaporation temperatures below – 60°C, which are seen in cryogenic applications, require the use of a three-stage refrigeration system (ASHRAE, 2010).

Using a multistage refrigeration cycle as opposed to a single-stage cycle improves the efficiency of the system in many ways. For reciprocating compressors, the pressure ratios required for a single stage of compression result in a loss of volumetric efficiency in the compressor (Gosney, 1982). Therefore, splitting the compression into two stages will lead to improved volumetric efficiency. Furthermore, splitting the compression process into stages and intercooling between stages reduces the work of compression for air compressors (Moran, Shapiro, Boettner, & Bailey, 2011). Similarly, the work of compression for refrigeration compressors can also be reduced through a reduction in gas temperature between stages of compression. In addition to improved compressor volumetric efficiency and intercooling there are several other methods of economizing the system that are compatible with multistage systems.

2.2.3 Economizing Methods

Ammonia refrigeration systems are typically economized in one of three ways. The methods of economizing are differentiated by how vapor at an intermediate pressure is produced, and how

the expansion process is performed. Figure 2-2 illustrates a Direct Expansion (DX) subcooler economized system. A DX subcooler utilizes a small shell and tube heat exchanger which subcools the liquid refrigerant leaving the condenser. The liquid ammonia leaving the condenser is subcooled on the shell side by evaporating liquid ammonia at the intermediate pressure on the tube side. The refrigerant on the tube side is expanded to the intermediate pressure using a thermal expansion valve which throttles the flow of refrigerant to maintain approximately 5°C of superheat leaving the subcooler (Gosney, 1982). The term *direct expansion* comes from the fact that the liquid refrigerant is being directly cooled using refrigerant. Subcooling the refrigerant lowers the temperature of the refrigerant entering the evaporator which increases the refrigeration capacity of the system. In addition, subcooling the refrigerant before the main expansion valve reduces the amount of liquid refrigerant that will flash to vapor in the expansion process, which in turn reduces the work of compression. The vapor produced in the subcooler is typically at a lower temperature than the vapor leaving the low-stage compressor. Therefore, the vapor from the subcooler will de superheat the vapor entering the high-stage compressor, further reducing the work of compression (Gosney, 1982).

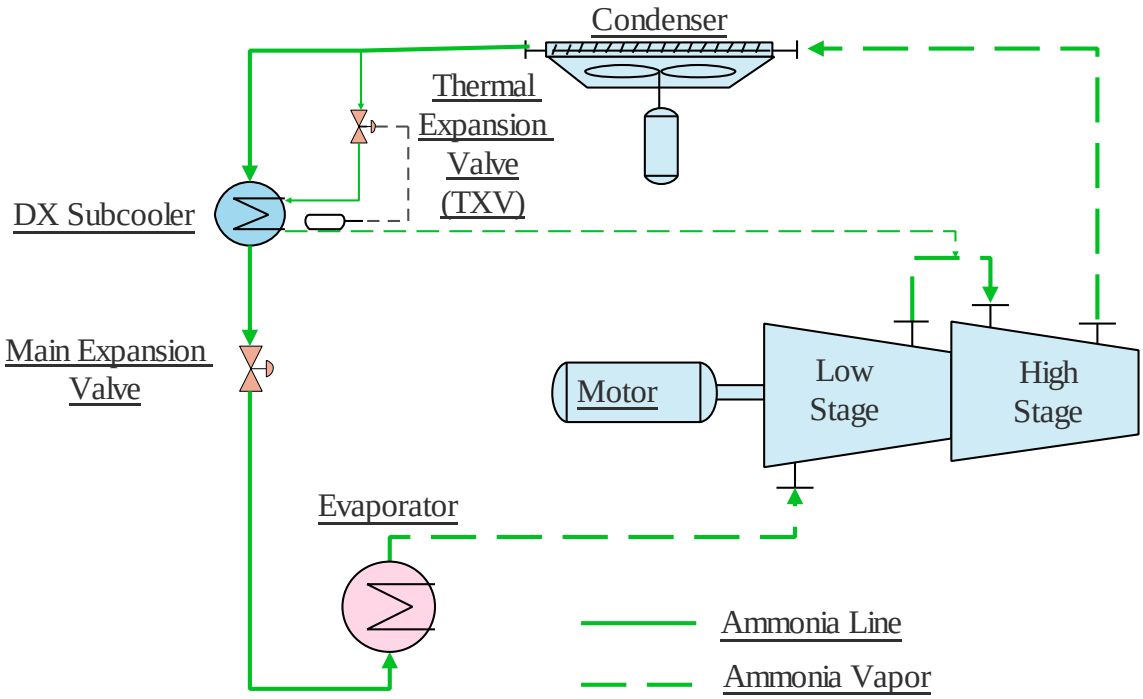

Figure 2-2 Direct Expansion (DX) Subcooled Refrigeration System (Gosney, 1982)

The next method of economizing the refrigeration system uses a shell-and-coil subcooler (Figure 2-3). The shell and coil economizer works in a similar manner to the DX sub cooler with two differences. Instead of a shell and tube heat exchanger, the shell-and-coil economizer utilizes a vessel with a coil of tube immersed in liquid refrigerant. As the liquid refrigerant leaving the condenser passes through the coil it is subcooled by evaporating liquid refrigerant in the vessel. In addition, a float valve maintains the liquid level in the vessel by varying the flow of liquid refrigerant through an expansion valve into the vessel rather than a thermal expansion valve (TXV) (Gosney,1982).

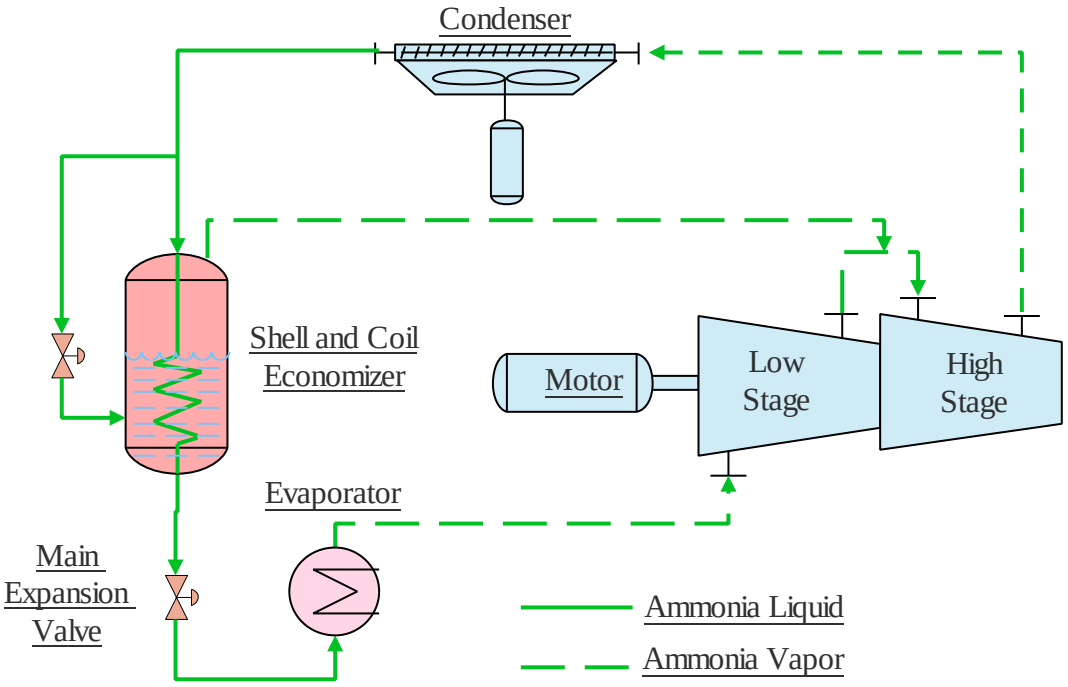

Figure 2-3 Shell-and-Coil Economized Refrigeration System (Gosney,1982)

The third method of economizing uses a flash chamber and two expansion valves to split the expansion into two separate stages (Figure 2-4). The flash chamber separates liquid and ammonia vapor between the two expansion steps. This reduces the amount of vapor that flows into the evaporator by removing it and returning it to the high-stage compressor. Vapor produced before the evaporator has no refrigeration effect. Therefore, it is advantageous to compress it from the intermediate pressure to the discharge pressure rather than from the evaporation pressure. The liquid leaving the flash chamber is cooled when some of it flashes to vapor at the intermediate pressure. Unlike the two subcoolers previously examined, the flash chamber will

only reduce the temperature of the liquid refrigerant leaving the chamber to its saturation temperature instead of subcooling it. However, the shell-and-coil economizer still produces colder liquid refrigerant than either the DX subcooler or the shell and coil subcooler (Gosney,1982).

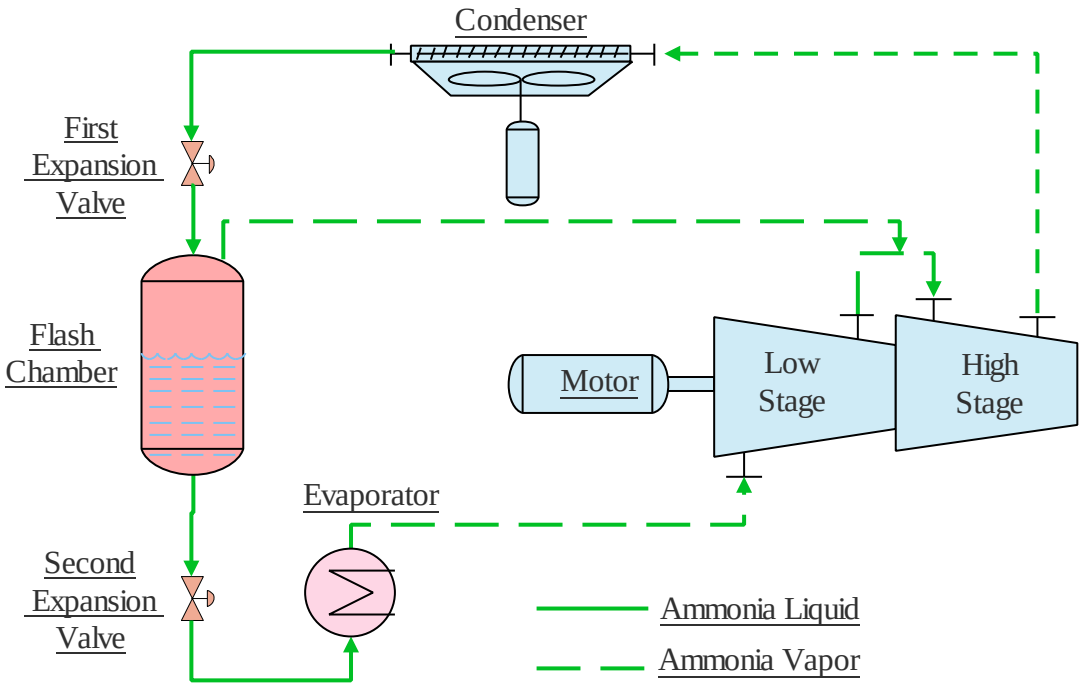

Figure 2-4 Flash Chamber Economized Ammonia Refrigeration System (Gosney,1982)

2.2.4 Selection of Intermediate Pressure

The pressure between the first and second stage of compression, known as the intermediate pressure (P_{int}) has an effect on the power consumption of the compressor and consequently the efficiency of the refrigeration system. In the case of an intercooled air compressor, the optimum intermediate pressure equalizes the high and low-stage pressure ratios. The optimum intermediate pressure for ammonia refrigeration systems is calculated by taking the saturation temperature corresponding to the intermediate pressure for equal pressure ratios and adding 5°C to it (Gosney, 1982).

2.3 Components used for Ammonia Refrigeration Systems

2.3.1 Evaporators

The evaporators required for ammonia systems are unique because of the low ammonia mass flow rates used as a result of ammonia's high net refrigeration effect. Low ammonia mass flow rates make direct expansion evaporators, which are common in most commercial and residential systems, inefficient. Furthermore, low mass flow rates make it difficult to uniformly feed a direct expansion evaporator. For this reason either a flooded evaporator or a liquid overfeed style evaporator will be used in an ammonia refrigeration system (ASHRAE, 2010). Liquid overfeed evaporators utilize a circulation pump to pump liquid ammonia at a higher mass flow rate through the evaporator from a low pressure flash tank. Flooded evaporators are evaporators in which the evaporator is flooded with liquid ammonia, the level of which is controlled by a float valve which throttles the high pressure ammonia into the evaporator. Figure 2-5 illustrates a flooded shell and tube heat exchanger and surge drum. The surge drum is responsible for ensuring that liquid ammonia cannot back up into the compressor and cause liquid slugging which would damage the compressor.

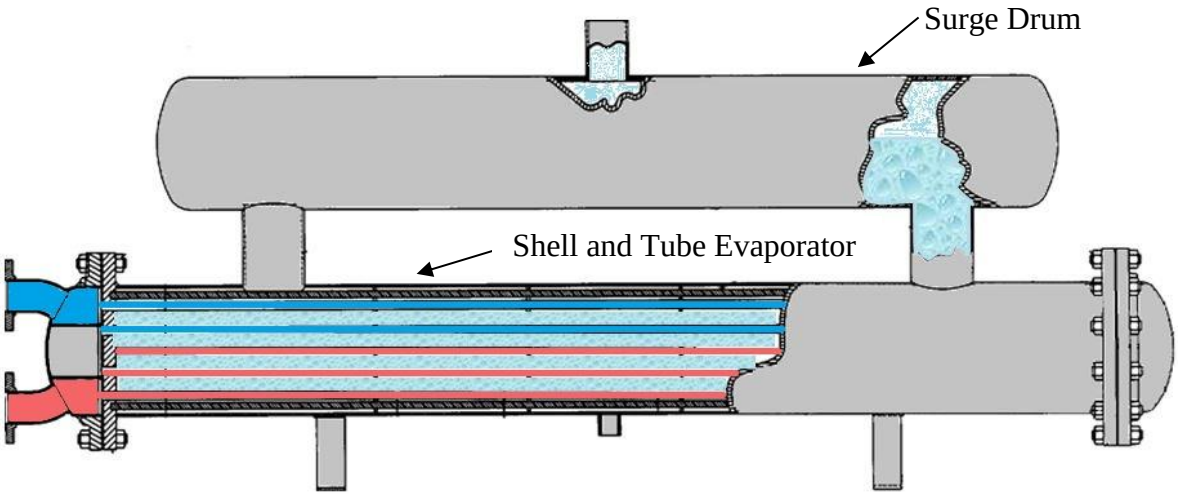

Figure 2-5 Flooded Shell and Tube Evaporator and Surge Drum

The control of the liquid level in a flooded evaporator is critical. Too much liquid creates a static head penalty and increases the saturation temperature of the liquid refrigerant near the bottom of the evaporator, and too little liquid will expose tubes near the top of the evaporator. An increase

in the evaporation temperature of the refrigerant reduces the performance of the evaporator (Webb, Choi, & Apparao, 1989).

2.3.2 Twin Screw Compressors

Ammonia refrigeration systems typically use either rotary screw compressors or reciprocating compressors. Reciprocating compressors are used in systems under 75 kW (21 TR) refrigeration capacity, and screw compressors are used for capacities above 75kW (ASHRAE, 2010). Twin screw compressors are positive displacement compressors that utilize two helically-shaped rotors to continuously trap and compress gas. The gas is drawn in through the suction housing, compressed by the rotors in the centre housing of the compressor, and then discharged. The capacity of the compressor, or the volume of gas that is compressed, is controlled using a sliding valve which allows some amount of the gas to recirculate to the suction side of the rotors. Figure 2-6 shows the arrangement of these components in a typical compressor.

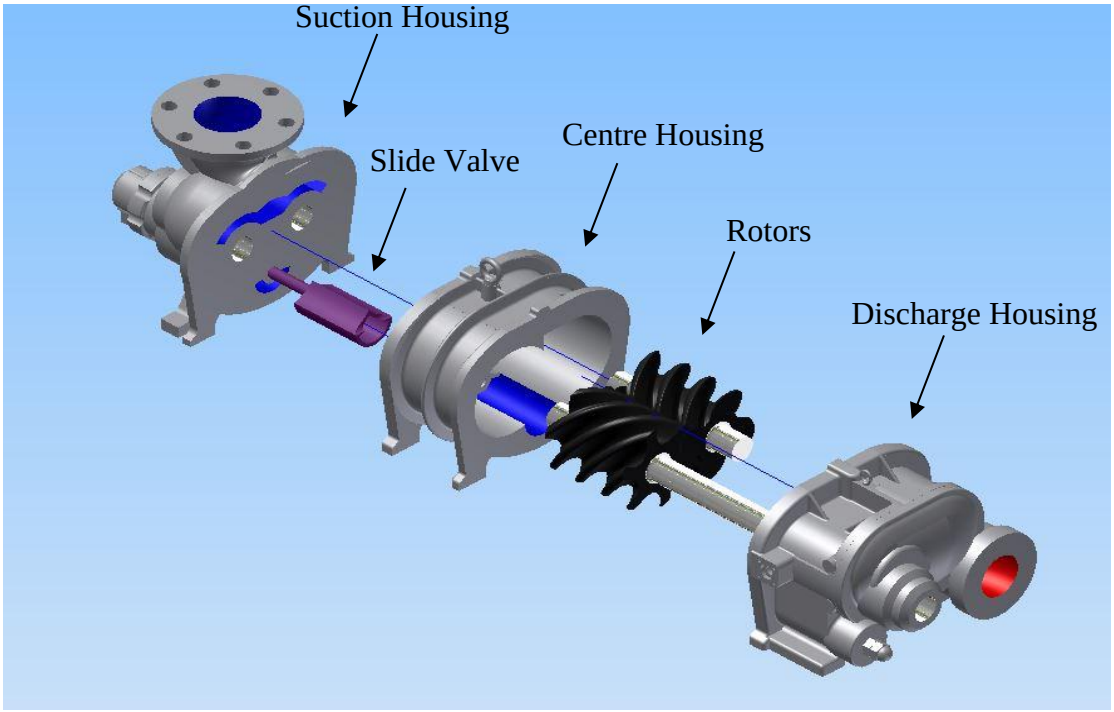

Figure 2-6 Screw Compressor Exploded View

Figure 2-7 illustrates the compression process in a typical screw compressor, which begins with refrigerant gas being drawn into the compressor through the suction port.

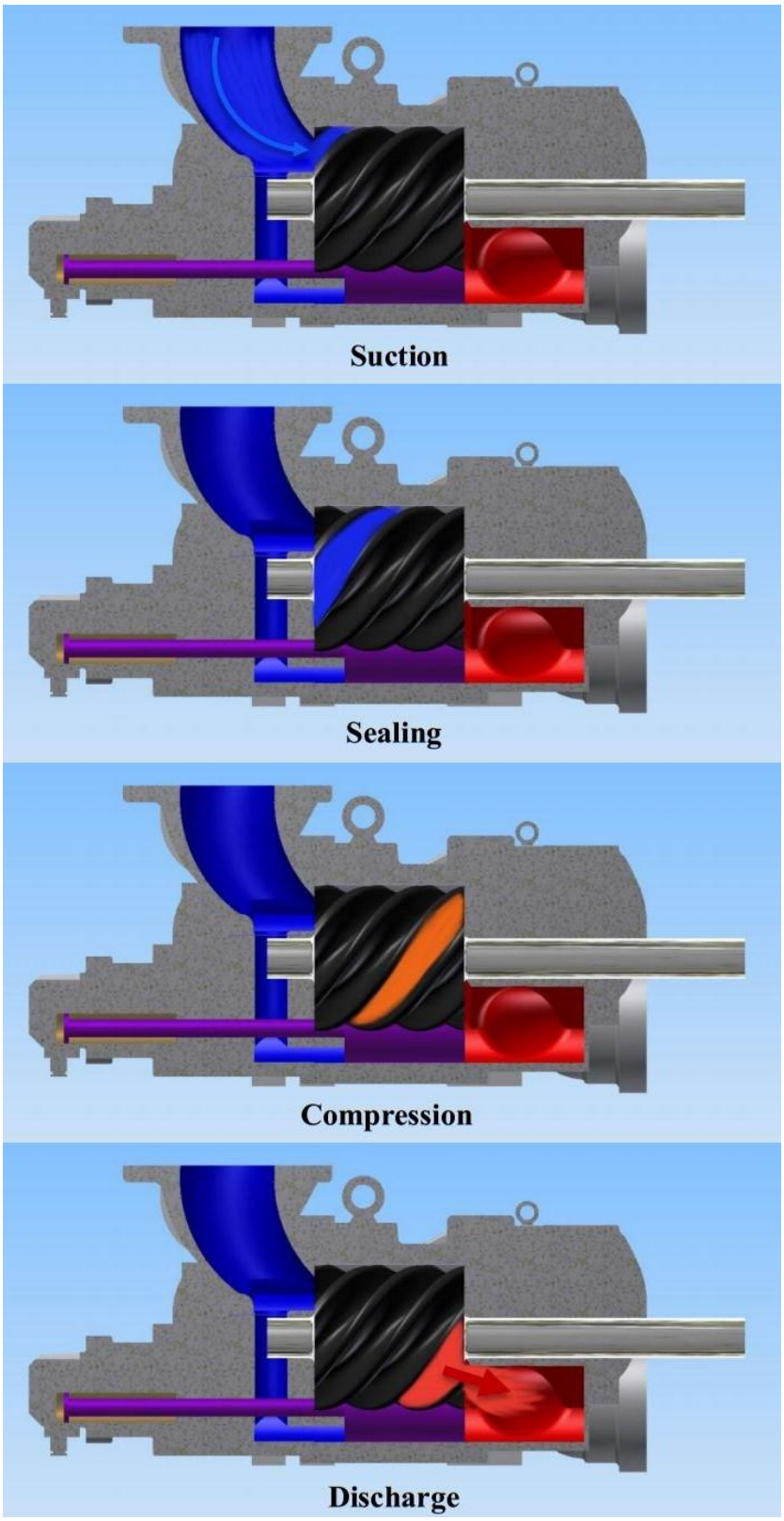

Figure 2-7 Screw Compressor Cross Section showing Gas Compression Process

As the rotors turn, voids between the rotors are exposed to the suction port creating a low pressure region and drawing gas into the voids. Further rotation causes the voids to move away from the suction port, sealing the low pressure gas between the rotors and the compressor housing. Trapped gas moves longitudinally through the compressor, and as it travels towards the discharge port the voids trapping it become progressively smaller. The compressed gas is discharged from the compressor when the voids are exposed to the discharge port.

The size and position of the compressor's discharge port is critical. The compressor's volume ratio (V_R) is defined as the ratio of the gas volume at suction (V_S) to the gas volume at discharge (V_D), and is determined by, among other things, the position and shape of the compressor's discharge port. (Gosney, 1982)

$$V_R = \frac{V_D}{V_S} \tag{2.1}$$

Figure 2-8 shows the discharge port, which allows the gas to escape radially past the end of the slide valve and axially into the discharge housing.

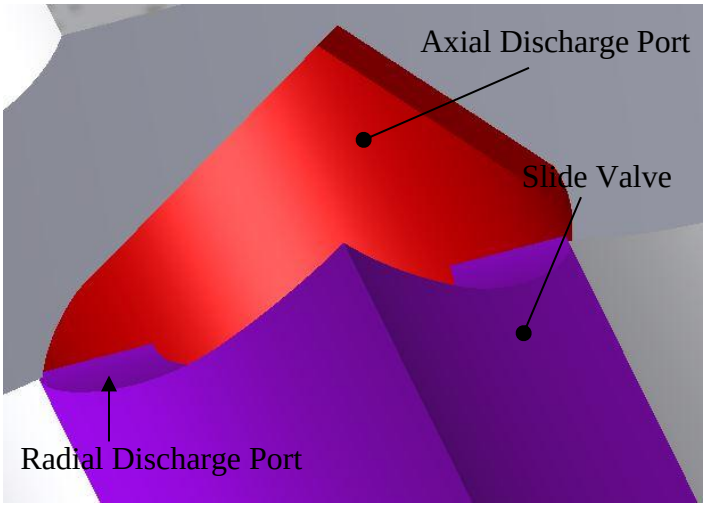

Figure 2-8 Twin Screw Compressor Discharge Port with Slide Valve

The volume of gas the compressor pumps for each revolution of the input shaft, known as the swept volume (V_{swept}), is determined by physical properties of the compressor itself such as the size of the rotors, and location / shape of the discharge port. The rate of gas flow through the compressor or swept volume rate ($\dot{V}_{swept}$) is equal to the swept volume for a single revolution of the compressor input shaft multiplied by the speed of the input shaft *n*, and the volumetric efficiency of the compressor (η_V).

$$\dot{V}_{\text{swept}} = (S)(V)(n)(\eta_{\text{V}}) \tag{2.2}$$

The swept volume rate needs to be varied in order to meet varying refrigeration loads, or other compressor requirements such as the maximum power consumption. In order to control the SVR, the speed of the compressor, or the swept volume can be varied. Typically the swept volume is varied using a sliding valve installed in the compressor housing.

The slide valve recirculates trapped gas back to the suction side of the compressor before it is compressed. Figure 2-9 illustrates how the position of the slide valve changes the volume of gas compressed. As the slide valve moves towards the discharge port the sealing of suction gas between the rotors is delayed, which reduces the volume of gas which is ultimately trapped and compressed. By changing the initial volume of the compressed gas, the position of the slide valve also changes the volume ratio of the compressor. The pressure of the compressor (P_{R}) can be related to the built-in volume ratio of the compressor (V_{R}), which is defined as the ratio of discharge volume (V_D) and suction volume (V_S) as

$$P_{\text{R}} = \left(\frac{V_{\text{D}}}{V_{\text{S}}}\right)^{K} \tag{2.3}$$

where K is the ratio of specific heats, $K = \frac{Cp}{Cv}$. If the built-in pressure ratio of the compressor does not match the operating pressure ratio of the refrigeration system, either under-compression or over-compression will occur. Under-compression and over-compression both lead to wasted energy and a reduction in compressor efficiency.

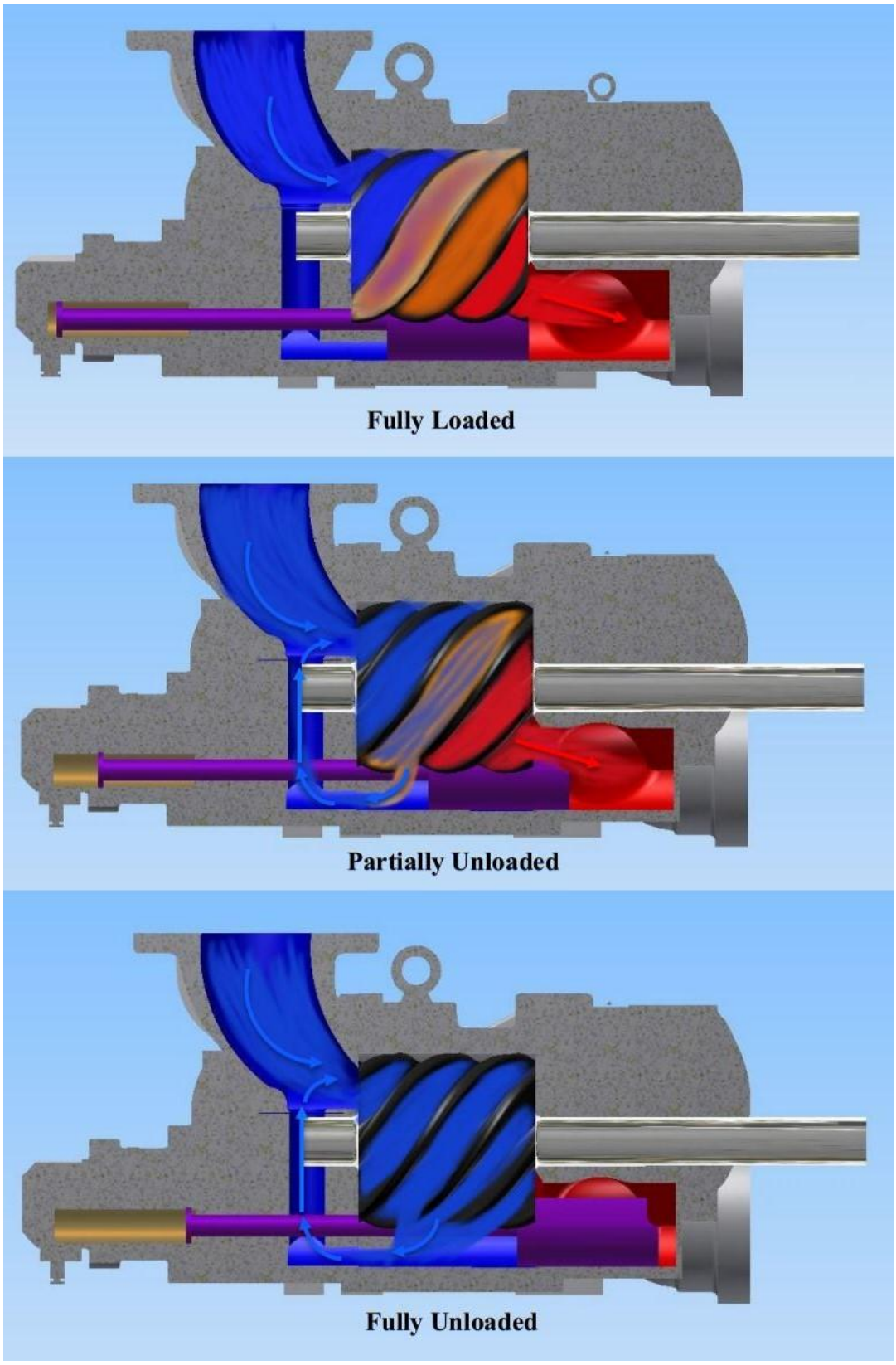

Figure 2-9 Compressor Slide Valve Operation

2.3.3 Condensers

Evaporative condensers are used almost exclusively in ammonia refrigeration systems. Air-cooled condensers can be used if water for the evaporative condensers is not available. Evaporative condensers are advantageous because they maintain low condensing pressures on days where the ambient air temperature is high (Scott, 2014). For example, to achieve a condensing temperature of 43°C, which might be required on a 30°C day with air cooled condensers, the condensing pressure will be 1555 kPa (225 psi). Lower condensing pressures are advantageous because they lower the work of compression, which can be calculated as

$$\dot{W}_{\text{Compressor}} = \frac{P_{\text{evap}} K}{\eta_{\text{i}}(K-1)} \left[\left(\frac{P_{\text{cond}}}{P_{\text{evap}}} \right)^{\frac{(K-1)}{K}} - 1 \right] \tag{2.4}$$

where K is the ratio of specific heats, η_{i} is the compressor isentropic efficiency, and P_{cond} and P_{evap} are the condensing and evaporation pressures respectively (Gosney,1982, p.270). Equation 2.4 demonstrates that the work of compression can be reduced by reducing the condensing pressure.

2.4 Rating Refrigeration Plant Performance

Commercial chillers are tested by their manufacturers to determine their capacity under a wide range of operating conditions. The performance of commercial chiller packages is typically determined under the guidelines of ASHRAE Standard 30: Method of Testing Liquid-Chilling Packages (ASHRAE, 1995) and AHRI Standard 550 / 590: Performance Rating of Water-Chilling and Heat Pump Water-Heating Packages Using the Vapor Compression Refrigeration Cycle (AHRI,2011). ASHRAE 30 describes the test methods, test procedures, and instrumentation that should be used for the tests. AHRI 550/590 sets out the conditions under which the tests should be performed, parameters that must be tested, minimum published data requirements, and nameplate requirements. Prescribed test conditions include part load conditions, required chiller leaving water temperature test points, and the required condenser entering dry bulb temperature for air cooled condensers. ASHRAE 30 does not prescribe test conditions, instead it refers to AHRI 550/590 for prescribed test conditions. Both standards require testing to be carried out under steady state conditions. Both standards require

measurements to include the compressor power consumption, the chiller water inlet temperature, the chiller leaving water temperature, the chiller water flow rate, and the power consumption of auxiliary components such as pumps and fans. All measurements are to be taken at five minute intervals as close to simultaneously as possible. The standards provide a consistent way for manufacturers to rate their chiller packages, so that end users can easily compare the performance of different chiller packages. Excluded from AHRI 550/590 are plants operating at chiller exit water temperatures less than 0°C (32°F). AGF plants always have brine temperatures leaving the chiller of less than 0°C. Therefore, they are automatically excluded from the standards. In addition, the size and complexity of AGF plants make it impractical to set up and test AGF plants in a laboratory setting. Laboratory tests are a requirement of AHRI 550/590 because field tests make it difficult to obtain consistent repeatable test results. Field tests do not allow the ambient air temperature, and brine temperatures to be held steady for testing.

2.5 Refrigeration Plant Modelling

A substantial number of models have been developed for simulating refrigeration plants and can be categorized based on whether they are steady state or transient. Steady state and transient models can be further subdivided into theoretical, empirical, or some combination of empirical and theoretical models. Most models are at least partially empirical, with correlations being used to predict the efficiency of the compressor. Transient models are usually based on theoretical models since data provided by manufactures, which is based on AHRI 550/590 or other test standards, is always for steady state conditions. Transient models such as the one developed by Zhang, Zhang, and Ding (2009), for an air cooled chiller with an economized screw compressor, are useful for plant control design and optimization. For the purpose of studying AGF refrigeration plants transient models are not required, because the ground's transient response to changes in brine temperature is orders of magnitude slower than the refrigeration plant's transient response.

Steady state models can be based on first principle thermodynamics, or empirical correlations developed from manufacture performance data. For example, Teyssedou (2007) presents a model of a refrigeration plant for an ice rink, based the TRNSYS Transient System Simulation Tool, and empirical data for simulating compressor performance. The refrigeration plant Teyssedou

considers consists of five, single stage reciprocating compressors, two evaporators, six condensers, and brine loop used to freeze the ice for the rink. The models of the compressors and other components are based on the ASHRAE HVAC 1 Toolkit for Primary HVAC System Energy Calculations, which is a collection of 38 separate subroutines for modeling the energy performance of different HVAC components (U.S. Department of Energy, 2011). The focus of Teyssedou's model is determining the energy consumption of the refrigeration system, as opposed to determining the overall performance of the refrigeration system under different conditions. Therefore, the control schemes that are studied are not directly applicable to a plant that is being operated in an overloaded state.

As it was previously mentioned, even models that rely on first principles may still rely on empirical correlations. Yu and Chan (2006) develop a model of an air cooled screw chiller using TRNSYS. The model uses theoretical models for the various system components, such as the compressor. Yu and Chan only use empirical correlations to model the volumetric and isentropic efficiency of the compressor. Their model is used to determine the energy consumption of the chiller package. Their primary goal is to find the optimum variable speed condenser fan control scheme that could be used to minimize the total compressor and condenser fan power consumption.

The models of Teyssedou (2007) and Yu and Chan (2006) give a representative sample of the refrigeration models that exist. Ding (2007) provides a critical overview of many of the models available and the different modeling techniques that are utilized.

2.5.1 Screw Compressor Models

Screw compressor models suitable for system modeling are either based on empirical data, or first principle thermodynamics. Numerous detailed models of the compression process exist which are suitable for optimizing the design of the compressor itself such as the models developed by Hsieh, Shih, Hsieh, Lin, and Tsai (2012) or Ghosh, Sahoo, and Sarangi (2007). Detailed compressor models are typically based on computational fluid dynamics (CFD) simulations and aim to optimize compressor parameters like rotor geometry. Therefore, they are not suitable for system modeling. Empirical models utilize compressor performance data provided by the compressor manufacturer to build correlations for a compressor's power

consumption, coefficient of performance (COP), and available nominal capacity ratio (ANCR), which is the ratio of available compressor capacity to nominal capacity as a function of the $T_{sat,S}$, and $T_{sat,D}$ (Solati, Zmeureanu, & Haghighat,2003). First principle models can determine the compressor power consumption and refrigerant flow rate using compressor specifications and operating conditions such as the swept volume rate, built in volume ratio, volumetric efficiency isentropic efficiency, suction pressure, and discharge pressure (Yu & Chan, 2006). The compressor power consumption can be calculated using Equation 2.4, and the refrigerant mass flow rate can be calculated using

$$\dot{m}_{\text{ref}} = \frac{\dot{V}_{\text{swept}} \cdot \eta_{\text{V}}}{v_{\text{ref}}} \tag{2.5}$$

where $\dot{m_{ref}}$ is the refrigerant mass flow rate in kg/s, $\dot{V}_{\text{swept}}$ is the compressor swept volume rate in m^3/s, v_{ref} is the specific volume of the refrigerant gas at the compressor suction in m^3/kg, and η_V is the compressor volumetric efficiency. The compressor volumetric efficiency can be calculated as

$$\eta_{\text{V}} = 0.925 - 0.009 P_{\text{R}} \tag{2.6}$$

where P_R is the compressor pressure ratio which is defined as the compressor discharge pressure divided by the compressor suction pressure (Yu & Chan, 2006).

2.5.2 Evaporator Models

AGF plants almost exclusively use flooded evaporators, utilizing either shell-and-tube or plate-and-frame heat exchangers. Evaporator models take either a detailed or a black box approach to modeling. The black box approach involves using either the log mean temperature difference method (LMTD) or the effectiveness-NTU method. Details about these methods can be found in any introductory heat transfer textbook such as (Bergman, Lavine, Incropera, & DeWitt, 2011). Using the black box approach only requires information about the overall heat transfer coefficient (*UA*) for the evaporator, which is assumed to be constant throughout the evaporator. The black box approach is commonly used by modeling packages such as TRNSYS (TRNSYS, 2010). The detailed modeling approach requires extensive information about the internal geometry of the heat exchanger in order to calculate the overall heat transfer coefficients. Finding sufficient information for an evaporator always presents the biggest modelling challenge. This is especially true with plate-and-frame heat exchangers where the

geometry of the plates is such that it enhances heat transfer. Therefore, without knowing the exact internal geometry of the plates it is not possible to use the detailed approach to model them. Furthermore, plate geometry is usually regarded as propriety information by heat exchanger manufacturers. Therefore, few detailed models exist for plate-and-frame heat exchangers that are practical to use. The majority of a shell-and-tube heat exchanger's geometry can be described using only a few basic specifications. Therefore, several detailed models exist for them. Webb et al. (1989) present a detailed model to predict the capacity of a flooded shell-and-tube evaporator. The model accounts for the effect of the refrigerant level in the evaporator including the static head penalty, and superheat that would occur if the refrigerant level in the evaporator dropped exposing some of the tubes.

A more practical model is presented by Vera-García et al. (2010) which does not require detailed information about the tube bundle geometry. The model only requires catalogue information for the heat exchanger including the exchanger's rated capacity, the evaporation temperature, the tube diameter, the secondary fluid inlet temperature, and the secondary fluid flow rate. In order to reduce the amount of information required the author assumed that the overall heat transfer coefficient at the design conditions on the inside of the tubes is equal to the overall heat transfer coefficient on the outside of the tubes:

$$\frac{1}{(UA)_{\text{brine}}} = \frac{1}{(UA)_{\text{ref}}} \tag{2.6}$$

This key assumption makes the model very practical because it is able to simulate the heat exchanger under different secondary fluid flow conditions with information that is easy to obtain from a manufacture's catalogue. However, the simplified model is limited by the author's use of the Dittus-Boelter correlation for the secondary fluid's convective heat transfer coefficient, which is only valid for: $0.7 \leq Pr \leq 160$, $Re_D \geq 10{,}000$, and $\frac{L}{D} \geq 10$ (Bergman et al., 2011). The effect of using a more accurate correlation for the convective heat transfer coefficient, such as the Gnielinski correlation is examined in Section 5.3.

2.5.3 Condenser Models

Like evaporator models, condenser models can take either a detailed or a black box modeling approach. For example, Yu and Chan (2006) used an LMTD approach to model an air cooled condenser by performing a regression analysis of the condenser manufacturer's provided performance data. The regression analysis was used to determine the local heat transfer coefficients as a function of operating conditions. In some situations air cooled condenser models may be as simple as assuming that the condensing temperature is equal to the ambient temperature plus an approach temperature, which is usually on the order of 8°C to 15°C (Scott, 2014). Detailed condenser models can be significantly more complex than detailed evaporator models. Unlike a flooded evaporator, condensers will have a region where the refrigerant is superheated, a two phase region where the refrigerant is being condensed, and some may have a subcooled region where the refrigerant is cooled beyond its saturation temperature. To account for the different refrigerant phases, detailed condenser models will break the condenser into multiple control volumes, essentially treating each control volume as a separate heat exchanger (Cuevas, Lebrun, Lemort, & Ngendakumana, 2009). Dividing the condenser into a larger number of control volumes will improve the accuracy of the model. However, the model must determine how much of the total condenser is dedicated to desuperheating, condensing, and subcooling.

2.6 Ground Freezing

The process of artificially freezing the ground for construction or mining has been used for over one hundred and fifty years. The first recorded application of artificial ground freezing was for a mine shaft in South Wales in the year 1862 (Sanger & Sayles, 1979). This section provides a brief overview of the ground freezing process and some of the physical processes involved.

To freeze groundwater, borehole heat exchangers, or freeze pipes, are cemented into the ground and a calcium chloride solution chilled to approximately -30°C is pumped through the freeze pipes. The calcium chloride solution is pumped down each freeze pipe's inner tube and then flows back up the annulus between the inner tube and the casing of the freeze pipes. As the brine flows up the annulus it removes heat from the surrounding ground through convective heat transfer (Figure 2-10).

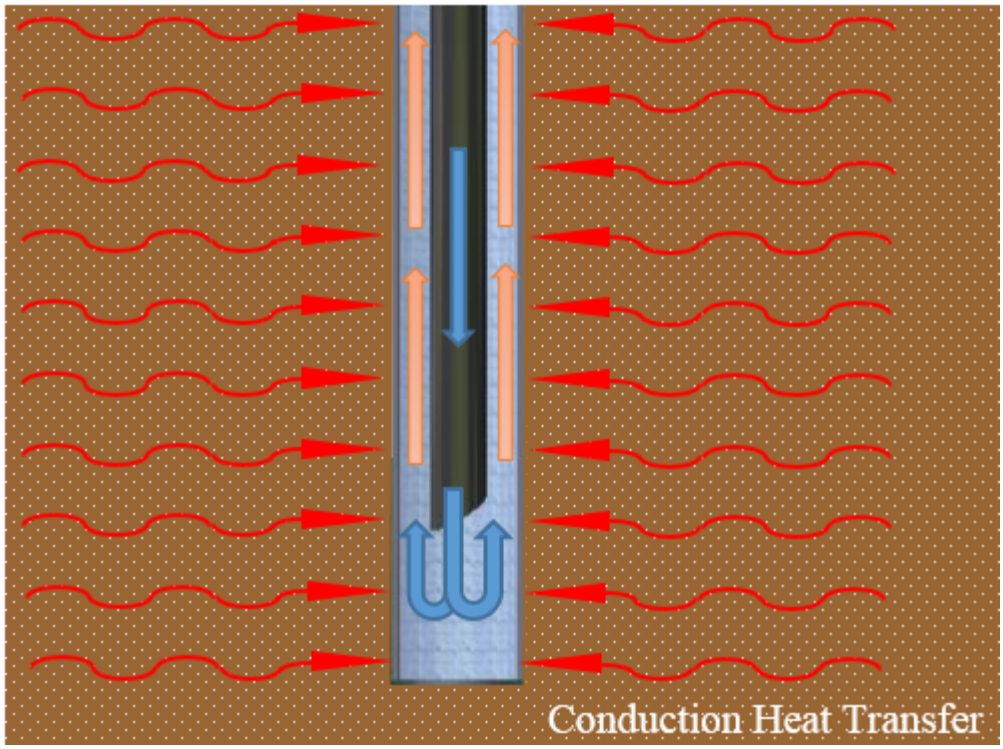

Figure 2-10 Freeze Pipe Brine Flow

The freezing process can be divided into three phases. In the first phase sensible heat is removed from the ground as its temperature approaches the freezing point of water, which can vary depending on the salinity of the ground water. In the second stage, phase change occurs at the zero degree Celsius, or phase change isotherm, removing latent heat from the water trapped in the soil and rock. Finally, in the third phase more sensible heat is removed from the frozen ground further reducing its temperature. These three phases occur simultaneously in a cylindrical column of ground surrounding the freeze pipe (Figure 2-11). After the freeze pipes are activated, the region of ground that is frozen grows and the phase change isotherm moves outwards from the freeze pipe (Andersland & Ladanyi, 2004). AGF projects typically aim to create a wall or block of frozen ground, which is accomplished by installing multiple freeze pipes in close proximity. As the columns of frozen ground grow they will eventually intersect closing the freeze wall or block of frozen ground.

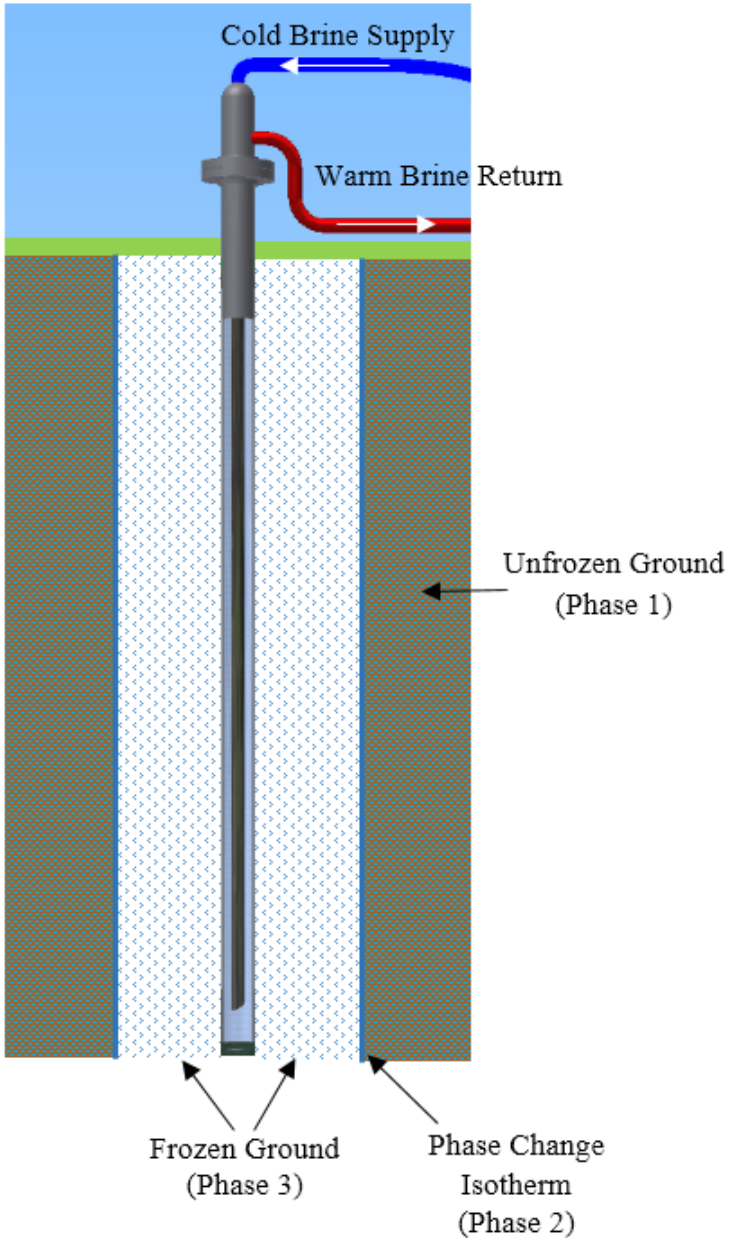

Figure 2-11 Stages of Ground Freezing

Before any freezing project is undertaken it is necessary to calculate the time required to freeze the ground and the required refrigeration capacity. In practice, phase change complicates the analysis of the ground heat transfer because the frozen ground's thermal conductivity is typically higher than that of the unfrozen soil. This along with phase change itself creates a discontinuity in the ground temperature distribution where phase change is occurring. As a result, rigorous closed-form solutions to the Fourier field equation are not possible (Sanger & Sayles, 1979). In

addition, modeling the freezing process requires coupling several thermophysical processes, including, heat and moisture transfer, ground water movement, and potential frost expansion (Eslami-nejad & Bernier, 2012). Therefore, the analysis of the freezing process typically requires numerical methods, such as the finite element method. Commercial software such as Geo-Slope's Temp/W (GEO-SLOPE International, 2015) can be used to accomplish this.

Despite the complexities of ground heat transfer, Sanger and Sayles (1979) developed a set of equations that can be used to roughly approximate heat transfer in frozen soil. They were able to do so by assuming that

- the isotherms move slowly enough that they resemble the isotherms that would exist under steady state conditions,
- the radius of the unfrozen soil affected by the temperature of the freeze pipe can be expressed as a multiple of the frozen soil radius, and
- the total latent and sensible heat can be expressed as specific energy, which when used to compute the energy removed from a soil column, gives the same energy as the latent heat and sensible heat added together.

Equation 2.7 was derived using these assumptions, and gives the refrigeration requirement per unit length of freeze pipe to freeze a column of soil as

$$\dot{Q}_{ground} = \frac{2\pi k(\Delta T)}{\ln(\frac{r}{r_0})} \tag{2.7}$$

where k is the thermal conductivity of the frozen soil, ΔT is the difference between the temperature at which the ground water freezes and the surface temperature of the freeze pipe, r is the radius of the phase change isotherm, and r_0 is the radius of the freeze pipe. Equation 2.7 is only a rough approximation yet it illustrates that the rate of heat removal from the ground is a direct function of the temperature of the brine circulating through the freeze pipes. Therefore, the temperature dependent freeze plant capacity is coupled to the rate of ground heat removal through the temperature of the brine circulating through the freeze pipes.

2.7 Literature Review Conclusions

Many different models exist for modeling refrigeration systems and their components. The models can be as simple as a correlation that can model the performance of the entire refrigeration system, or as complex as a detailed thermodynamic model of each and every component in the system. The model that is used depends on what information is available about the refrigeration system, and the purpose of the model. Every system model considered in the literature review is used for modeling and optimizing the energy efficiency of the refrigeration system.

No literature was found pertaining to modeling industrial refrigeration systems for the purpose of predicting its refrigeration capacity and optimizing the capacity of the refrigeration system. The difference between the two modeling/optimization approaches is analogous to the difference between modifying an engine to maximize fuel economy versus modifying it to maximize its power output. In order to use a model to maximize the performance of a refrigeration system the model must be able to predict how the system responds to the plant controls when the compressor and other components are operating at full capacity. Therefore, the primary goal of this research is to develop a model that can calculate the capacity of the refrigeration plant over the plant's entire operating envelope based on component specifications. The model must be capable of predicting which system components will limit the refrigeration capacity under different operating conditions. The results of this model can be used to help address the coupling of the plant’s capacity with the rate of heat removal from the ground for AGF. The basis for the model is an existing plant at Cameco’s Cigar Lake mine, which will be described in the next chapter.

CHAPTER 3: CIGAR LAKE REFRIGERATION PLANTS

3.1 Cigar Lake Surface AGF system

The Cigar Lake Uranium mine, located 675 km north of Saskatoon SK, is the world's largest high grade uranium deposit with proven and probable reserves of $1.05 \cdot 10^8$ kg (232 million pounds) of U_3O_8 at an average grade of 18%. The orebody which is located 450 m below ground is an unconformity type deposit, meaning that it lies at the boundary between basement metasediments and overlying Athabasca sandstone. The crescent shaped orebody is approximately 7 m in thickness, and is a mixture of pitchblende and clay (Edwards, 2004). Both the orebody and surrounding sandstone, which is highly fractured, are very weak and contain a large amount of ground water under extremely high pressures.

During the test mining phase for the Cigar Lake project, several hydrogeological studies were carried out. The studies found that in the region of extremely altered sandstone surrounding the ore body the hydraulic conductivity of the sandstone is $1 \cdot 10^{-5}$ m/s. In the basement rock below the orebody, where all of the mine workings are constructed, the hydraulic conductivity of the rock is $1 \cdot 10^{-9}$ m/s. Groundwater modeling indicated that the measured hydraulic conductivities and hydraulic gradients in the vicinity of the orebody result in potential inflow rates from the sandstone formation of 2,700 m^3/hr. The large inflow potential made conventional dewatering using a network of dewatering wells cost prohibitive and logistically impractical. Curtain grouting utilized during test mining was effective in reducing the inflow of water to levels which could be pumped out of the mine in a cost effective manner. However, AGF which was also utilized during test mining almost completely stemmed the flow of water and therefore also reduced the amount of radon gas entering the mine along with the water (Cigar Lake Mining Corporation (CLMC), 1995).

In order to safely mine the uranium ore the entire orebody and all of the surrounding weak ground is frozen using AGF. The freezing is accomplished using freeze pipes installed both from the surface and the underground mine workings as shown in Figure 3-1. The freeze pipes installed from the surface are approximately 460 m long and are run from the surface to just below the ore body. In an attempt to reduce the heat load on the refrigeration plant, the surface freeze pipes use an isolating packer along with an extra inner tube to create an air gap between

the cold brine and the outermost freeze pipe casing. This air gap spans 400 m from the surface to just above the ore body. The underground freeze pipes, which are approximately 60 m long, are installed from underground drifts by drilling upwards with a specially designed drill that uses a preventer to seal the drill string and stop water from flowing into the mine.

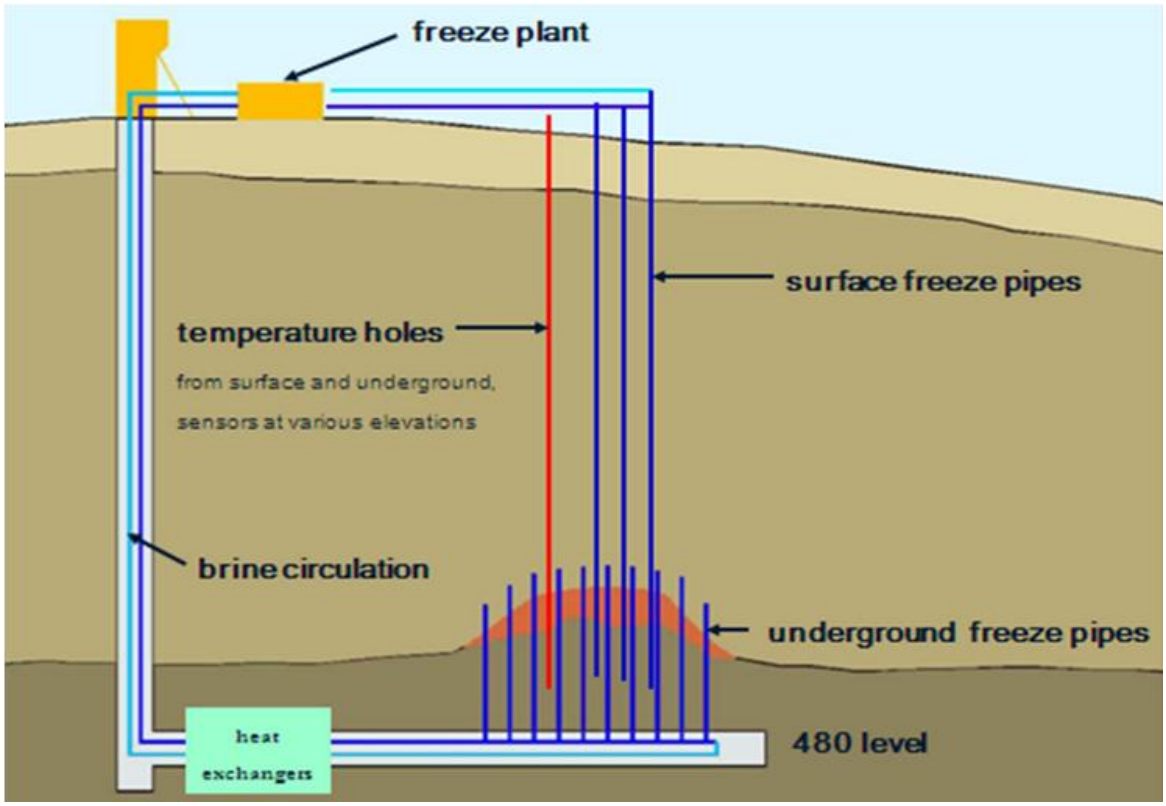

Figure 3-1 Cigar Lake Mine Cross Section (Used with permission of Cameco Corp.)

To remove heat from the ground, calcium chloride brine is chilled using three different refrigeration plants. The smallest of the three refrigeration plants, commonly called the FRICK plant, is rated for 317 kW (90 TR) at $T_{sat,s}$ =-40°C. The second refrigeration plant, called the Primary plant, is rated for 3165 kW (900 TR) at $T_{sat,s}$ =-40°C. The third and largest plant, called the modular plant, is rated for 4407 kW (1253 TR) at $T_{sat,s}$ =-40°C and $T_{sat,D}$=43.3°C. The FRICK and primary plants are responsible for chilling the brine used in the underground freezing circuit, and a portion of the surface freeze pipes. The modular plant is responsible for chilling the brine for the remaining surface freeze pipes.

3.2 Cigar Lake Modular Plant Description

The modular refrigeration plant (Figure 3-2), which will be the focus of this research, consists of five separate refrigeration plants or modules, which are the individual red buildings in Figure 3-2.

Figure 3-2 Cigar Lake Modular Refrigeration Plant with Five Modules and Condensers

The five different refrigeration modules are coupled together using large brine tank capable of holding approximately 72,000 L of brine (Figure 3-3). The tank has a baffle installed with an opening in it that divides the tank into two separate compartments. The baffle allows for different flow rates on the freeze pipe (field) side of the tank and the refrigeration plant (module) side of the tank. The flow on the module side of the tank is always maintained at a rate higher than on the field side, which induces flow through the hole in the tank baffle from the cold to the warm side of the tank.

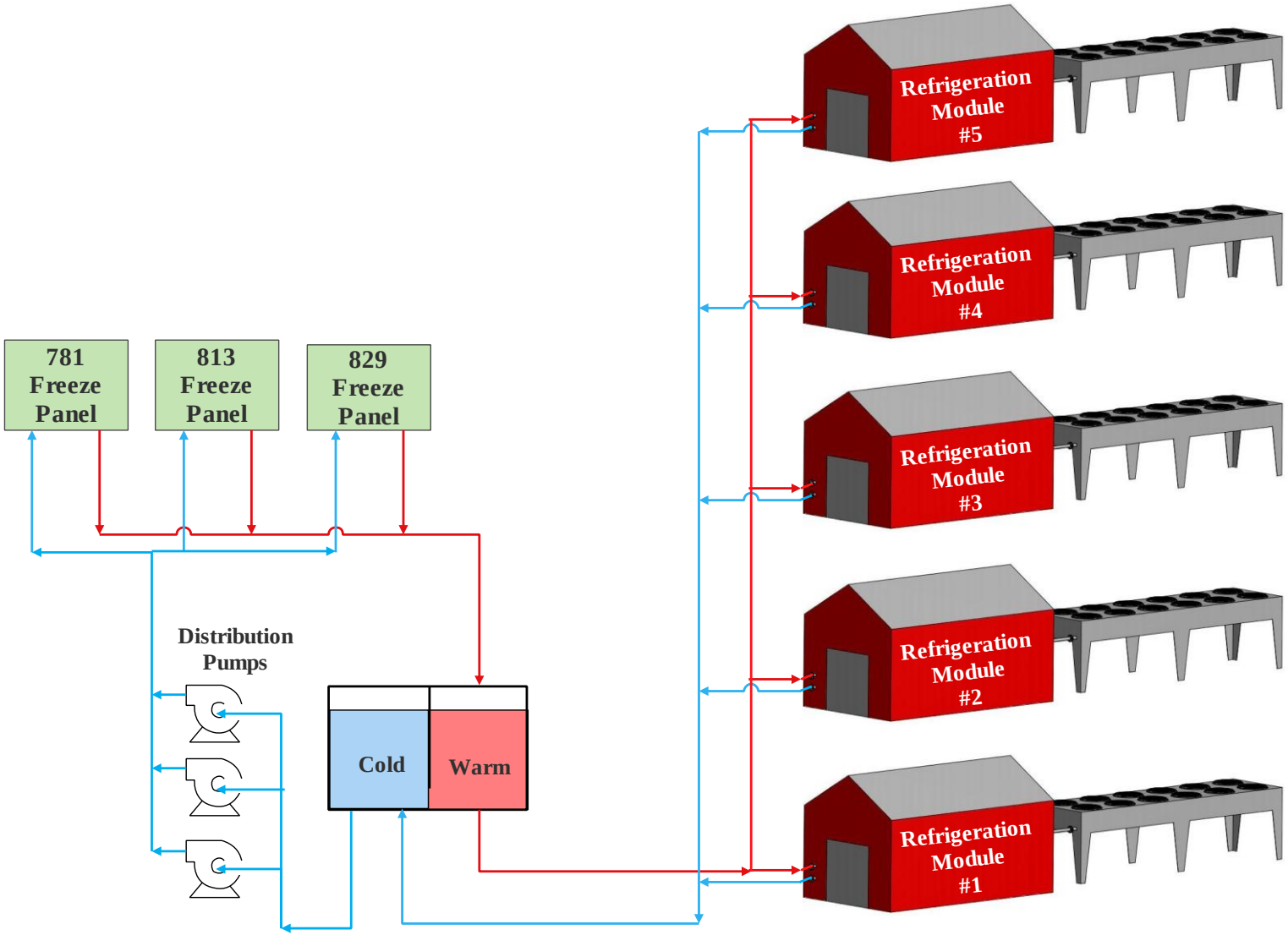

Figure 3-3 Cigar Lake Modular Refrigeration Brine Flow Diagram

Eight different centrifugal pumps are used in the system for brine distribution. One pump is installed in each refrigeration module, and three large pumps plumbed in parallel distribute brine to the freeze pipes. Only two of the distribution pumps are required to meet the freeze pipe flow requirements, leaving the third pump as a backup for maintenance.

Each refrigeration module can be divided into four different loops (Figure 3-4) based on process fluid including

- the brine chilling loop,
- the ammonia refrigeration loop,
- the oil injection loop, and
- the glycol cooling loop.

The brine chilling loop consists of a circulation pump, and an evaporator, which is a shell-and-tube heat exchanger. Brine pumped from the tank flows on the tube side of the heat exchanger. The brine on the tube side transfers heat to liquid ammonia on the shell side causing the ammonia to evaporate.

The ammonia refrigeration loop consists of nine main components including

- a flooded shell-and-tube evaporator,
- a surge drum,
- a two stage compound twin screw compressor,
- an oil separator,
- an air cooled condenser,
- a direct expansion shell and tube subcooler,
- a thermal expansion valve (TXV) , and
- a float controlled expansion valve.

The oil injection loop consists of a coalescing filter type oil cooler, oil pump, and a shell-and-tube heat exchanger which cools the oil using glycol. The glycol is pumped through the oil cooler, and then an air cooled heat exchanger which rejects the heat gained in the oil cooler to the atmosphere. The two stage ammonia refrigeration cycle begins in the evaporator, which is flooded with liquid ammonia. As the ammonia is evaporated, the ammonia vapor flows through the surge drum which is designed to reduce the velocity of the vapor sufficiently to ensure that no liquid ammonia can reach the compressor.

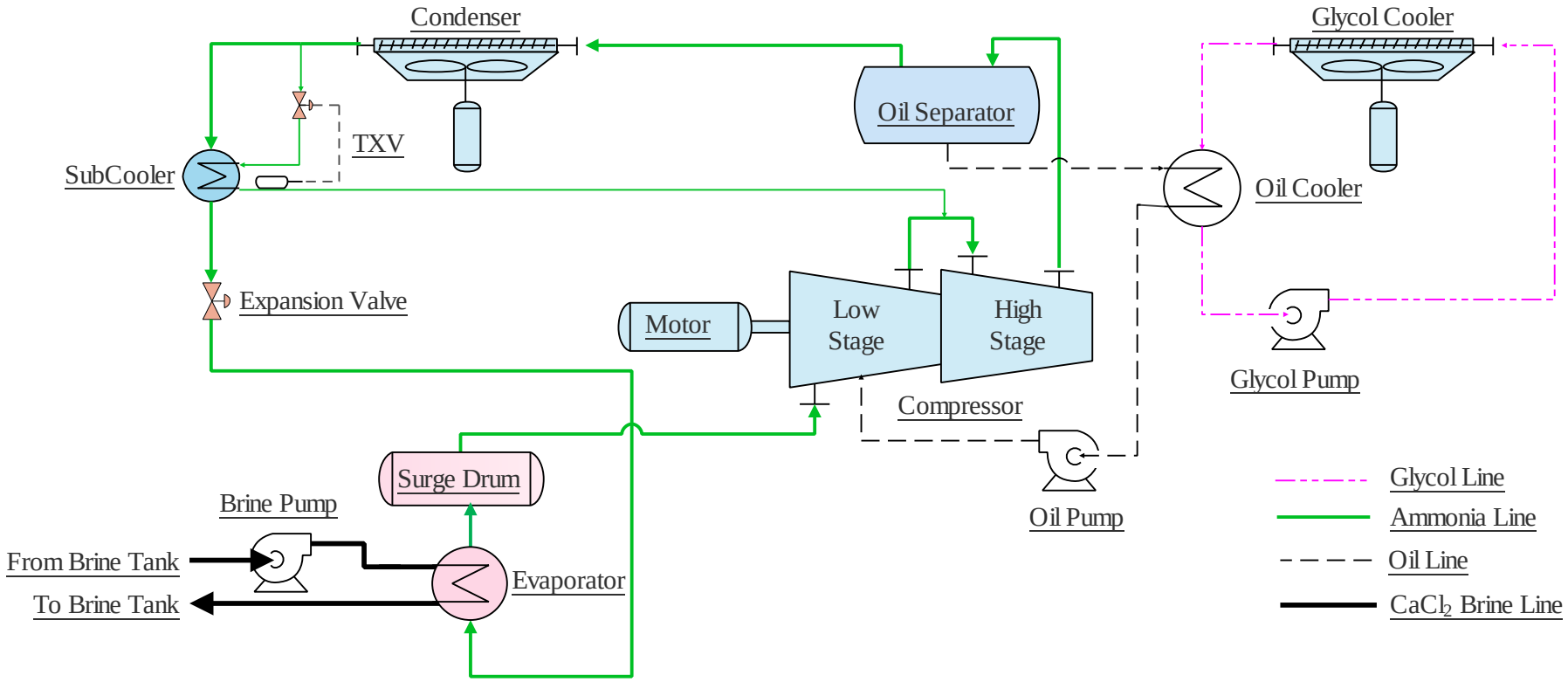

Figure 3-4 Refrigeration Module Process Flow Diagram

The compressor is a two stage compound twin screw compressor. In the compressor's low-stage oil is injected and mixed with the ammonia vapor to seal lobes of the compressor and cool the ammonia vapor. After the first compression stage the ammonia-oil mixture is combined with ammonia vapor at the intermediate pressure that is produced in the subcooler. After being compressed in the high-stage the ammonia /oil mixture passes through the oil separator which uses coalescing filters to separate the oil from the ammonia vapor.

3.3 Cigar Lake Modular Plant Specifications

The modular plant was custom built, and most of the components used in the plant were made-to-order. Since the plant was custom built, the specifications available for the individual components are not as numerous or detailed as those that would be available for a commercial refrigeration system. Evaporator and condenser specifications were provided by their manufacturers for a single operating point. Compressor specifications were obtained from software produced by the compressor manufacturer, Mycom, which calculates the compressor capacity based on operating parameters such as suction, and discharge pressure. Similarly specifications for the brine pumps were obtained from software produced by Goulds Pumps. The main component specifications are summarized in Table 3-1.

3.4 Cigar Lake Modular Plant Instrumentation

Figure 3-5 is a simplified Piping and Instrumentation Diagram (P&ID) for the refrigeration plant. The symbols used in Figure 3-5 are described in the abbreviations section of this thesis. Only piping and instrumentation pertinent to the data analysis in this thesis is shown. In addition, only one module is shown as all of the modules have identical instrumentation. Table 3-2 lists the instrumentation shown on the plant P&ID and gives the specifications for the instrumentation. There was no information available on the accuracy of instrumentation that was included with the compressor. Therefore its accuracy was assumed to be the same as the other instrumentation used in the system.

Table 3-1 Modular Plant Specifications

Component	Manufacture	Type	Model Number	Rating	Rating Conditions
Compressor	Mayekawa	Compound Twin Screw Oil Injected Ammonia Compressor.	N3225LS C-MBM	1066 kW (303 TR)	$T_{sat,s}$ = -42.8°C $T_{sat,D}$ = 43.3°C
Compressor Motor	N/A	3 Phase, 600V Electric	N/A	746 kW (1000 hp)	N = 3550 RPM
Evaporator	Chilcon	Flooded Evaporator	FA-24288-410	881 kW (250 TR)	T_{evap} = -40°C $\dot{V}_{brine}$ = 249.7 m^3/hr $T_{brine,in}$ = -31.4°C
Condenser	Colmac	Air Cooled Condensers	ACV-90324-11126L-G-36-3-DT-E	2x (841.8 kW) = 1684kW (479 TR)	T_{cond} = 43.3°C T_{amb} = 30.0°C Airflow = 211,885 m^3/hr (124711 cfm)
Compressor Heat Exchanger Pumps	Goulds Pumps	Centrifugal Pump	3196: 4x6-13	204 m^3/hr	42 m Total Discharge Head (TDH)
Brine Distribution Pumps	Goulds Pumps	Centrifugal Pump	3196: 3x4-13	195 m^3/hr	107 m Total Discharge Head (TDH)

.

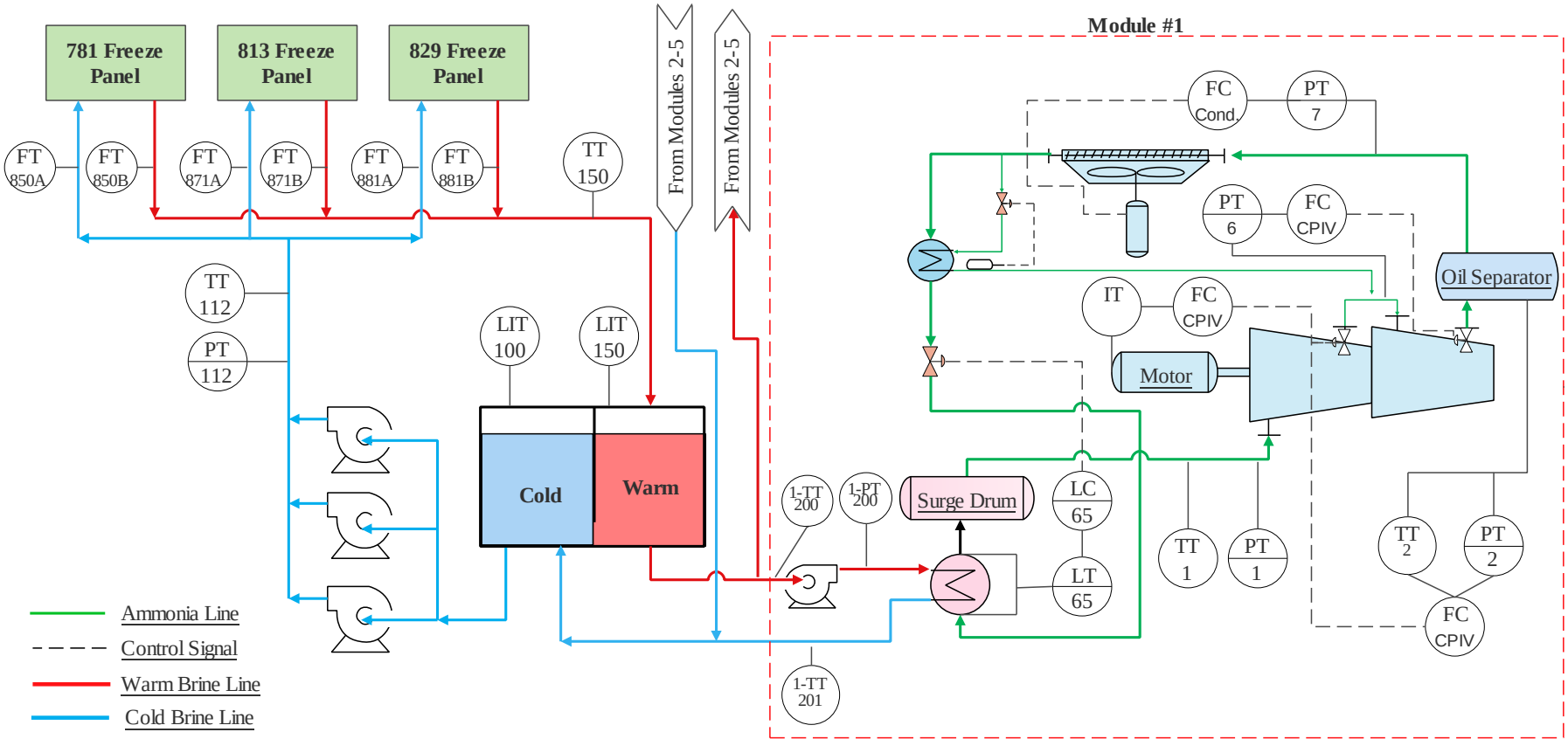

Figure 3-5 Modular Refrigeration Plant Process and Instrumentation Diagram

Table 3-2 Freeze Plant Instrumentation Specifications

Instrument	Type	Manufacturer	Measurement Range	Accuracy	Reference
FT-850A	Magnetic Flow Tube	Foxboro	26 m^3/hr to 554 m^3/hr	±.25%	(Invensys Systems, Inc.,2013)
FT-850B					
FT-871A					
FT-871B					
FT-881A					
FT-881B					
PT-1	Pressure Transducer	Mycom	-101.4 kPa to 980.4 kPa -14.7 (psi) to 142.2 (psi)	±.25%	Mycom Piping and Instrumentation Diagram Legend and Equipment Data Cover Sheet Drawn in 2011.
PT-2					
PT-6					
PT-112	Pressure Transducer	Wika	0-2068 kPa (0-300 psig)	(±0.25% of Span) ±5.17 kPa (±0.75 psi)	(Wika Instrument Corporation, 2011)
TT-112	RTD	Wika	-200°C to +250°C	Din Class A $\pm(0.15 + 0.002\|T\|)$℃	(Wika Corporation, N.D.) (Acromag Inc., 2011)
TT-150					
TT-200					
TT-201					
TT-1	RTD	Mycom	-50°C to +50°C	$\pm(0.15 + 0.002\|T\|)$℃ $\pm(0.15 + 0.002\|T\|)$℃	Mycom Piping and Instrumentation Diagram Legend and Equipment Data Cover Sheet Drawn in 2011.
TT-2	RTD	Mycom	0°C to +150°C		Mycom Piping and Instrumentation Diagram Legend and Equipment Data Cover Sheet Drawn in 2011.
LT-65	Float Switch	Hansen	N/A	N/A	N/A
LIT-100	Guided Radar	Profibus	0 to 35m	±3mm	(Endress + Hauser, 2012)
LIT-150	Guided Radar	Profibus	0 to 35m	±3mm	(Endress + Hauser, 2012)
PT-7	Pressure Transducer	Johnson Controls	0 to 3447 kPa (0 to 500psig)	(±1% of Span) ±34 kPa (±5 psi)	(Johnson Controls, 2014)

3.5 Cigar Lake Modular Plant Controls

Three main control systems are utilized on the refrigeration plants during normal operation. They include a condenser control system, a compressor control system, and an evaporator liquid level control system. Different aspects of the refrigeration plant's operation are controlled by each of the three controllers. However, the condenser control system and the compressor control system are both responsible for controlling the condensing pressure.

The condenser control system is used to prevent the condensing pressure (which can be directly converted to the Saturated Discharge Temperature ($T_{sat,D}$)) from dropping below a predetermined set point during times of low ambient temperature such as winter. This minimum $P_{sat,D}$ must be sufficient to overcome system pressure losses and to operate control valves (COLMAC COIL Manufacturing, N.D.). The condenser controller shuts down or cycles the twelve fans installed on each condenser to keep the condensing pressure at or above the minimum $P_{sat,D}$, which is set to approximately 1132 kPa (164 psi). A condensing pressure of 1132 kPa is equivalent to a saturation temperature of 29°C.

The screw compressors are controlled by a Mycom Mypro-CPIV compressor controller, which is used to keep the compressor within an operating envelope (Figure 3-6) defined by operator set points and machine limits. Critical set points and machine limits include the compressor pressure limits, including the suction pressure ($P_{sat,S}$) limit, the discharge pressure limit $P_{sat,D}$, and horsepower limits. The minimum suction pressure is set by the operator to maintain an evaporation temperature several degrees higher than the freezing temperature of the brine which is -47°C at a concentration of 29% $CaCl_2$ (DOW Chemical Corporation, 2003). The maximum $T_{sat,D}$ is set by the operator at approximately 1724 kPa (250 psi) which is less than the compressor's physical discharge pressure limit. The power consumption of the compressor, determined by the compressor motor size, is limited to 746 kW (1000 hp). In Figure 3-6 lines of constant horsepower are shown in green. The shaded green area in Figure 3-6 represents operating conditions where the compressor capacity is limited by the CPIV in order to keep the compressor power draw at or below 746 kW (1000 hp).

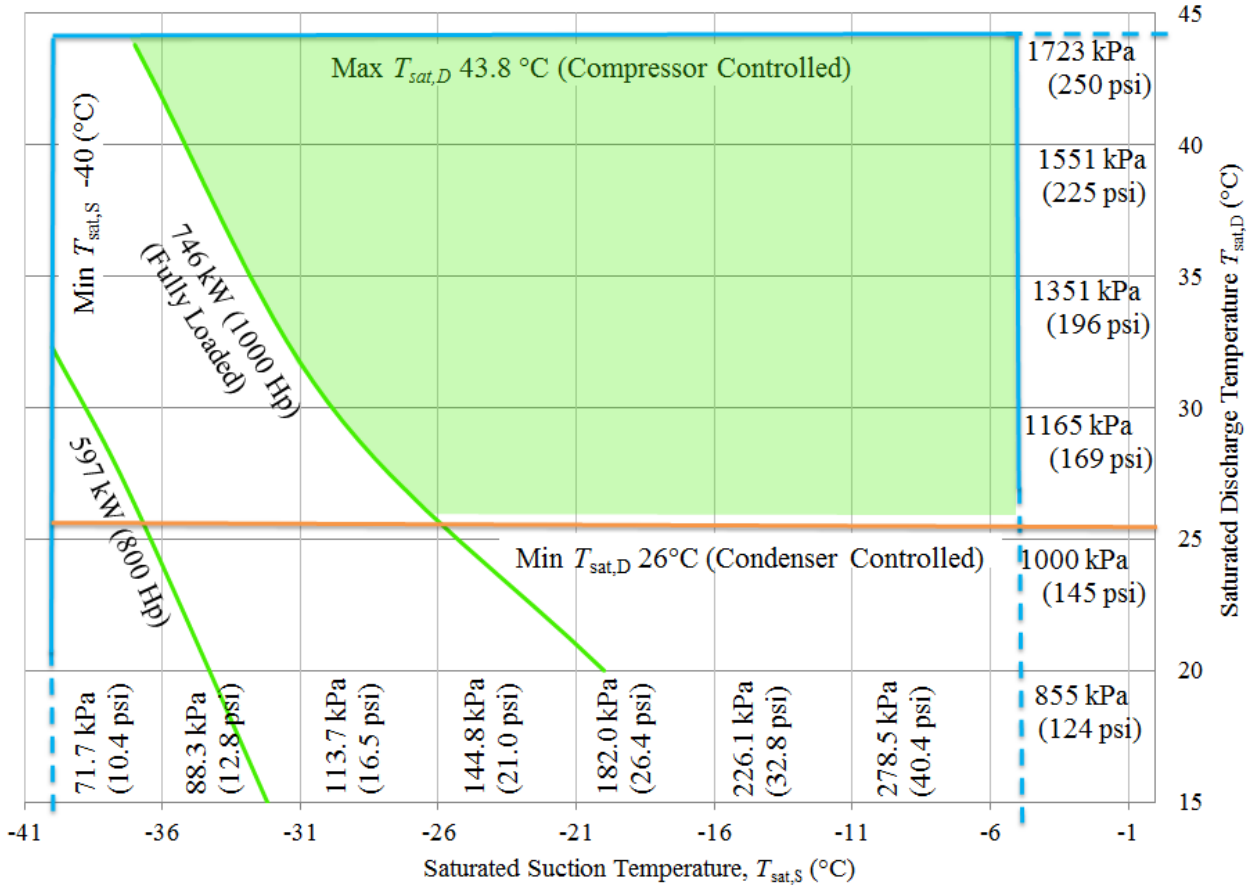

Figure 3-6 Compressor Operating Envelope

To keep the compressor operating within its envelope the CPIV uses both the high-stage and low-stage slide valves. The low-stage slide valve is used to maintain

- the minimum suction pressure set point,
- the maximum power absorption (measured using motor current draw), and
- the maximum discharge temperature.

The high-stage slide valve is used to only to maintain the intermediate pressure set point.

The CPIV automatically determines the required slide valve position using a proportional-integral-derivative (PID) control algorithm that compares operating parameters to limits set by the operator. The PID algorithm maintains the compressor's operating parameters at the set points selected by the operator, within operator selected dead band values. The dead band values, which are selected by the user, are used to prevent the PID controller from over controlling the slide valves, which could cause the slide valves to oscillate when the system is

near the desired set points. In the case of the modular refrigeration plants, the controlled parameter for the first stage is the suction pressure set point, and the intermediate pressure is the controlled parameter for the second stage.

To prevent the compressor overloading the CPIV uses the low-stage slide valve to force the compressor to unload if the compressor meets and of the conditions listed in Table 3-3, which are based on operator set points.

Table 3-3 Compressor Unload Conditions

Conditions
If motor Amps > high motor amps unload set point
If discharge pressure > high discharge pressure unload set point
If suction pressure < low suction pressure unload set point
If intermediate pressure > intermediate pressure unload set point

Load forbid set points are used to help prevent the controller from hunting near the unload set points and to help prevent control overshoot. If any of the conditions listed in Table 3-4 are met, the controller will not move the compressor's slide valve to increase compressor capacity.

Table 3-4 Conditions that Prevent an Increase in Compressor Capacity

Conditions
If motor Amps > high motor amps forbid set point
If discharge pressure > high discharge pressure forbid set point
If suction pressure < low suction pressure forbid set point
If intermediate pressure > intermediate pressure forbid set point

The command to unload the compressor will continue to be issued to the slide valve actuator until all of the conditions in Table 3-3 cease to be met. Once the unload conditions cease to be met, as long as none of the load forbid set points are exceeded, normal PID control will resume (Mayekawa MFG. CO., LTD., 2011).

The ammonia liquid level in the evaporator is controlled by a magnetic float switch (Figure 3-7) and a Hansen HS4A solenoid valve (Figure 3-8). The float switch cycles the solenoid valve on and off as the liquid level in the evaporator changes. If the solenoid valve is unable to maintain

the appropriate liquid level in the tank a secondary bypass expansion valve can be manually opened or closed to fine tune the flow of liquid ammonia into the evaporator (Figure 3-8).

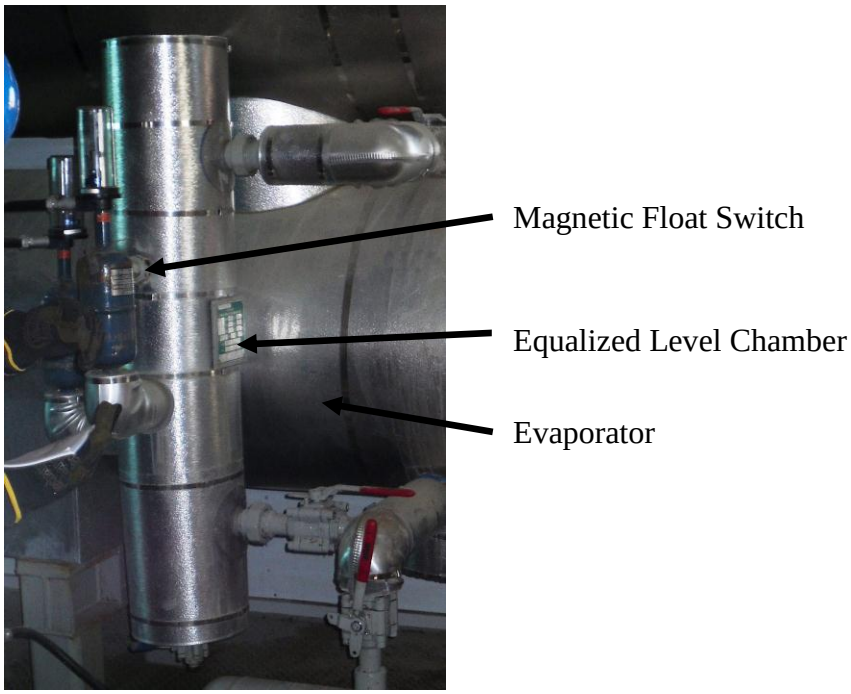

Figure 3-7 Equalized Liquid Level Chamber and Magnetic Float Switch

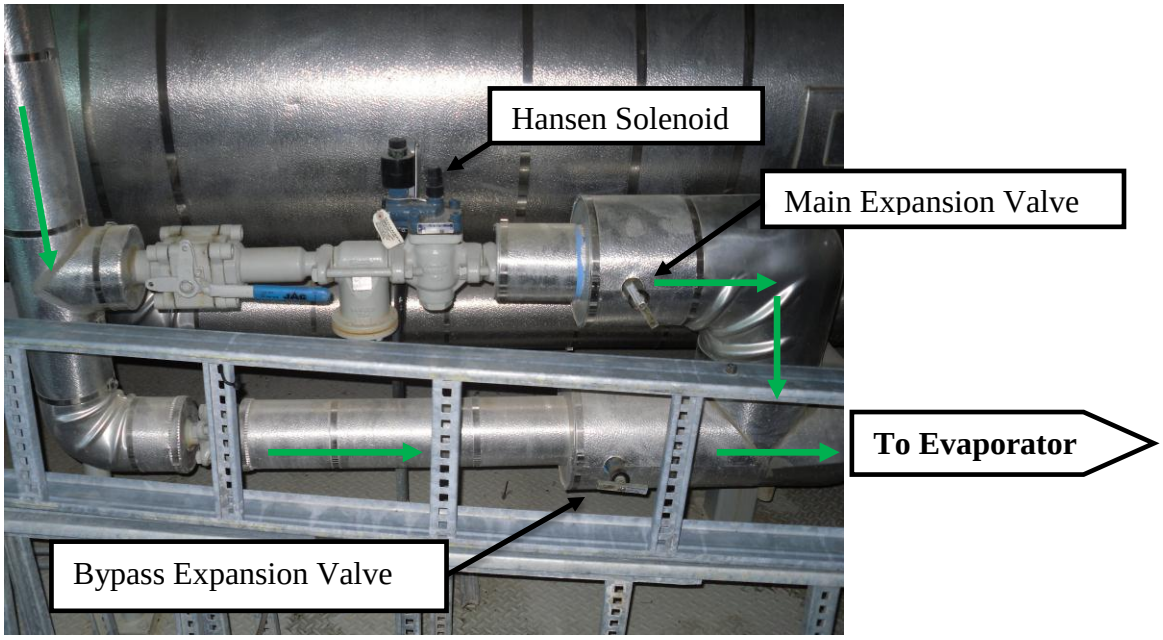

Figure 3-8 Expansion valves and Hansen Solenoid Valve

CHAPTER 4: MODEL DEVELOPMENT

The capacity of the refrigeration plant is calculated using a system model that is a combination of models for the evaporator, compressor, and condenser. The system model couples the individual component models together and determines the refrigerant pressures and mass flow rates that balance compressor and evaporator capacity while satisfying the requirements of the compressor controller. The evaporator, compressor, condenser, and overall system models are implemented as separate subroutines in an Excel spreadsheet. Several different software packages were considered during the modeling process including TRNSYS, Thermolib, which is a MATLAB add in, Aspen HYSYS, which is a standalone package for chemical process simulation, and OpenModelica, which is an open source Modelica based simulation package for transient simulation of physical systems. None of the packages considered could represent all of the refrigeration system components and the compressor control system without modifying default models included with the software. Therefore, Excel was the simplest option for developing the model. In addition, developing the model in Excel afforded complete control over the equations and solution methods used by the model.

4.1 Thermodynamic Properties

Thermodynamic and transport properties of the refrigerant and secondary fluid (brine) are of critical importance when developing a numeric model of the system. The open source fluid property library CoolProp was used to provide thermophysical properties for both the primary refrigerant (ammonia) and the secondary coolant (calcium chloride brine) (Bell, Wronski, Quoilin, & Lemort, 2014). CoolProp was developed using the C++ programming language and has high level interfaces compatible with most programming languages including C++, Visual Basic, and Microsoft Excel (Bell et al., 2014). The high level interface manifests itself in Excel as a single command that will return the desired property. For example, to obtain the saturated pressure of Ammonia (R717) in kPa, at -40°C, the following command can be typed into any Excel cell or macro

$$= \text{Props}(\text{"}P\text{"},\text{"}T\text{"},-40+273.15,\text{"}x\text{"},1,\text{"R717"})$$

where x is the vapor quality, with a vapor quality of one being a saturated vapor. The variables, P, T, and x can be substituted for any of the properties supported by CoolProp as long as the

combination of the second two variables gives enough information for CoolProp to determine the thermodynamic state for the property being queried.

CoolProp uses multiparameter Helmholtz-energy-explicit equations to obtain the thermodynamic properties, such as enthalpy, density, and the specific heats of pure and pseudo-pure fluids such as ammonia. Correlations based on experimental data are used to obtain the transport properties of pure and pseudo-pure fluids such as viscosity and thermal conductivity (Bell, et.al., 2014). When compared with the data provided by the more widely used fluid property database RefProp, the largest deviation for any single property of Ammonia occurred for the specific heats c_p and c_v and was on the order of 10^{-4} (Bell, 2015a). RefProp, is a commercial Thermophysical property, and transport property database that was developed by the National Institute of Standards and Technology (NIST) (NIST, 2010).

Thermodynamic and transport properties, such as density, thermal conductivity, heat capacity, dynamic viscosity, enthalpy, and freezing temperature, for binary mixtures such as Calcium Chloride brine are calculated using correlations fitted to experimental data. CoolProp is capable of determining the properties for Calcium Chloride brine in concentrations ranging from 0 to 30% and temperatures ranging from -100°C to +40°C. The uncertainty in the properties predicted by CoolProp for Calcium chloride brine over the range of -40°C to +40°C are at most ±0.04% (Bell, 2015b).

4.2 Evaporator Model

The evaporator was modeled using two different approaches. The first model, developed by Vera-García et al. (2010), is a simplified evaporator model that requires a minimal number of evaporator specifications. The model only requires the evaporator's catalogued working conditions or CWC, and information about the operating point at which the evaporator is being modeled to predict its performance. The CWC, which are typically provided in a manufacturer's catalogue or on the specification sheet that accompanies an evaporator when it is purchased are

- the rated evaporator capacity $\dot{Q}_{\text{evap}}^{\text{cwc}}$ (kW or TR),
- the brine flow rate $\dot{V}_{\text{brine}}^{\text{cwc}}$ (m^3/hr),
- the evaporation temperature $T_{\text{evap}}^{\text{cwc}}$ (°C), and

- the brine inlet temperature to the evaporator $T_{\text{brine,in}}^{\text{cwc}}$(°C).

The required operating conditions at the operating point to be modeled include

- the brine flow rate $\dot{V}'_{\text{brine}}$,
- the evaporation temperature T'_{evap}, and
- the brine inlet temperature to the evaporator $T'_{\text{brine,in}}$.

The approach used by the simplified evaporator model is based on a combination of both the LMTD and effectiveness-NTU approaches. Using the LMTD approach, the model first calculates the combined overall heat transfer coefficient and surface area (UA) for the evaporator at the CWC as follows:

$$UA^{\text{CWC}} = \frac{\dot{Q}_{\text{evap}}^{\text{cwc}}}{LMTD^{\text{CWC}}} \tag{4.1}$$

where:

$$LMTD^{\text{CWC}} = \frac{\left(\left(T_{\text{brine,out}}^{\text{CWC}} - T_{\text{evap}}^{\text{CWC}}\right) - \left(T_{\text{brine,out}}^{\text{CWC}} - T_{\text{evap}}^{\text{CWC}}\right)\right)}{\log\left(\left(T_{\text{brine,out}}^{\text{CWC}} - T_{\text{evap}}^{\text{CWC}}\right)/\left(T_{\text{brine,out}}^{\text{CWC}} - T_{\text{evap}}^{\text{CWC}}\right)\right)}. \tag{4.2}$$

The outlet brine temperature $T_{\text{brine-out}}^{\text{CWC}}$ at the CWC can be calculated as:

$$T_{\text{brine-out}}^{\text{CWC}} = T_{\text{brine,in}}^{\text{CWC}} - \frac{\dot{Q}_{\text{evap}}^{\text{cwc}}}{\dot{m}_{\text{brine}} Cp_{\text{brine}}}. \tag{4.3}$$

The fluid properties such as density and the specific heat are evaluated at the evaporator brine inlet temperature.

To simplify the calculation of the overall heat transfer coefficient for the new operating conditions Vera-García et al. (2010) made the simplifying assumption that the UA on the brine side of the evaporator tubes is equal to the UA on the ammonia side of the tubes:

$$\frac{1}{(UA)_{\text{brine}}} = \frac{1}{(UA)_{\text{ref}}} \tag{4.4}$$

Using the simplifying assumption, the Dittus-Boelter correlation for the brine side heat transfer coefficient, and the heat transfer coefficient for stable film boiling on the refrigerant side Vera-García et al. (2010) were able to show that the combined UA at the new operating point (UA') can be calculated as

$$UA' = UA^{\text{CWC}} \frac{2\beta_{\text{brine}}\beta_{\text{ref}}}{\beta_{\text{brine}+}\beta_{\text{ref}}} \tag{4.5}$$

where

$$\beta_{\text{brine}} = \left(\frac{c'_{\text{p,brine}}\,\mu'}{c^{\text{cwc}}_{p,\text{brine}}\,\mu^{\text{cwc}}}\right)^{0.4} \left(\frac{k'_{\text{brine}}}{k^{\text{cwc}}_{\text{brine}}}\right)^{0.6} \left(\frac{\dot{m}'_{\text{brine}}}{\dot{m}^{\text{cwc}}_{\text{brine}}}\right)^{0.8}, \text{ and} \tag{4.6}$$

$$\beta_{\text{ref}} = \left(\frac{k'_{\text{g,ref}}\,h'_{\text{fg}}\,\rho'_{\text{g}}(\rho'_{\text{L}} - \rho'_{\text{g}})^{1/4}}{k^{\text{cwc}}_{\text{g,ref}}\,h^{\text{cwc}}_{\text{fg}}\,\rho^{\text{cwc}}_{\text{g}}(\rho^{\text{cwc}}_{\text{L}} - \rho^{\text{cwc}}_{\text{g}})^{1/4}}\right)^{4/3} \left(\frac{\dot{Q}'_{\text{evap}}}{\dot{Q}^{\text{cwc}}_{\text{evap}}}\right)^{1/3} \tag{4.7}$$

where $k_{\text{g,ref}}$ is the thermal conductivity of the saturated ammonia vapor at the evaporation temperature, h_{fg} is the latent heat of vaporization at the evaporation temperature, ρ_{g} is the density of the saturated ammonia vapor at the evaporation temperature, and ρ_{L} is the density of the saturated liquid ammonia at the evaporation temperature. Variables with the $'$ superscript are based on the modeled operating point and ($^{\text{cwc}}$)variables are based on the catalogued working conditions. Once UA' has been calculated the effectiveness-NTU method is used to calculate the performance of the evaporator at the new operating point as follows:

$$\dot{Q}'_{\text{evap}} = \varepsilon \dot{Q}_{\text{max}} \tag{4.8}$$

where

$$\varepsilon = 1 - \exp(-NTU), \tag{4.9}$$

$$\dot{Q}_{\text{max}} = C'_{\text{p,brine}} \dot{m}'_{\text{brine}} (T'_{\text{brine,in}} - T'_{\text{evap}}), \text{ and} \tag{4.10}$$

$$NTU = \frac{UA'}{m' c'_p}. \tag{4.11}$$

Equation 4.7 illustrates that, in boiling heat transfer, the heat transfer coefficient is a function of the rate of heat transfer itself. Thus, in order to calculate UA', iteration is required. Figure 4-1 illustrates how the evaporator model is implemented including the iterative calculation procedure.

A second evaporator model was also included in the program that allows the user to use a constant *UA* value for the evaporator. This option allows evaporators other than shell-and-tube evaporators to be used with the system model as long as sufficient information is available to determine the *UA* for the evaporator. This model only requires Equations 4.8, 4.9, and 4.11 which makes it substantially easier to implement than the first model.

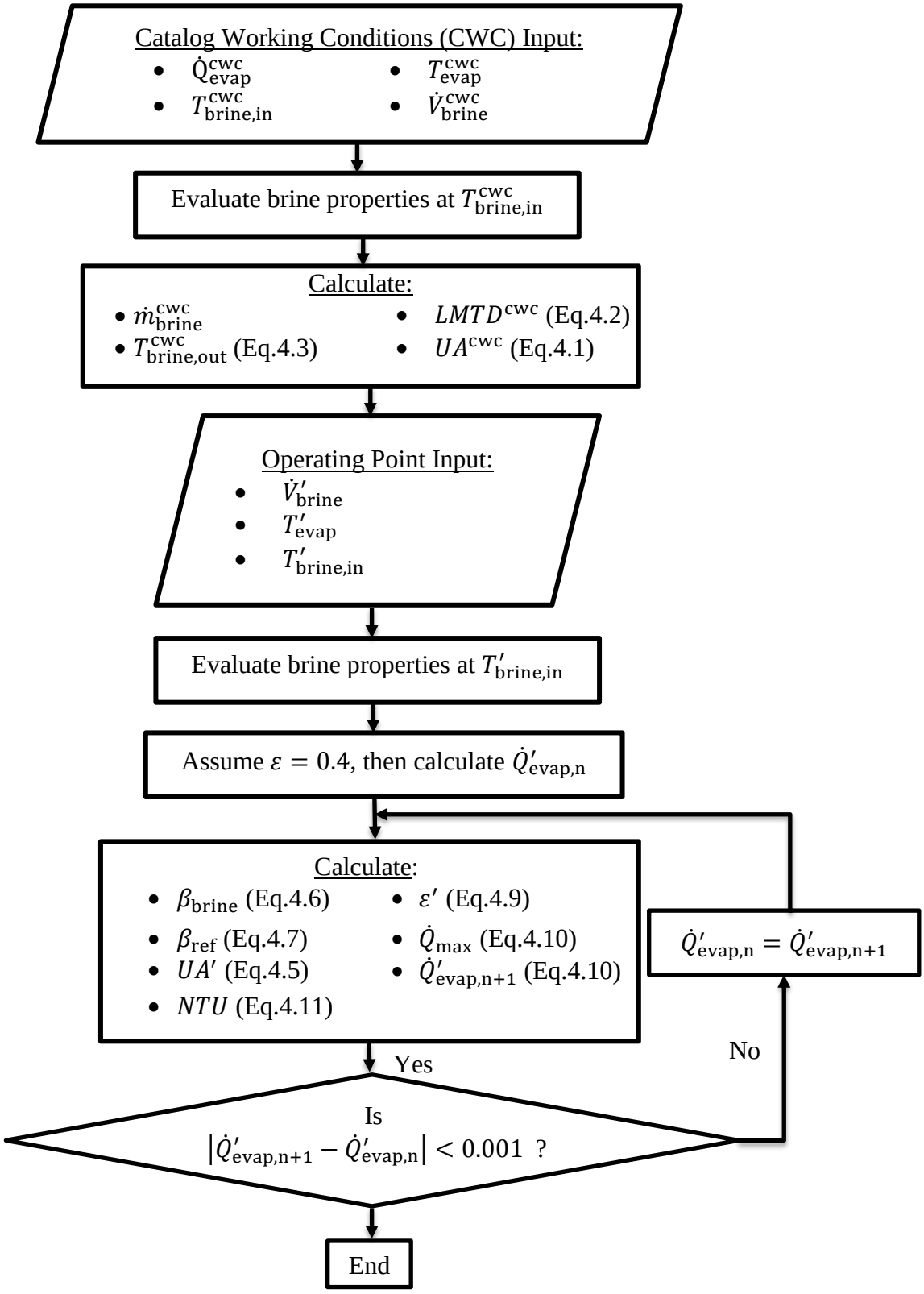

Figure 4-1 Evaporator Model Flow Chart

4.3 Condenser Model

The condenser model is used to calculate the saturated condensing temperature of for each refrigeration module using the ambient air temperature as an input. The condenser model uses a similar approach to Scott (2014) where a constant approach or constant temperature difference between the ambient and condensing temperature is used to calculate the condensing temperature. This simple model does not require any information about the condenser geometry or performance which makes it very convenient if little information is available about the condenser geometry. The model simulates the condenser control system, which shuts condenser fans off progressively to control the minimum condensing temperature. The Cigar Lake operating data indicates the minimum condensing temperature is 29°C on average. Therefore, the model uses 29°C as the lower bound on condensing temperature. Figure 4-2 illustrates how the model works, by comparing the ambient temperature to the modeled condensing pressure.

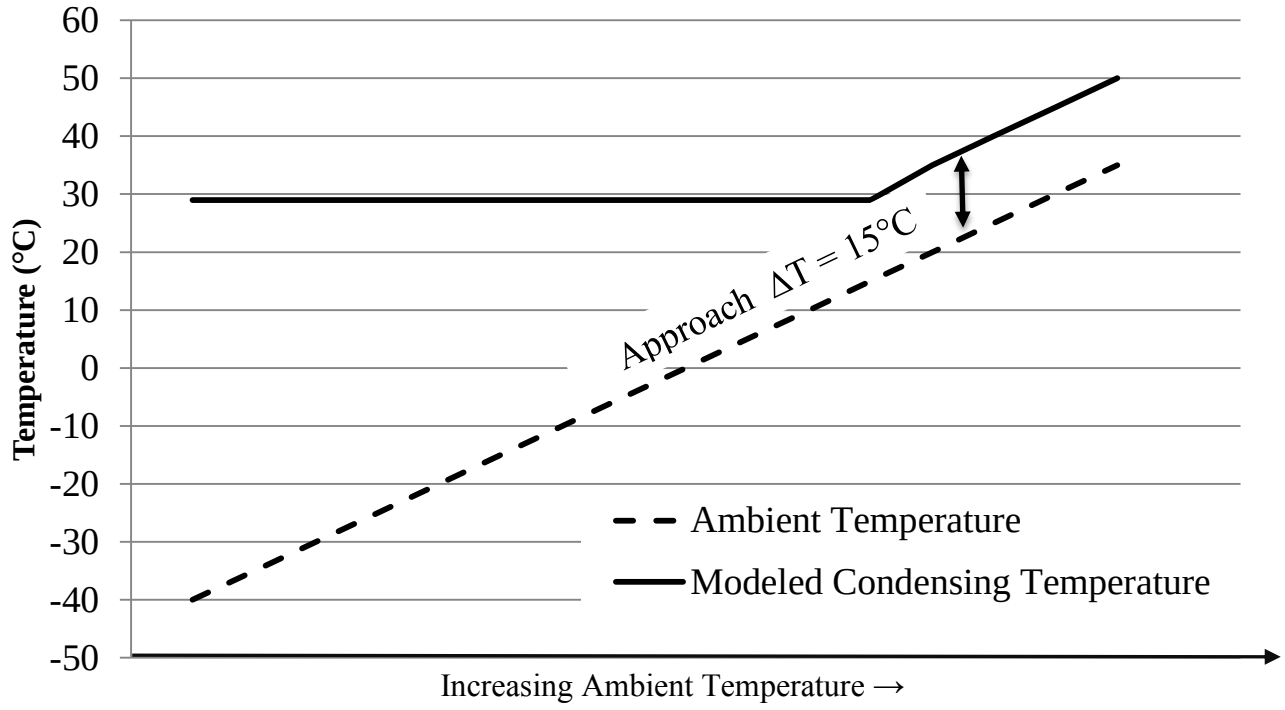

Figure 4-2 Modeled Condensing Temperature and Ambient Temperature Comparison

4.4 Compressor Package Model

The two-stage, twin-screw, oil-injected, compressors used in the modular freeze plants are modeled using a first principle thermodynamic model. The primary purpose of the compressor model is to calculate the work of compression and the refrigeration capacity of the compressor package, which includes the compressor, subcooler, and oil injection system. The compressor package capacity is defined as the theoretical refrigeration capacity of the system operating between a given condensing temperature T_{cond} and a given evaporation temperature T_{evap}. The compressor package model also emulates the actions of the compressor control system (CP4), which were described in Section 3.5. The CP4 controls the compressor's slide valves to limit the capacity of the compressor. The compressor package model presented differs from the existing models presented in the current literature because it models the CP4, the oil injection process, and the subcooler. The injection of oil during the compression process is assumed to transfer heat to the surroundings. Furthermore it is assumed oil injection does not have any effect on the power consumed by the compressors. The oil seals, lubricates, and cools the compressor carrying away the majority of the heat of compression and ensuring the high-pressure-stage discharge temperature never exceeds 90°C (Bloch, 2006, p.150). Therefore, the compressor model assumes that the rate of oil injection is controlled by either the refrigerant plant operator in order to maintain constant high-stage and low-stage discharge temperatures. Cigar Lake operating data shows that the high-stage discharge temperature, $T_{\text{dis,high}}$, is very nearly constant at 90°C, and the low-stage discharge temperature, $T_{\text{dis,low}}$, is very nearly constant at 60°C regardless of the evaporation and condensing temperatures. To calculate the work of compression the compressor's isentropic efficiency is used, which is assumed to be constant at

$$\eta_{i,high} = 0.75, \text{ and}$$

$$\eta_{i,low} = 0.75.$$

The isentropic efficiencies are based on an analysis of a very limited amount of catalog data provided by the Mycom compressor software. The power consumption of the compressor is inversely proportional to the isentropic efficiency. Therefore, inaccuracy in the isentropic efficiency assumptions will directly affect the compressor power consumption predictions. In addition the isentropic efficiency affects capacity predictions when the compressor capacity is

limited by power consumption. Using the isentropic efficiencies, the work of compression for either stage was calculated as

$$\dot{W}_{\text{comp}} = \dot{m}_{\text{ref}} \frac{\Delta h_{\text{i}}}{\eta_{\text{i}}} \tag{4.12}$$

Where Δh_{i} is the change in enthalpy across a compressor for an isentropic compression. During an isentropic compression the change in entropy (ies) (s) is zero, therefore $s_{\text{S}} = s_{\text{D}}$. Δh_{i} can be calculated using the relationship ($s_{\text{S}} = s_{\text{D}}$), and the thermophysical properties of the refrigerant at the suction and discharge pressure of each compression stage.

The refrigeration capacity of the compressor is equal to

$$\dot{Q}_{\text{comp}} = \dot{m}_{\text{ref}}(h_1 - h_9) \tag{4.13}$$

where h_1 is the enthalpy of the refrigerant vapor leaving the evaporator, and h_9 is the enthalpy of the liquid refrigerant entering the evaporator (Figure 4-3). It is assumed that no superheating occurs in the evaporator, and the surge drum is correctly sized to remove all liquid in the vapor stream leaving the evaporator. Therefore, the vapor leaving the evaporator is saturated. To calculate the refrigeration capacity the compressor model must fix the remaining states in the system (states 2 through 9 inclusive). Two independent refrigerant properties are required to fix each of the states. In all cases the first property is the pressure of the refrigerant which will either be the evaporation, intermediate, or condensing pressure. The compressor model does not determine the evaporation or condensing pressures, instead they are determined by the system model using the saturated condensing and evaporation temperatures then passed to the compressor model as inputs. The compressor model determines the intermediate pressure which is either fixed by the user or set to the optimum intermediate pressure. This can be calculated from the optimum intermediate saturation temperature (Gosney, 1982).

$$T_{\text{int,optimum}} = T_{\text{int,GM}} + 5°C \tag{4.14}$$

where $T_{\text{int,GM}}$ is the saturation temperature corresponding to the geometric mean intermediate pressure

$$P_{\text{int,GM}} = \sqrt{P_{\text{evap}} \cdot P_{\text{cond}}}. \tag{4.15}$$

State one is fixed using the evaporation pressure, and the assumption that there is no superheat in the evaporator. Any superheating of the vapor before it enters the compressor is assumed to occur in the suction lines between the evaporator and the compressor. State two is fixed by the

intermediate pressure and the assumption that the low-stage discharge temperature is constant at 60°C. State three is fixed by assuming the vapor leaving the subcooler is mixed adiabatically with the vapor leaving the low-stage compressor. Therefore, the enthalpy at state three can be calculated as

$$h_3 = \frac{\dot{m}_{\text{int}} h_7 + \dot{m}_{\text{low}} h_2}{\dot{m}_{\text{high}}} \tag{4.16}$$

where

$$\dot{m}_{\text{int}} = \dot{m}_{\text{high}} - \dot{m}_{\text{low}} \,. \tag{4.17}$$

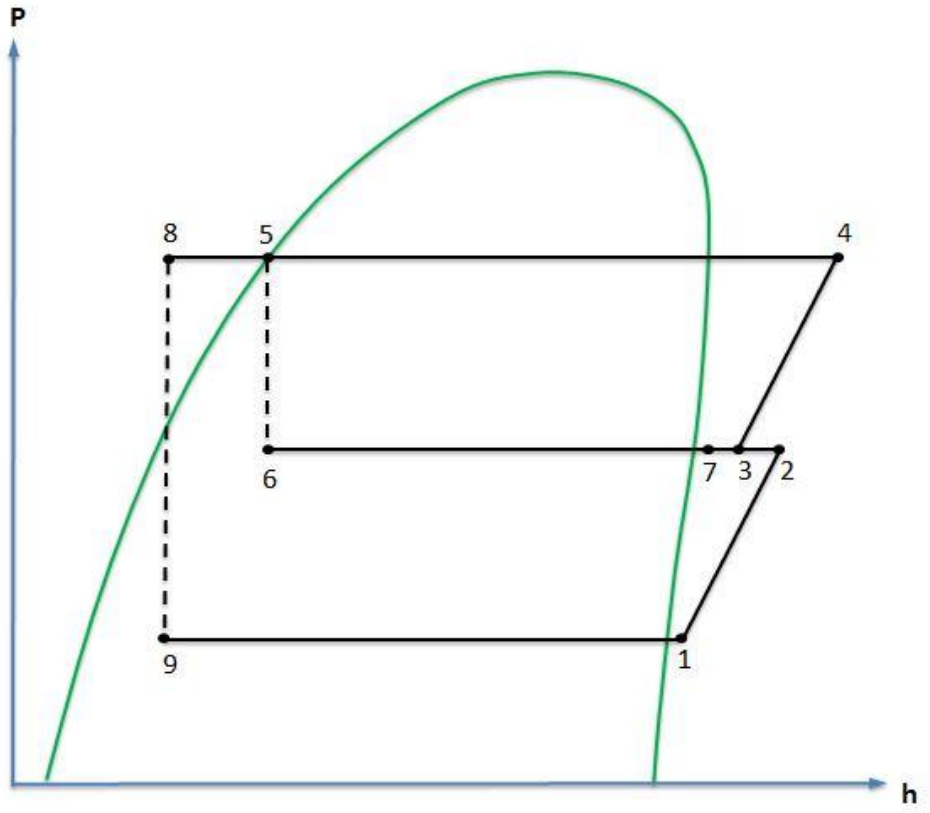

Figure 4-3 Pressure Enthalpy Diagram for DX Subcooled Refrigeration System

State four is fixed by the condensing pressure and the assumption that the high-stage discharge temperature is constant at 90°C. It is assumed that the liquid refrigerant leaving the condenser is not subcooled because the condensers are designed such that all of the liquid drains into large receivers and should never back up into the condensers. Therefore, at state five the liquid leaving the condenser is saturated. The expansion from state five to six is assumed to be a throttling process or an irreversible adiabatic expansion. When a fluid undergoes a throttling process

changes in velocity, and gravitational potential are assumed to be negligible and heat transfer to the surroundings is ignored. Therefore, it is assumed that the enthalpy of the refrigerant at state six is equal to the enthalpy of the refrigerant at state five (Moran et al. 2011, p.195).

$$h_6 = h_5 \tag{4.18}$$

The superheat of the vapor leaving the DX subcooler at point seven is controlled by a thermal expansion valve (TXV) with its bulb situated at the exit of the subcooler (Figure 4-4). The TXV throttles the flow of liquid refrigerant into the tube side of the subcooler to maintain a constant amount of superheat at the location of the TXV bulb, which is typically 5°C (Gosney, 1982). Therefore, state seven is fixed by the intermediate pressure and a constant 5°C superheat.

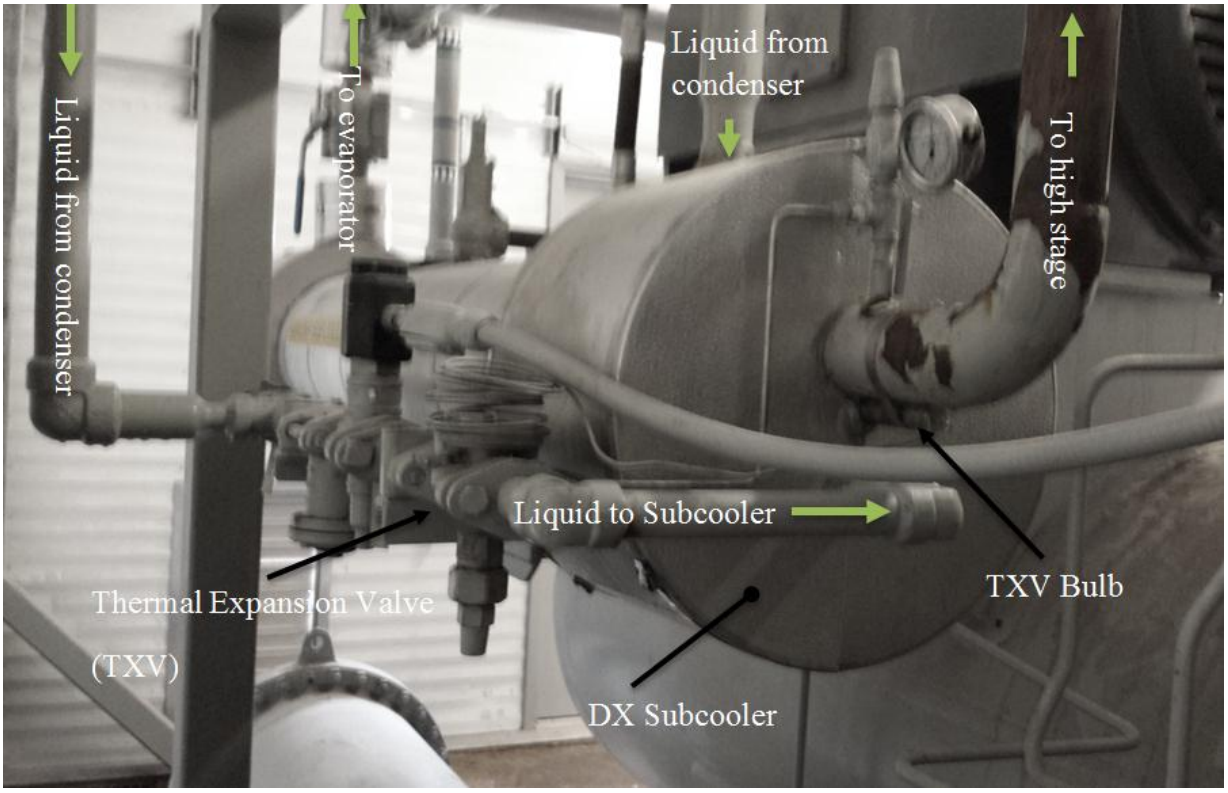

Figure 4-4 Modular Plant Subcooler and Thermal Expansion Valve (TXV)

During process five to eight the liquid refrigerant leaving the condenser is subcooled on the shell side of the DX subcooler. Limited information is available on the capacity of the subcooler. Therefore, it is modelled in a similar fashion to the condenser where it is assumed that the liquid approach temperature or ΔT for the subcooler is constant at 5°C. Therefore, the liquid temperature at state eight can be calculated as (Gosney, 1982, p.111)

$$T_8 = T_6 + 5°\text{C} \tag{4.19}$$

Process eight to nine is another reversible adiabatic expansion. Therefore, in an identical fashion to process five to six the enthalpy at point nine is equal to

$$h_9 = h_8. \tag{4.19}$$

To calculate the refrigeration capacity and power consumption the mass flow rates in the system must be calculated. If the slide valves are in their fully-loaded positions, the maximum theoretical refrigerant mass flow rates in both the high and low-stages can be calculated as

$$\dot{m}_{\text{ref}} = \frac{\dot{V}_{\text{swept}}\,\eta_{\text{V}}}{v_{\text{ref}}}. \tag{4.20}$$

The specific volume of the refrigerant is evaluated at the inlet to either compression stage. For the high-pressure stage, in order to determine the temperature of the refrigerant at the compressor inlet Equation 4.16 must be used. Therefore, an iterative process is required to calculate the high-pressure stage suction temperature and the high-pressure stage mass flow rate. The swept volume rates for the compressor are (Mayekawa MFG. CO., LTD., 2014):

$$\dot{V}_{\text{swept,low}} = 5700\ m^3/hr, \text{and}$$

$$\dot{V}_{\text{swept,high}} = 1900\ m^3/hr.$$

Using limited data available from the Mycom Compressor Capacity calculation software (Mayekawa MFG. CO., LTD., 2014) the volumetric efficiencies for the high and low-stages were calculated to be

$$\eta_{\text{V,low}} = 0.894, \text{and}$$

$$\eta_{\text{V,high}} = 0.874.$$

The refrigerant mass flow rates are directly proportional to the compressor's volumetric efficiency if the slide valves are fully closed. Therefore, the accuracy of the assumed volumetric efficiencies is important. A full compressor run sheet, which was used to obtain the swept volume and compressor efficiency data is available in Appendix A.

Under all operating conditions the mass flow rates in both the high and low-stages are dependent on the positions of the compressor slide valves which are determined by the CP4. The high-stage slide valve is used to maintain the intermediate pressure at a set point determined by the operator.

To calculate the high-pressure stage mass flow rate a control volume can be drawn around the subcooler. A steady state energy balance performed on the control volume (Figure 4-5) allows the high-stage mass flow rate to be calculated as (Gosney, 1982)

$$\dot{m}_{\text{high}} = \dot{m}_{\text{low}} \frac{(h_2 - h_6)}{(h_3 - h_5)}. \tag{4.21}$$

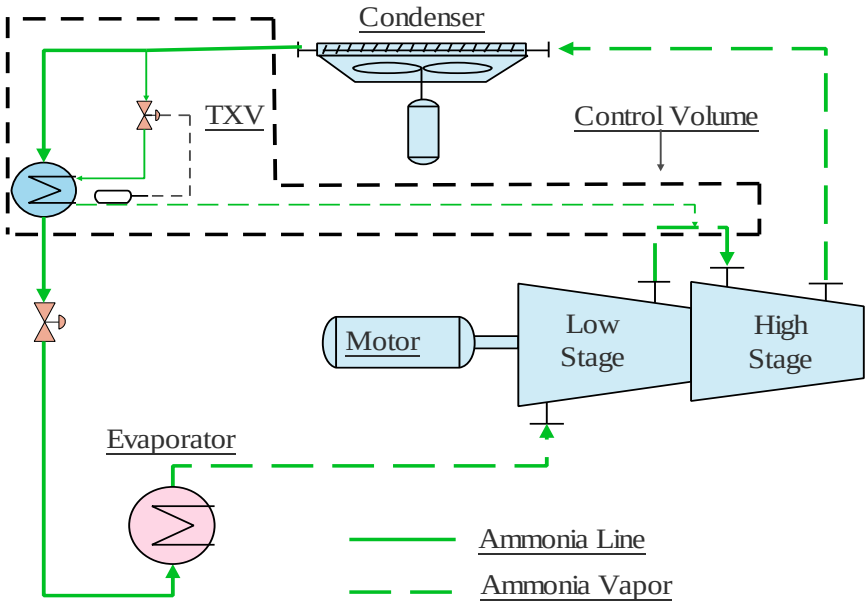

Figure 4-5 Control Volume for Subcooler energy Balance (Gosney, 1982)

The compressor model simulates the control action of the CP4 by ensuring that the total compressor power consumption does not exceed the power of the electric motors and by limiting the minimum suction pressure. For the Cigar Lake modular plants the compressor power draw cannot exceed 746 kW (1000 hp) and the minimum suction pressure is typically limited to71.7 kPa (10.4 psi) which corresponds to an ammonia saturation temperature of -40°C. Each iteration of the model checks to see if the total absorbed compressor power is less than or equal to 746 kW (1000 hp). If the total absorbed power is greater than 746 kW the model reduces the mass flow rate and recalculates the absorbed power and compressor capacity. When the system model determines that the compressor capacity needs to be reduced to keep the suction pressure within the operating envelope, it calculates the evaporator capacity at the minimum suction temperature and forces the compressor model to limit the compressor capacity to match. The compressor model matches the evaporator capacity by an appropriate low side mass flow rate. Figure 4-6 illustrates the calculation procedure for the compressor model.

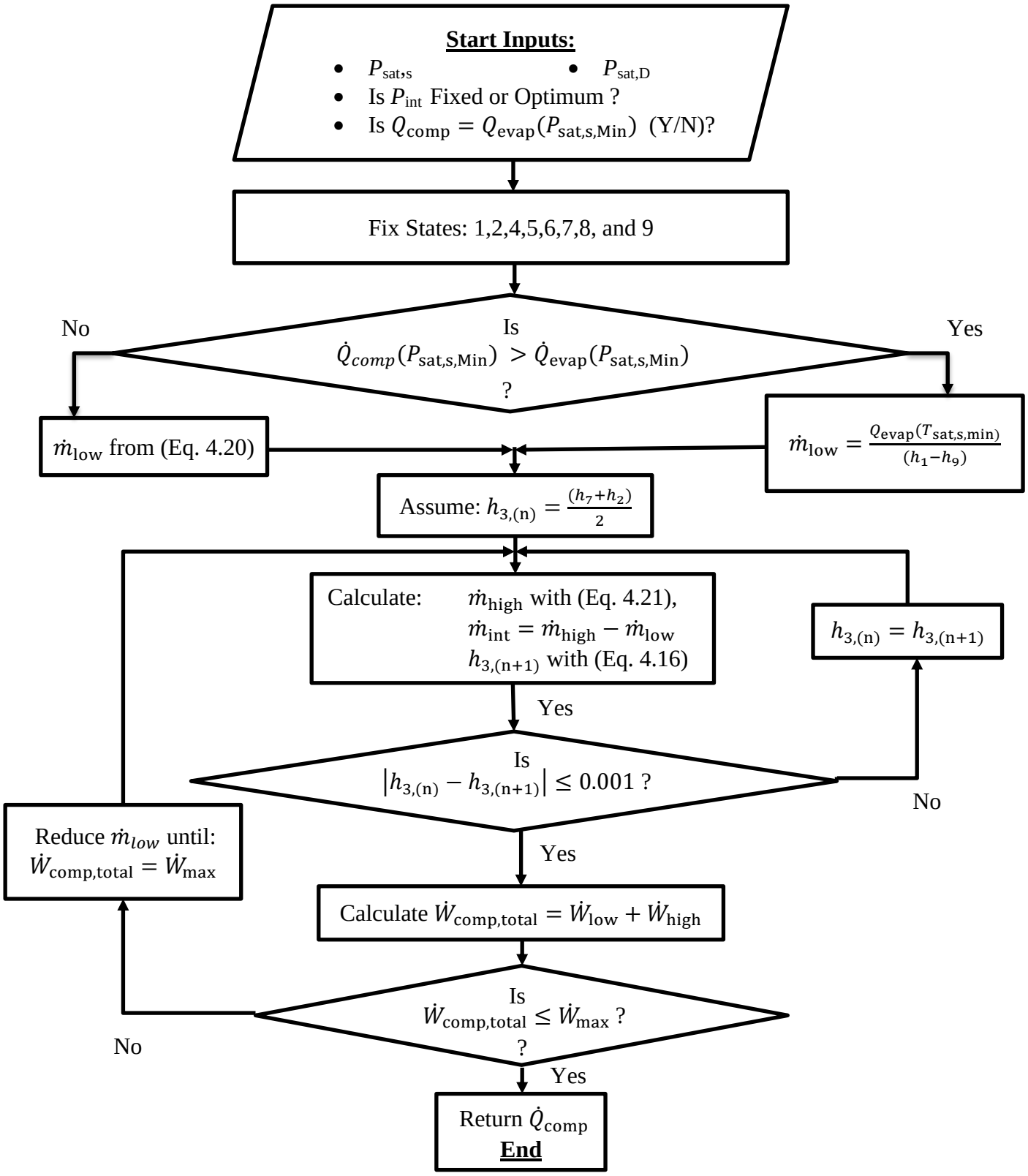

Figure 4-6 Compressor Model Algorithm Flow Chart

4.5 Refrigeration System Model

The refrigeration system model couples the individual compressor, evaporator, and condenser models together to predict the overall system refrigeration capacity. The models are coupled together using the condensing and evaporation temperatures. The evaporation and condensing temperatures can easily be used to calculate the evaporation and condensing pressures because the refrigerant is undergoing a phase change in both the evaporator and condenser. The condensing temperature is calculated by the condenser model without any iteration, and passed to the compressor model. In order to determine the evaporation temperature, an iterative procedure is required. The iterative calculation determines the evaporation temperature where the compressor capacity is equal to the evaporator capacity. With increasing evaporation temperature the compressor capacity will increase while the evaporator capacity decreases. Therefore, the evaporation temperature that the system will operate at is given by the intersection of the evaporator and compressor capacity curves shown in Figure 4-7.

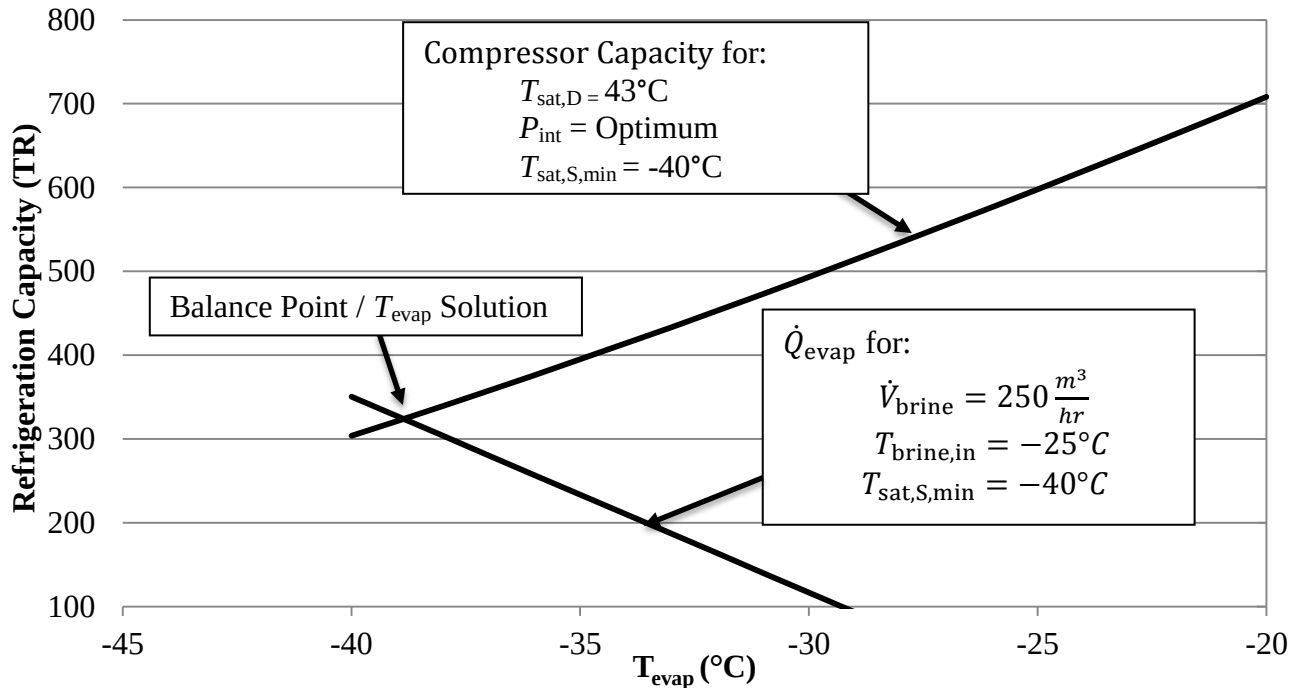

Figure 4-7 Example of Evaporator and Compressor Capacity versus Evaporation Temperature

The solution is determined using the false position (FP) technique, which confines the solution to a domain which shrinks with each iteration. The solution has to fall between the minimum evaporation temperature and the evaporator inlet brine temperature. Therefore, the initial solution domain is

$$T_{\text{evap,min}} \leq T_{\text{evap}} \leq T_{\text{brine,evap,in.}} \tag{4.22}$$

Before trying to find a solution, the model checks to make sure that the solution will not fall below the minimum evaporation temperature using the inequality

$$\dot{Q}_{\text{evap}}\left(T_{\text{evap,min}}\right) \leq \dot{Q}_{\text{comp}}\left(T_{\text{evap,min}}\right). \tag{4.23}$$

If the inequality holds true, the evaporation temperature is set to the minimum evaporation temperature, and the compressor model is forced to reduce the compressor capacity to meet the evaporator capacity at the minimum evaporation temperature.

False position progressively makes the solution domain smaller until the solution is found within a predetermined tolerance. The method of false position is slower than other iterative solution methods. However, it guarantees convergence as long as a solution exists within the initial solution domain (Stroud & Booth, 2003, p.807). Other solution methods, such as the secant method, will diverge if the initial guess at the solution is not sufficiently close to the final solution. Figure 4-8 illustrates the algorithm used by the system model.

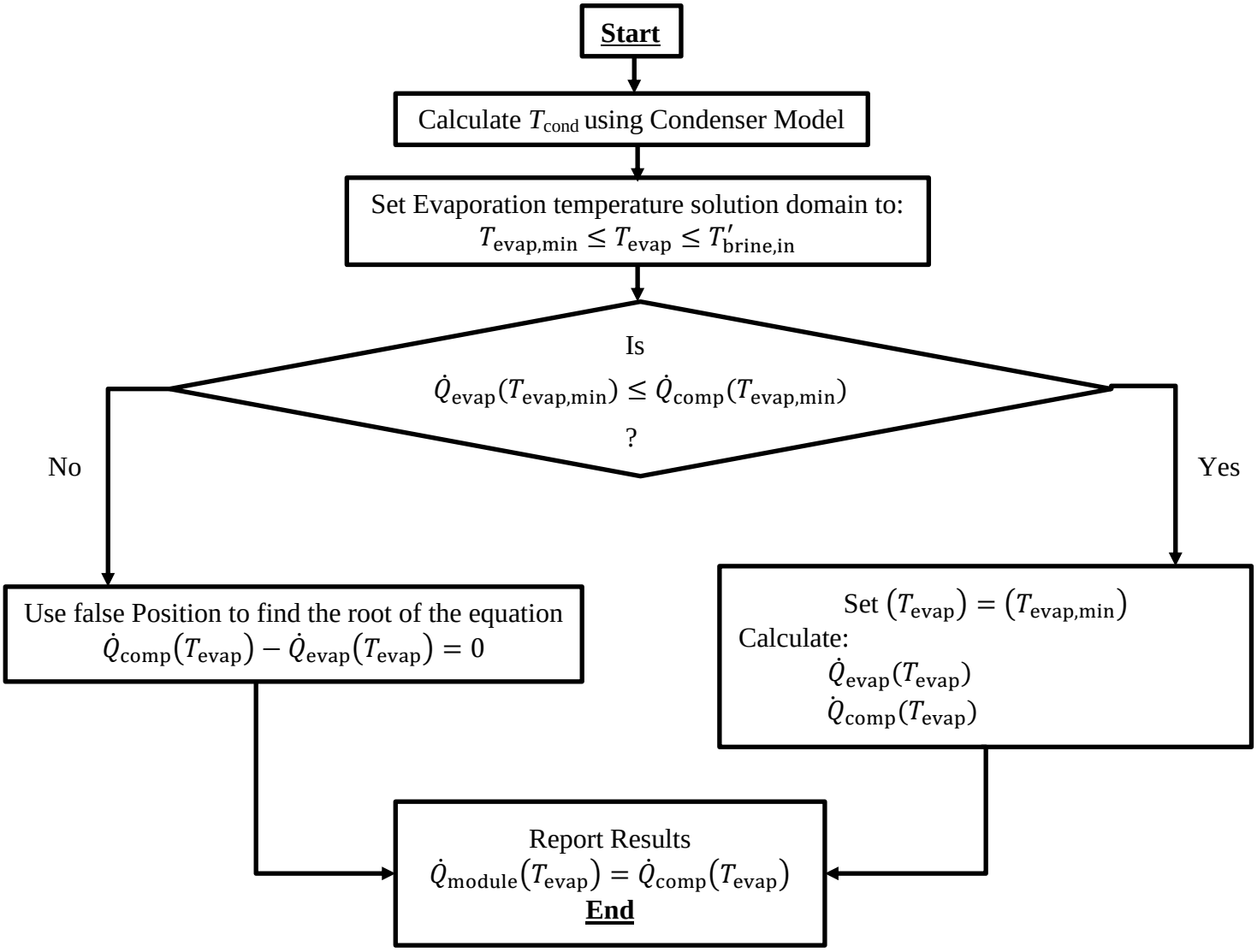

Figure 4-8 System Model Flow chart

4.6 Refrigeration Plant Model

The system model described in Chapter Four calculates the performance of the five individual refrigeration modules. The plant model determines how the entire system, including the brine pumps and five refrigeration modules perform together. Specifically, it calculates the temperature of the brine supplied to the freeze panels based on the brine temperature returning to the plant from the freeze panels. The plant model assumes heat gain from the surroundings to the brine pipes is negligible, because all of the brine lines are well insulated. Therefore, the plant model only includes the brine tank, the brine distribution pumps, and the module heat exchanger pumps.

The brine tank is modeled using mass and energy balances performed on two control volumes drawn around both sides of the brine tank (Figure 4-9).

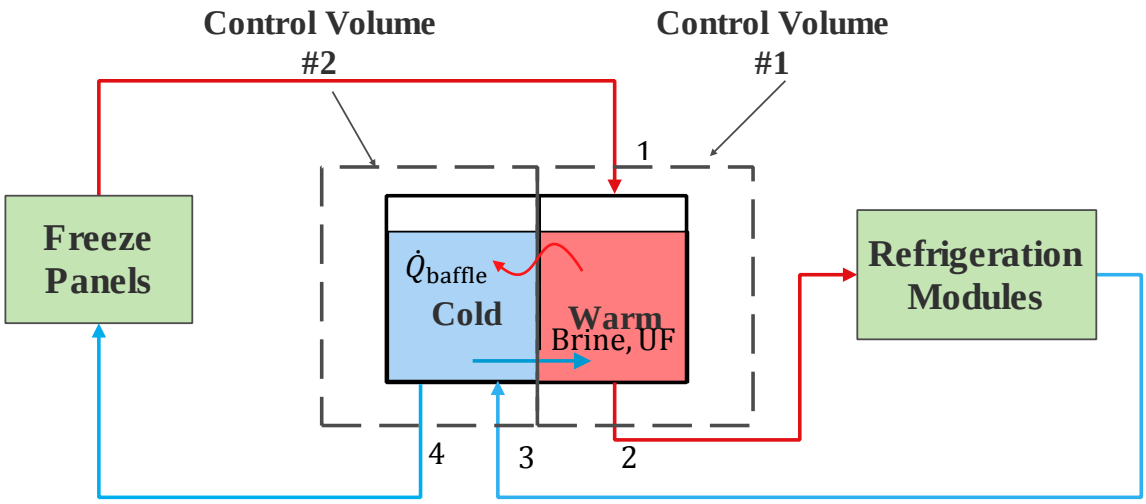

Figure 4-9 Brine Tank Model Control Volumes

Warm brine from the freeze panels returns to the warm side of the brine tank (1), where it mixes with cold brine that flows to the warm side of the tank through the hole in the baffle (brine, UF). The warm brine flows to a header that distributes it to each of the five refrigeration modules (2). After the brine is cooled by the refrigeration modules it returns to the cold side of the tank (3) before being pumped back to the freeze panels (4). The baffle in the brine tank is constructed of 6.4 mm (1/4 inch) steel plate therefore, it has very low thermal resistance and the heat transfer between the hot and cold brine ($\dot{Q}_{\text{baffle}}$) in the tank cannot be ignored. Again because the transient response time of the ground is several times greater than the refrigeration plant`s transient response time only steady state conditions will be considered. Performing steady state mass and energy balances on each control volume and assuming each side of the tank is well mixed gives

$$h_2 = \frac{(\dot{m}_{\text{F}} h_1 + \dot{m}_{\text{UF}} h_4 + \dot{Q}_{\text{baffle}})}{\dot{m}_M} \tag{4.24}$$

and,

$$h_4 = \frac{(\dot{m}_M h_3 - \dot{Q}_{\text{baffle}})}{\dot{m}_M} \tag{4.25}$$

where $\dot{m}_{\mathrm{M}}$ is the brine mass flow rate on the refrigeration module side of the tank, $\dot{m}_{\mathrm{F}}$ is the brine mass flow rate on the freeze panel side of the refrigeration tank, and

$$\dot{m}_{\mathrm{UF}} = \dot{m}_M - \dot{m}_F. \tag{4.26}$$

The heat transfer across the tank baffle, $\dot{Q}_{\mathrm{baffle}}$, can be calculated as

$$\dot{Q}_{\mathrm{baffle}} = UA_{\mathrm{baffle}} L(T_W - T_C) \tag{4.27}$$

where *UA* is the overall heat transfer coefficient times area for the tank baffle, *L* is the brine level in the tank as a percentage, T_{w} is the brine temperature on the warm side of the tank, and T_{C} is the brine temperature on the cold side of the tank.

The temperature of the brine returning to the tank from the refrigeration modules (T_3) is calculated using Equation 4.28 and the refrigeration module capacity, which is calculated using the refrigeration system model.

$$T_3 = T_{2\mathrm{P}} + \frac{\dot{Q}_M}{\frac{\dot{m}_M}{N_M} Cp_{\mathrm{brine}}} \tag{4.28}$$

where $T_{2\mathrm{P}}$ is the temperature of the brine entering the module heat exchangers after it has passed through the module circulation pumps, and N_{M} is the number of refrigeration modules working to cool the brine.

In a similar fashion the overall capacity of the refrigeration system can be calculated as:

$$\dot{Q}_{\mathrm{plant}} = \dot{m}_F Cp_{\mathrm{brine}}(T_1 - T_{4\mathrm{P}}) \tag{4.29}$$

where $T_{4\mathrm{P}}$ is the temperature of the brine supplied to the freeze panels after the three module distribution pumps (Figure 3-3). It is assumed that the pumps do not exchange heat with their surroundings. Therefore, any pump work that does not increase the head or velocity of the brine adds heat to the brine causing the brine temperature to increase. Using these assumptions the heat gain across any of the pumps in the system can be calculated as:

$$\Delta T_{\mathrm{brine}} = \frac{(1 - \eta_{\mathrm{pump}})}{\eta_{\mathrm{pump}}} \frac{(9.81\ m/s^2)\Delta H}{c_{p_{\mathrm{brine}}}} \tag{4.30}$$

where η_{pump} is the pump efficiency at the operating point, ΔH is the change in total head across the pump in meters, and $c_{P,\mathrm{brine}}$ is the specific heat of the brine evaluated based on the fluid

temperature at the pump inlet. A full derivation of Equation 4.30 is provided in Appendix B, and Figure 4-10 illustrates the calculation procedure used by the refrigeration plant model including the iterative procedure required to calculate the brine temperature leaving the tank for the modules.

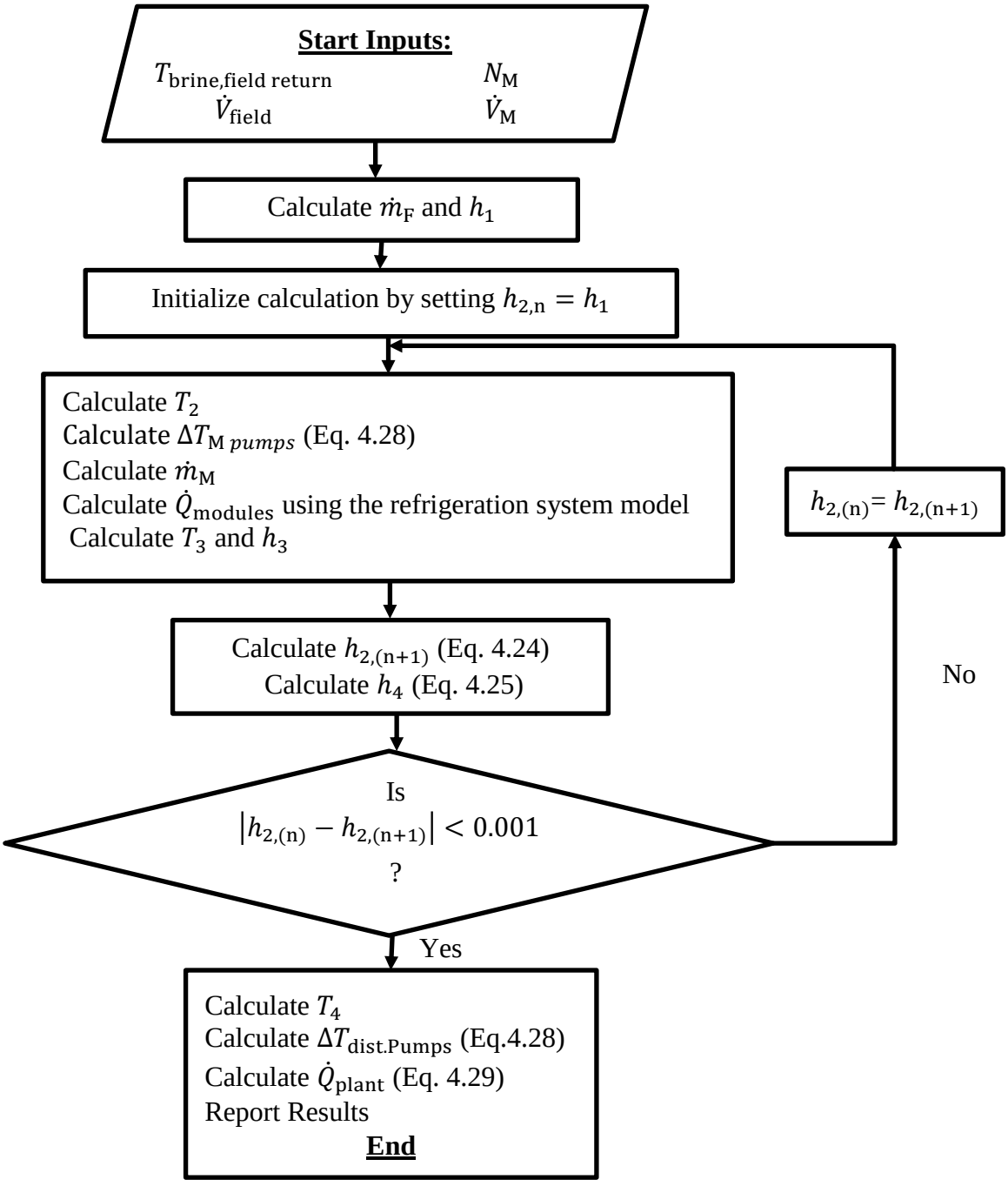

Figure 4-10 Refrigeration Plant Model Flow Chart

4.7 Model Implementation

The models developed for the Plant, Refrigeration System, compressor, evaporator, and condenser were implemented in a Microsoft Excel® spreadsheet using VBA macros. Each of the models was implemented as a separate subroutine to make the program more flexible. Figure 4-11 illustrates how the program is structured and how the five subroutines collect data.

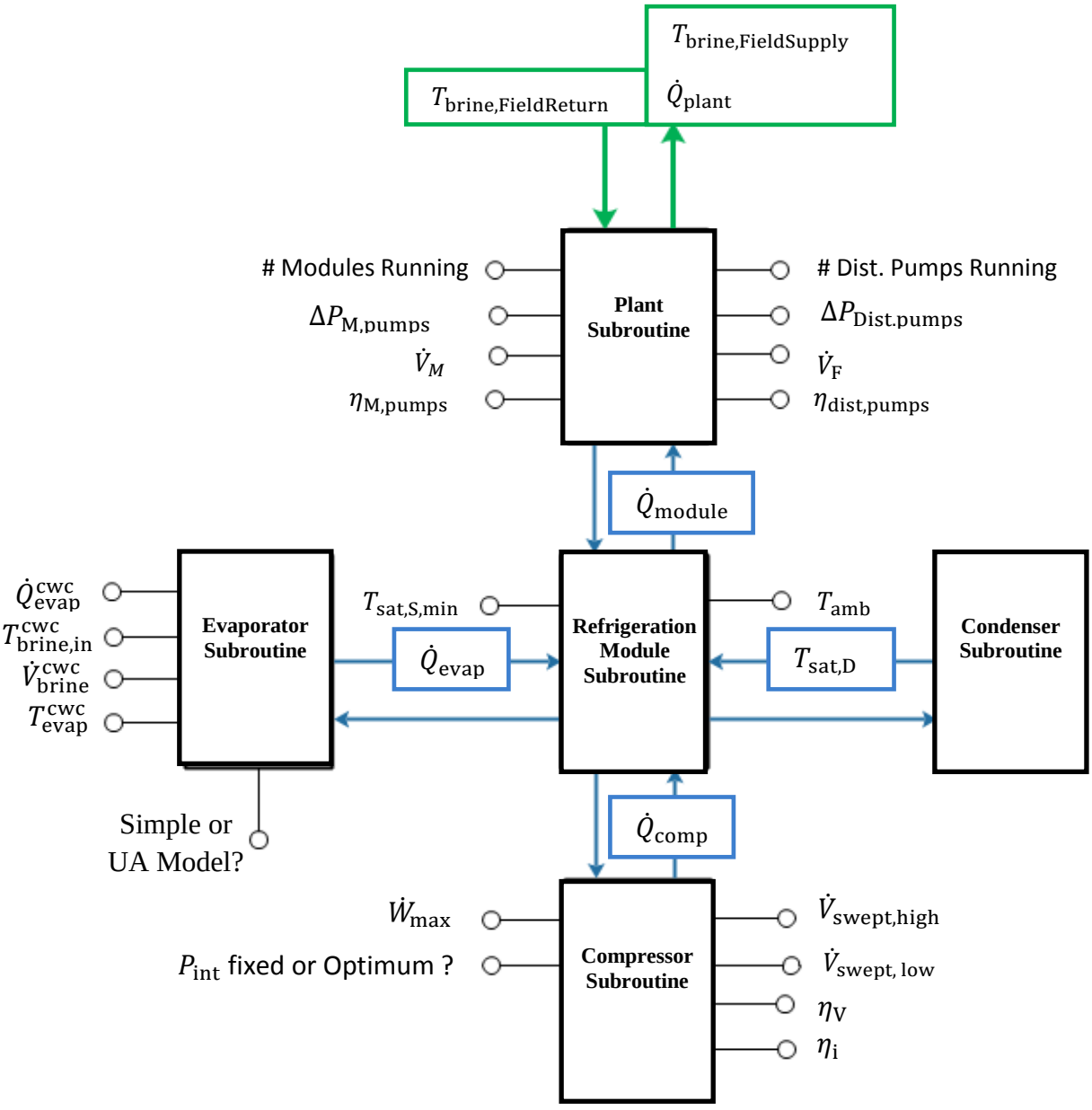

Figure 4-11 Refrigeration Plant Model Subroutine Callout Diagram

CHAPTER 5: MODEL VALIDATION

To validate the model developed in Chapter Four, two sets of data collected by Cigar Lake plant operators over a period of nine months were used. The plant performance predicted by the models is compared with the actual plant performance determined using the two data sets. Where it is available, the data collected by the operators was also used to validate individual component models.

5.1 Description of Data

The Cigar Lake plant data used to validate the model was collected by Cameco's refrigeration plant operators on a daily basis. Data collection occurred a minimum of once per twelve hour shift for the refrigeration systems and four times per twelve hour shift for the brine distribution system. The data, which is based on readings from the instrumentation detailed in Figure 3-5 and Table 3-2, was manually transferred from a display located in the Cigar Lake main control room into a Microsoft Access database (Figure 5-1) or onto run sheets (Figure 5-2). The data was manually collected because the modular refrigeration plant's instrumentation had not yet been integrated into Cigar Lake's main distributed control system (DCS), which is capable of automatically recording data. There were no specific procedures or protocols in place for when and how the data was to be collected. Therefore, some of the data was collected when the plant was operating in a transient state and some was incorrectly recorded due to human errors.

The data is divided into two sets based on how it was recorded. The data collected from January to May of 2014, Dataset 1, was collected using run sheets. Dataset 1 differs from the second set of data, Dataset 2, primarily because it includes the temperature of the brine entering and leaving each evaporator (chiller supply temperature and chiller discharge temperature in Figure 5-2). Therefore, it was suitable for validating both the evaporator model, and the model of the refrigeration modules. Dataset 2 was recorded using the process database from the beginning of May of 2014 to the end September 2014. The only brine temperature information in Dataset 2 is the field supply and field return brine temperature. Therefore, the second data set is only suitable for validating the model of the plant as a whole.

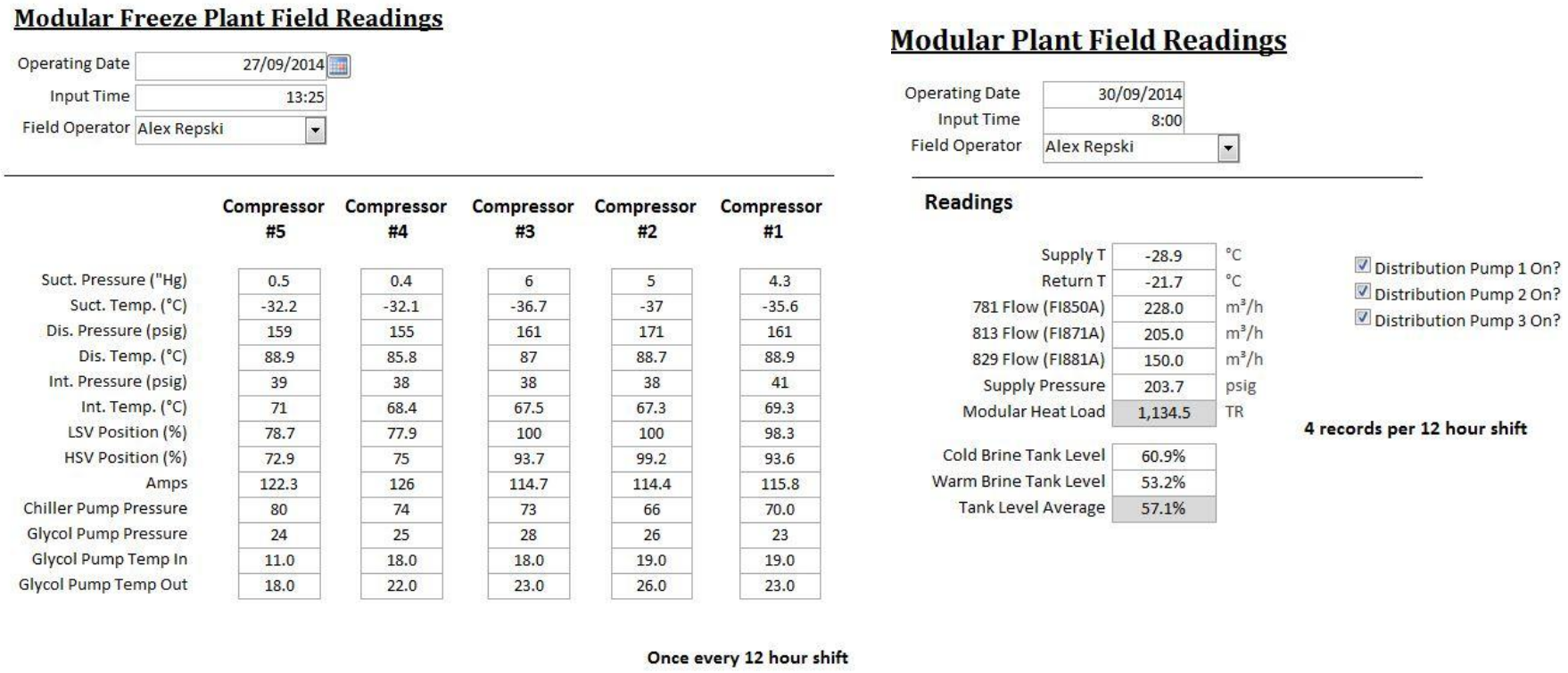

Modular Freeze Plant Field Readings

Operating Date: 27/09/2014
Input Time: 13:25
Field Operator: Alex Repski

	Compressor #5	Compressor #4	Compressor #3	Compressor #2	Compressor #1
Suct. Pressure ("Hg)	0.5	0.4	6	5	4.3
Suct. Temp. (°C)	-32.2	-32.1	-36.7	-37	-35.6
Dis. Pressure (psig)	159	155	161	171	161
Dis. Temp. (°C)	88.9	85.8	87	88.7	88.9
Int. Pressure (psig)	39	38	38	38	41
Int. Temp. (°C)	71	68.4	67.5	67.3	69.3
LSV Position (%)	78.7	77.9	100	100	98.3
HSV Position (%)	72.9	75	93.7	99.2	93.6
Amps	122.3	126	114.7	114.4	115.8
Chiller Pump Pressure	80	74	73	66	70.0
Glycol Pump Pressure	24	25	28	26	23
Glycol Pump Temp In	11.0	18.0	18.0	19.0	19.0
Glycol Pump Temp Out	18.0	22.0	23.0	26.0	23.0

Once every 12 hour shift

Modular Plant Field Readings

Operating Date: 30/09/2014
Input Time: 8:00
Field Operator: Alex Repski

Readings

Supply T	-28.9	°C
Return T	-21.7	°C
781 Flow (FI850A)	228.0	m³/h
813 Flow (FI871A)	205.0	m³/h
829 Flow (FI881A)	150.0	m³/h
Supply Pressure	203.7	psig
Modular Heat Load	1,134.5	TR
Cold Brine Tank Level	60.9%	
Warm Brine Tank Level	53.2%	
Tank Level Average	57.1%	

☑ Distribution Pump 1 On?
☑ Distribution Pump 2 On?
☑ Distribution Pump 3 On?

4 records per 12 hour shift

Figure 5-1 Cigar Lake Modular Refrigeration Plant Database Example Screenshot

Date: May 17/14 Operator: _____

		Module 1		Module 2		Module 3		Module 4		Module 5	
Time		AM	PM	AM	PM	AM	PM	AM	PM	AM	PM
Suction Temperature	°C	-37.3	-38	-38.5	-38.7	-38.5	-38.6	-37	-37.7		
Suction Pressure	"Hg	7.1	7.5	8.0	8.1	8.2	7.4	6.1	7.4		
Discharge Pressure	psig	156	157	169	168	159	158	152	151		
Discharge Temperature	°C	88.7	87.5	89.2	87.8	88.5	89.7	87.3	88.4		
Int. Pressure	psig	34	33	36	34	33	33	31	33		
Int. Temperature	°C	72	71.4	71.4	70.1	73.5	73.6	65.5	70.1		
LS Slide Valve Position	%	92	91.7	94.5	94.7	87	93.4	93	94.1		
HS Slide Valve Position	%	77	74.9	84	81.8	64	72.5	76	74.2		
Motor Current	Amps	94	92.3	94	93	90	93	94	96.9		
Auto Purger	On/Off	off	off	off	off	off	off	off	off		
Oil Pressure	psig	46	46	43	46	46	45	45	46		
Oil Temperature	°C	54	53.1	54.6	53	52.3	52.3	52.4	53.6		
Oil Filter Differential	psig	4	3	5	6	1	1	4	4		
Glycol Pump Pressure	psig	24	23	26	26	26	26	25	25		
Glycol Pump Temp In	°C	16	16	18	19	17	17	19	21		
Glycol Pump Temp Out	°C	22	22	26	26	20	23	23	25		
Level		●	●	●	●	●	●	●	●	○	○
Chiller Ammonia Level	Top	⊖	⊖	⊖	⊖	⊖	⊖	⊖	⊖	○	○
	Bottom	●	●	●	●	●	●	●	●	○	○
Chiller Pump Pressure	psig	63	64	67	66	63	74	64	66		
Chiller Supply Temp	°C	-29.3	-29.6	-29.1	-29.1	-29	-29.3	-28.7	-29.1		
Chiller Discharge Temp	°C	-32.5	-32.5	-32.2	-32.4	-32.3	-32.9	-33	-32.9		
Building Temperature	°C	24.5	27.3	25.8	26.4	26.5	25.7	30.2	29.1		
Run Hours (NS Only)	h		8453		7192		8470		8264		

Brine Distribution						
Time		7:00	11:00	17:00	23:00	5:00
Supply Pressure PT-112	psig	205	209.04	206.34	210.21	209.49
Comments:						

Figure 5-2 Cigar Lake Modular Refrigeration Plant Example Run Sheet

5.2 Evaporator Model Validation

Dataset 1 was used to validate the evaporator model by comparing the evaporator capacity calculated from the data to the evaporator model predictions. To determine the evaporator capacity from the measured data, Equation 5.1 is used which requires the brine inlet temperature, outlet temperature, and brine flow rate.

$$\dot{Q} = \rho \dot{V}_{\text{brine}} Cp\left(T_{\text{brine,in}} - T_{\text{brine,out}}\right) \qquad (5.1)$$

The Cigar Lake modular refrigeration plants do not have flow meters to measure the flow of brine through the evaporators. To overcome this difficulty the discharge pressure of chiller pump in each module is used along with a model of the chiller pumps to calculate the flow of brine through the evaporators. The development of the chiller pump model is detailed in section 5.3.1. The data used to validate the evaporator model consisted of 194 operating points, all from Dataset 1 with

$$-39.7°C \leq ST_{\text{evap}} \leq -35.5°, C$$

$$232.4\ m^3/hr \leq \dot{V}_{\text{brine}} \leq 291.2 m^3/hr, \text{and}$$

$$-33.0°C \leq T_{\text{brine,in}} \leq -26.7°C.$$

The range of calculated evaporator capacities was

$$122\ TR \leq \dot{Q}_{\text{evap}} \leq 443\ TR.$$

Figure 5-3 compares the evaporator capacity calculated using the simplified evaporator model described in Section 4.3, which uses the Dittus-Boelter correlation, to the evaporator capacity that was calculated using Dataset 1. On average the model predicts an evaporator capacity 26% higher than the measured capacity with a standard deviation of 18%. This is represented in Figure 5-3 by the data points being shifted above the solid black line that represents a zero percent difference between measured and modeled capacity. The black dotted lines in Figure 5-3 represent the uncertainty in the calculated evaporator capacity.

The uncertainty in the capacity ($u_{\dot{Q}}$) is calculated using Equation 5.2, the derivation of which is detailed in Appendix C.

$$u_{\dot{Q}} = \pm\left(\left(\rho c_p\left(T_{\text{brine,in}} - T_{\text{brine,out}}\right)u_{\dot{V}}\right)^2 + \left(\rho C p \dot{V}_{\text{brine}} u_{T_{\text{out}}}\right)^2 + \left(\rho C p \dot{V}_{\text{brine}} u_{T_{\text{in}}}\right)^2\right)^{1/2} \quad (5.2)$$

In Equation 5.2 ($u_{T_{\text{out}}} and\ u_{T_{\text{in}}}$) are the uncertainties in the measured brine outlet and inlet temperatures respectively. The uncertainty in the brine temperatures is a combination of resolution uncertainty (±0.1°C) and resistance temperature detector (RTD) accuracy which is given in Table 3-2. Using the average brine flow rate, average brine inlet temperature, and average brine outlet temperature the average uncertainty in the evaporator capacity determined using the Data Set 1 is ±311 kW (±88.4 TR).

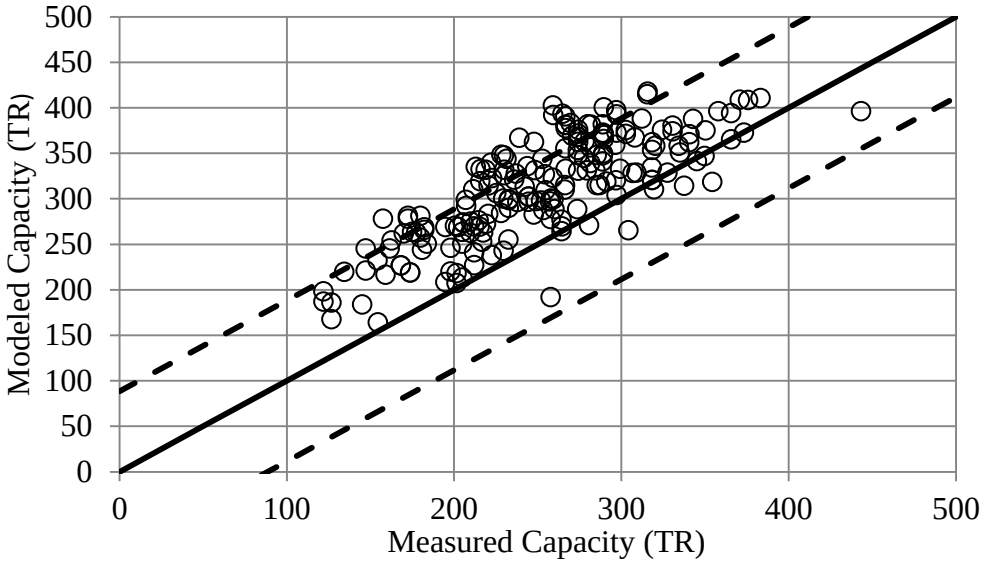

Figure 5-3 Modeled and Measured Evaporator Capacity Comparison (Dittus-Boelter)

Although the uncertainty in the measured capacity is large there is still room for improvement in the evaporator model's predictions. The Dittus-Boelter correlation is known to produce errors as large as 25% whereas correlations such as the Gnielinski correlation are more accurate with errors closer to 10% (Bergman et al., 2011, p.515). In addition the Dittus-Boelter correlation is only valid for Reynolds numbers greater than 10,000 and brine flow rates through the evaporator resulted in Reynolds numbers ranging from 2500 to 3100.

For comparison the Gnielinski correlation, which is valid for $Re \leq 5 \cdot 10^6$ (Bergman et al., 2011,p.515), is used to modify the simplified evaporator model. On average the modified evaporator model predicts an evaporator capacity that is 31% higher than the measured capacity and the standard deviation for the percent difference of 18% (Figure 5-4), which is not an improvement over the Dittus-Boelter correlation in this case. The lack of improvement might be attributed to the uncertainty in the correlations. It might also be attributed to uncertainty in the measured capacities, or possible inaccuracies resulting from other assumptions used in the evaporator model.

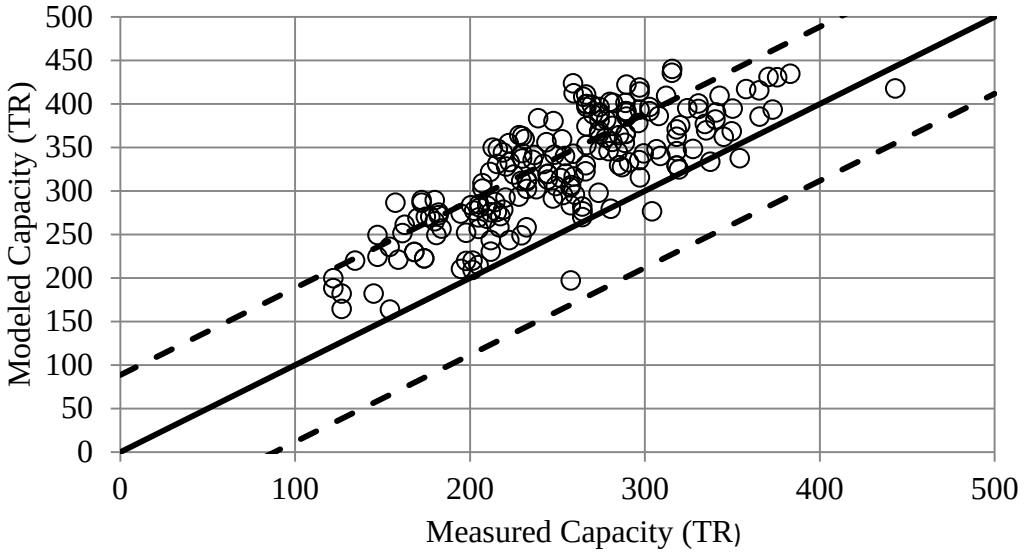

Figure 5-4 Modeled and Measured Evaporator Capacity Comparison (Gnielinski)

The second evaporator model, which assumes a constant *UA* of 172 kW/K under all operating conditions, was also validated using Dataset 1.The constant *UA* value is based on calculations that use the manufacturer's specifications for the evaporator. On average the constant *UA* model predicts an evaporator capacity 36% higher than the measured capacity with a standard deviation of 21% (Figure 5-5). The constant *UA* model results in a greater standard deviation than the simplified evaporator model because it is unable to account for changes in brine flow rate, or changes in brine viscosity as the brine temperature changes.

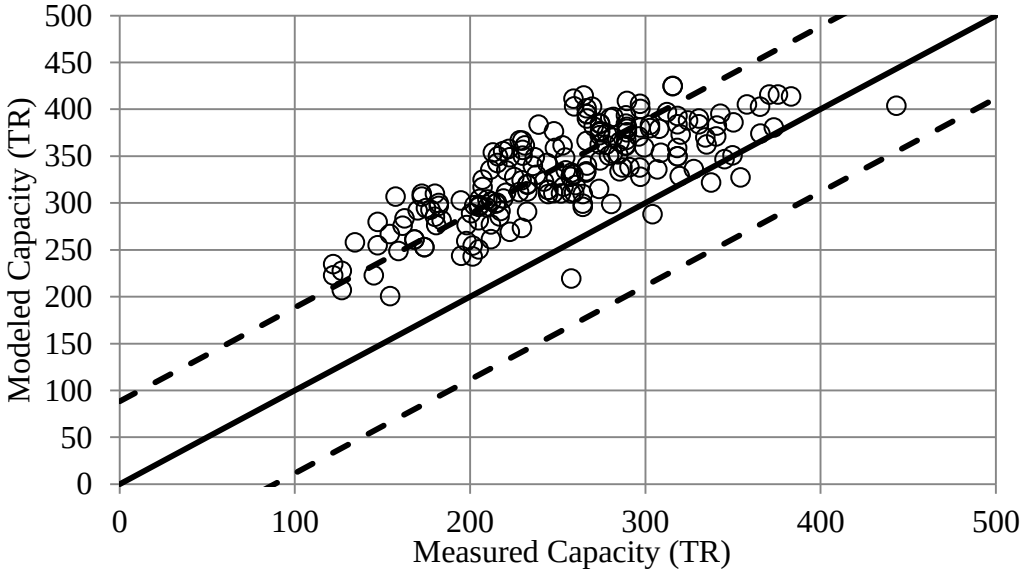

Figure 5-5 Modeled and Measured Evaporator Capacity Comparison (Constant *UA*)

The evaporator capacity predicted by all three models is greater than the measured capacity. All three of the models rely on the manufacturer's rated evaporator performance, which is based on their own proprietary model. The difference between the rated and actual performance could be a combination of uncertainty in the original manufacturer's ratings and a loss of evaporator capacity due to fouling. A study performed by the Cigar Lake process department demonstrated that by removing heavy fouling from the plate and frame heat exchangers in the primary refrigeration plant the performance of the evaporators could be improved by 15% (L. Verhelst, personal communication, May 19, 2014). This study illustrates that heavy fouling can have a significant impact on evaporator capacity and may help account for difference between modeled and measured evaporator capacities. To correct for the evaporator models over-predicting the evaporator performance, a calibration factor of 0.7 is applied to the *UA* used by the evaporator model for all subsequent modeling. After adjustment, the predictions of the evaporator model easily fall within the uncertainty in the measured capacity.

5.2.1 Chiller Pump Model Development

The brine flow through the evaporators is calculated using the chiller pump discharge pressure and a model based on the chiller pump curve. The pump curves provided by the pump manufacturer (Goulds Pumps) plot pump flow in m^3/hr against the change in total water head across the pump. The change in total head across the pump is

$$\Delta h_{\text{total}} = \left(H_{\text{stat,out}} + H_{\text{u,out}}\right) - \left(H_{\text{stat,in}} + H_{\text{u,in}}\right) \quad (5.3)$$

where H_{stat} is the static head and H_{u} is the velocity head which can be calculated as

$$H_{\text{u}} = \frac{u^2}{2g} = \frac{\left(\frac{\dot{V}}{A}\right)^2}{2g} \quad (5.4)$$

where $\dot{V}$ is the pump flow, A is the cross sectional area of the pump inlet or outlet, and g is the acceleration due to gravity. The static head at the pump inlet is calculated using the brine tank level and the distance from the pump inlet to the bottom of the brine tank

$$H_{\text{stat,in}} = (3.21 + 0.0443L) \quad (5.5)$$

where L is the brine tank level as a percentage e.g., 80.

The static discharge head can be calculated using the pump discharge pressure as:

$$H_{\text{stat,out}} = \frac{\left(P_{\text{pump,D}} \cdot 6894.7572\right)}{\rho g} \tag{5.6}$$

where $P_{\text{pump,D}}$ is the pump discharge pressure in psi and ρ is the brine density calculated based on the brine temperature at the pump discharge.

The pump curve for the chiller pumps which are Goulds Pumps 3196 4"x6" – 13 pumps (101 mm (4") inlet, 152 mm (6") discharge, and 330 (13") maximum impeller size, 303 mm (12") impeller used) has been re-produced in Figure 5-6. To model the pump curve Excel was used to fit a second-order polynomial (Equation 5.7) which is used with the quadratic formula to calculate the chiller brine pump flow rate.

$$H_{\text{Tot}} = (-2.6127 \cdot 10^{-4})\dot{V}^2 + (2.8798 \cdot 10^{-2})\dot{V} + 47.2866 \tag{5.7}$$

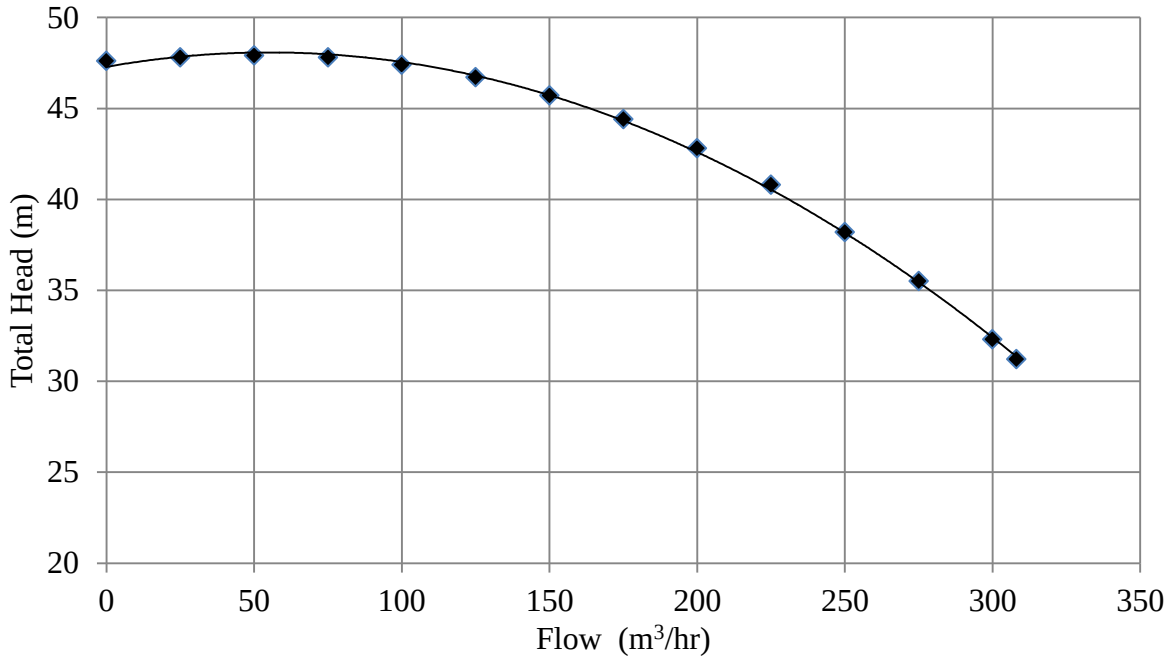

Figure 5-6 Chiller Circulation Pump Curve fit to Manufacturer's Data

As previously mentioned, the pump curves provided by Goulds Pumps are based on water. Pumping fluids with a higher viscosity than water will result in lower pump performance. ANSI 9.67 (2010) provides a method based on empirical relationships to correct pump curves so they can be used with fluids with higher viscosities. Using the ANSI standard, a water head of 23 m (at a flow rate of 364 m^3/hr) decreases by 0.2% when it is corrected for a brine viscosity of 19

centipoise. Therefore, the effects of viscosity on the pump performance are negligible and the model does not need to include the viscosity correction.

The pressure transducer used to measure the chiller pump discharge pressure has an accuracy of ±0.25% (see Table 3-2). Figure 5-7 illustrates the effect of the pressure transducer accuracy on the chiller pump model's flow predictions. At low flow rates small changes in pressure result in large changes in the calculated pump flow rate because the slope of the pump curve at low flow rates is very low. Fortunately the brine flow rate through the evaporators does not fall below 232 m^3/hr in Dataset 1. Therefore, the uncertainty, based on instrumentation accuracy, in the brine flow predicted by the pump model is acceptable.

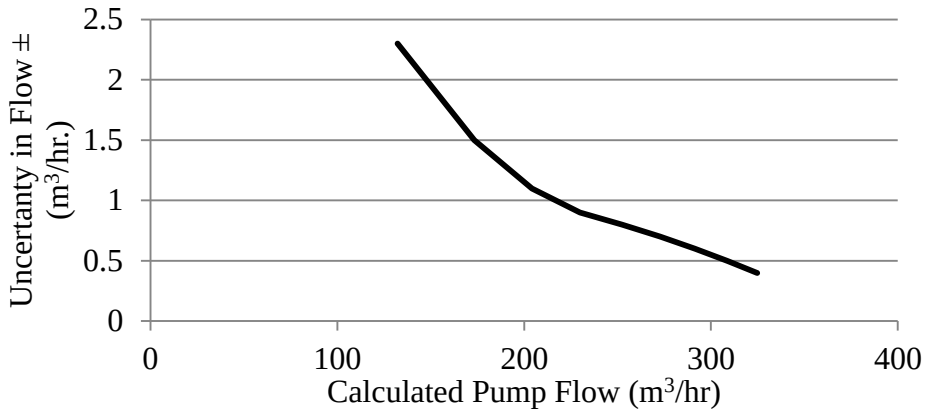

Figure 5-7 Uncertainty in Chiller Pump Model due to Instrument Accuracy

The operators recording the pump discharge pressure data typically only recorded pressures to the nearest whole number, and did not include any decimal points. Therefore, an additional uncertainty associated with the resolution of the measurements, which is estimated to be ±3.5 kPa (±0.5 psi) must be considered. The effect of this additional uncertainty is significant, especially at low flow rates as shown in Figure 5-8. The average evaporator brine flow rate for the first set of data is 261 m^3/hr. Therefore, the uncertainty in the pump model's predicted flow rate is ±4.5 m^3/hr.

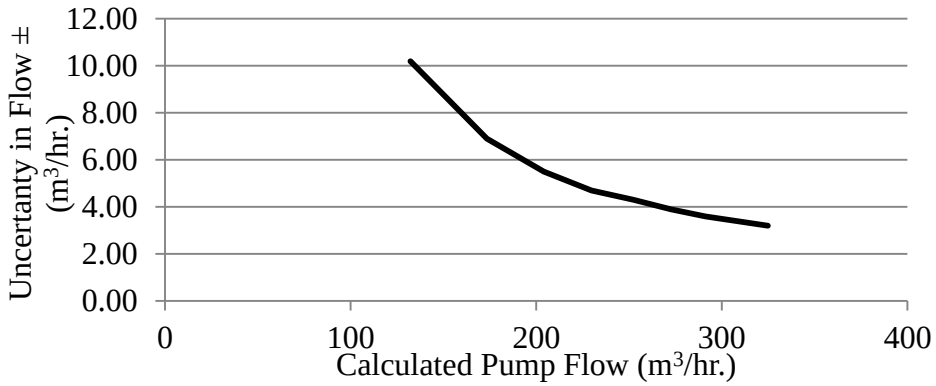

Figure 5-8 Uncertainty in Chiller Pump Model due to Resolution Error

5.3 Condenser Model Validation

Figure 5-9 shows the average daily ambient temperature at Cigar Lake and the condensing temperature averaged between the five modules from April 21, 2014 to September 27, 2014. The average daily temperature data was obtained from The Government of Canada Environment Canada (2014) and was collected by a weather station located at the Cigar Lake mine site. Unfortunately, hourly temperature data is not available for the Cigar Lake mine site. The condensing temperatures were measured and recorded at times of the day which do not necessarily correspond to the time of day the average daily temperature occurred at. Therefore, comparing the modeled condensing temperatures to measured condensing temperatures, based average daily temperatures, is inaccurate. In addition as Figure 5-9 illustrates the range of daily temperatures relative to the average daily temperature is significant. Despite the inaccuracies introduced by the limited amount of temperature data, the modeled condensing temperatures agree quite well with the measured condensing temperature with an average percent difference of 5.4% with a standard deviation of 8.1%.

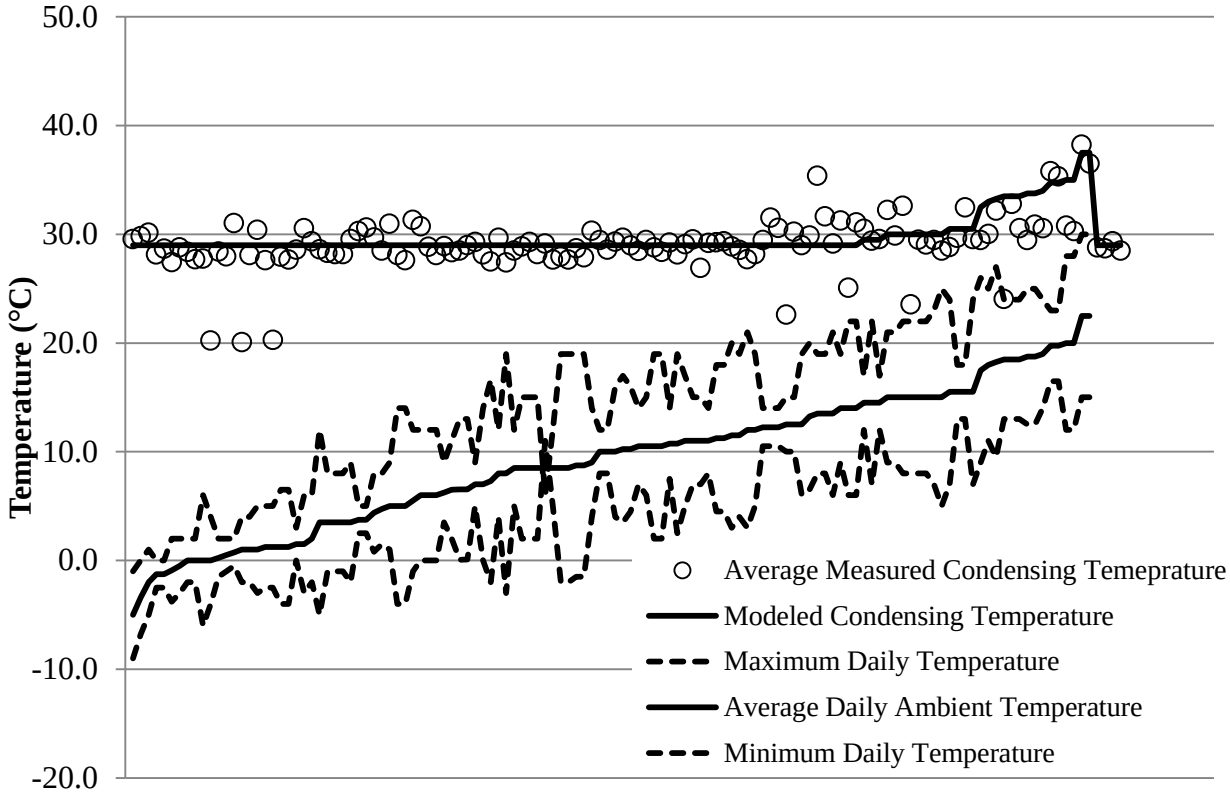

Figure 5-9 Ambient Temperature and Condensing Temperature (Measured and Modeled)

5.4 Compressor Model Validation

The compressor model was validated by comparing the calculated compressor capacity at various suction and discharge temperatures to the capacity given by the Mycom compressor software under the same operating conditions. In all cases the compressor capacity calculated by the compressor model was in excellent agreement with the capacities provided by the Mycom software. In addition, the effect of changes in assumed values of the compressor constants were examined to determine how much they affect the predictions of the compressor model. Table 5-1 summarizes the analysis of the compressor model constants, using a suction temperature of -29°C and a condensing temperature of 35°C.

Table 5-1 Analysis of Compressor Constants

Constant	Variation		Base Capacity kW (TR)	Total Variation kW (TR)	Total Variation (%)
$\dot{V}_{swept,low}$ (m^3/hr)	5700	±10%	1808 (514)	355 (101)	20%
$\dot{V}_{swept,high}$ (m^3/hr)	1900	±10%	1808 (514)	0	0%
Suction Superheat (°C)	2	±10%	1794 (510)	25 (7)	1.4%
$T_{D,high}$ (°C)	90	±10%	1808 (514)	0	0%
$T_{D,low}$ (°C)	60	±10%	1808 (514)	0	0%
$\dot{W}_{max}$ (kW (hp))	746 (1000)	±10%	1808 (514)	7 (2)	0.4%

As Table 5-1 shows, the assumed values for the compressor constants have very little effect on the predicted compressor capacities. The swept volume rate has a large effect on the compressor's predicted capacity. However, it is a function of the physical design of the compressor and can only be changed by modifying the compressor or changing the speed of the electric motor.

5.5 Refrigeration System Model Validation

The Refrigeration System Model, which predicts the capacity of each of the five refrigeration modules, was validated using Dataset 1. Again, Equation 5.1 was used to calculate the plant capacity based on the Cigar Lake data. The average uncertainty in the measured capacity is ±25.1 kW (±88.4 TR). The refrigeration module's predictions for plant capacity represent the measured capacities very well with an average percent difference of -2.6%, and a standard deviation of 13%. In addition, as Figure 5-10 illustrates, the predicted capacities match the

measured module capacity within the uncertainty bounds. The predictions for module brine exit temperatures (T_{supply}) match the measured exit temperatures with an average percent difference of -0.1% and a standard deviation of 1.5% (Figure 5-11).The predicted values for the supply temperature do not match the measured values within the uncertainty in the measured T_{supply} which is ±0.22°C on average. However, because the return temperature is an input to the model the uncertainty in the measured temperatures will affect the results of the model. Therefore, it is unlikely the measured temperature would match the modeled temperatures within uncertainty.

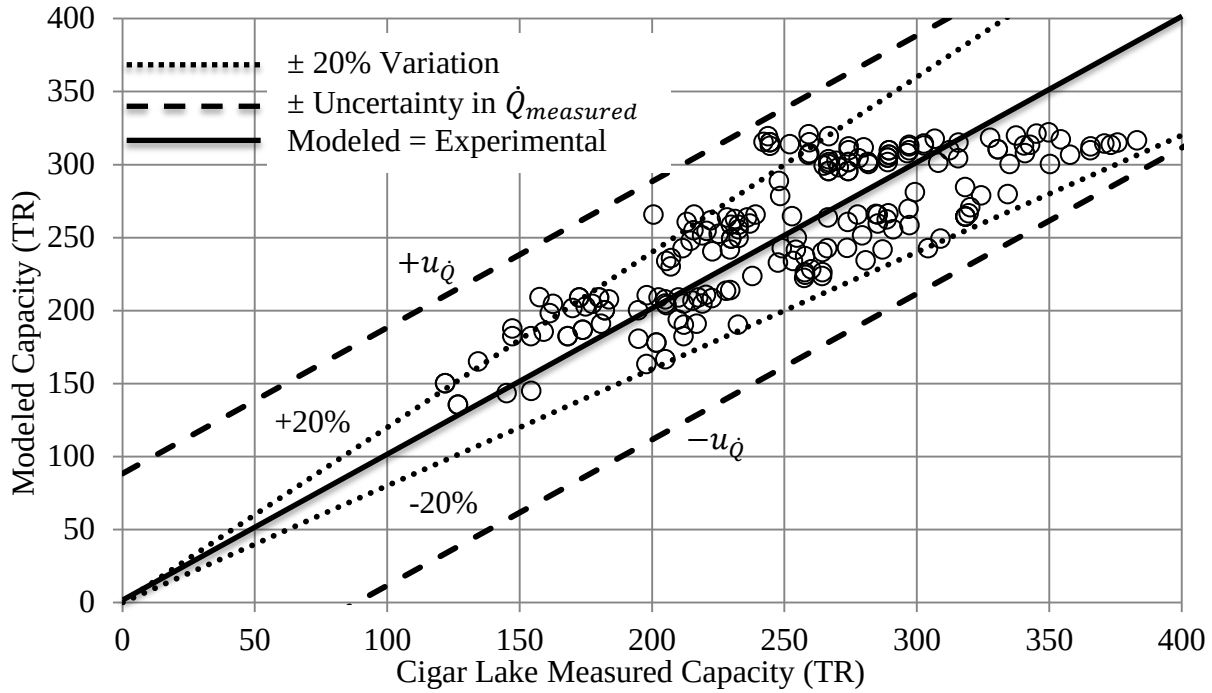

Figure 5-10 Comparison of Modeled Module Capacity with Measured Capacity

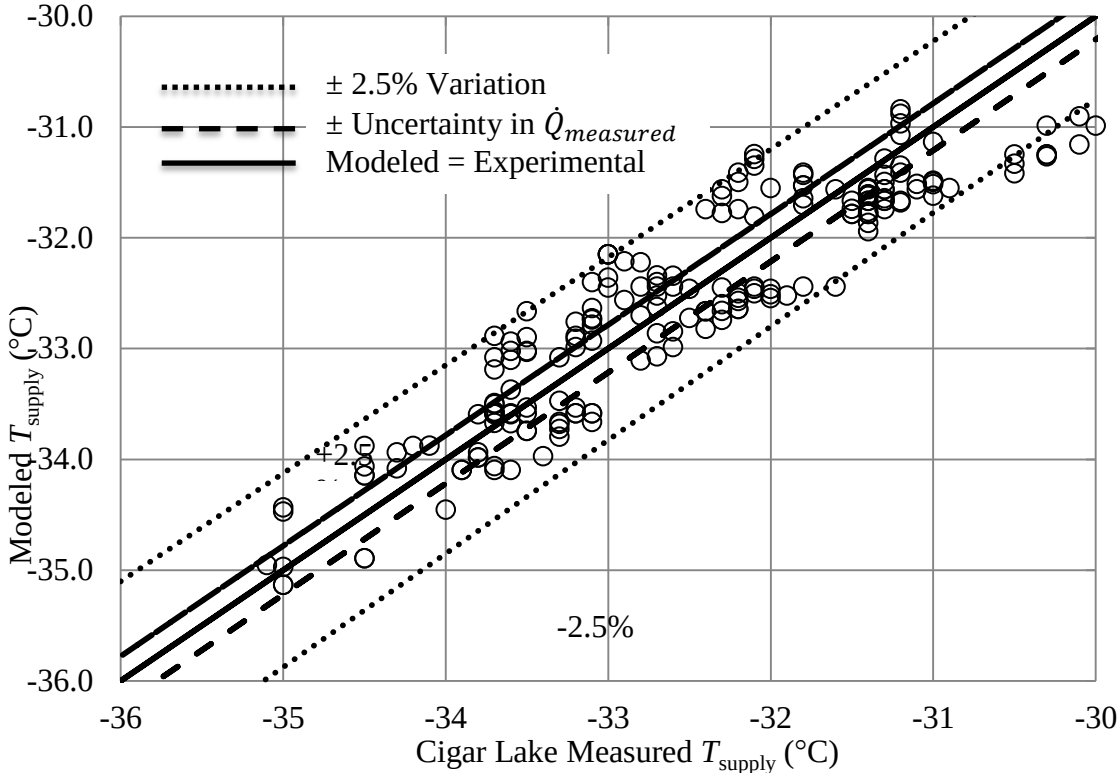

Figure 5-11 Comparison of Modeled and Measured Module Exit Brine Temperature

5.6 Refrigeration Plant Model Validation

Dataset 2 was used to validate the model of the refrigeration plant as a whole, which includes the five refrigeration modules, the brine tank and the brine pumps. Dataset 2 was collected from May, 2014 to the end of September, 2014. Dataset 2 represents the summer months with a mean maximum daily ambient temperature of 30°C, which allows the model's performance in high ambient temperature conditions to be evaluated. Dataset 2 contains 128 operating points with

$$295.3\ \mathrm{m^3/hr} \leq \dot{V}_{\mathrm{brine,F}} \leq 588.4\ \mathrm{m^3/hr},$$

$$-16.8°C \leq T_{\mathrm{brine,F-return}} \leq -23.0°C, \text{and}$$

$$-23.5°C \leq T_{\mathrm{brine,F-supply}} \leq -30.9°C.$$

The range of calculated evaporator capacities was

$$882\ \mathrm{TR} \leq \dot{Q}_{\mathrm{evap}} \leq 1250\ \mathrm{TR}.$$

Again the plant capacities were calculated from Dataset 2 using Equation 5.1, the average uncertainty in which was ±127.6 TR. Figure 5-12 compares the modeled refrigeration plant capacity to the capacities calculated for the same operating conditions using Dataset 2. On

average the capacities predicted by the model match the measured capacities within 4.21%, and with a standard deviation of 11%. As Figure 5-12 shows, only a few of the modeled capacities do not match the measured capacities within the bounds of uncertainty, which are shown by the black dotted lines. The predicted field brine supply temperature is compared with the measured supply temperature in Figure 5-13. The supply temperature predictions match the measured supply temperatures with an average percent difference of 1% with a standard deviation of 4%.

The models for the evaporator, condenser, refrigeration modules, and the refrigeration plant are able to predict the performance of the refrigeration plant with sufficient accuracy. The capacity predictions match the capacities determined using the Cigar Lake data within measurement uncertainty. Only a few of plant model's capacity predictions fall outside of the range of measurement uncertainty. During the summer months the refrigeration plants frequently operate in a transient state due to power outages and maintenance. These transient conditions could explain why some of the predicted plant capacities do not match the measured capacities within the bounds of uncertainty. The brine supply temperature predictions for both the module model, and plant model match the measured supply temperature within ±5%; however, like the predicted module supply temperatures they do not fall within the bounds of uncertainty. Again this could be a result of the uncertainty in the brine return temperatures, which are an input to the plant model, reducing the accuracy of the plant model's predictions.

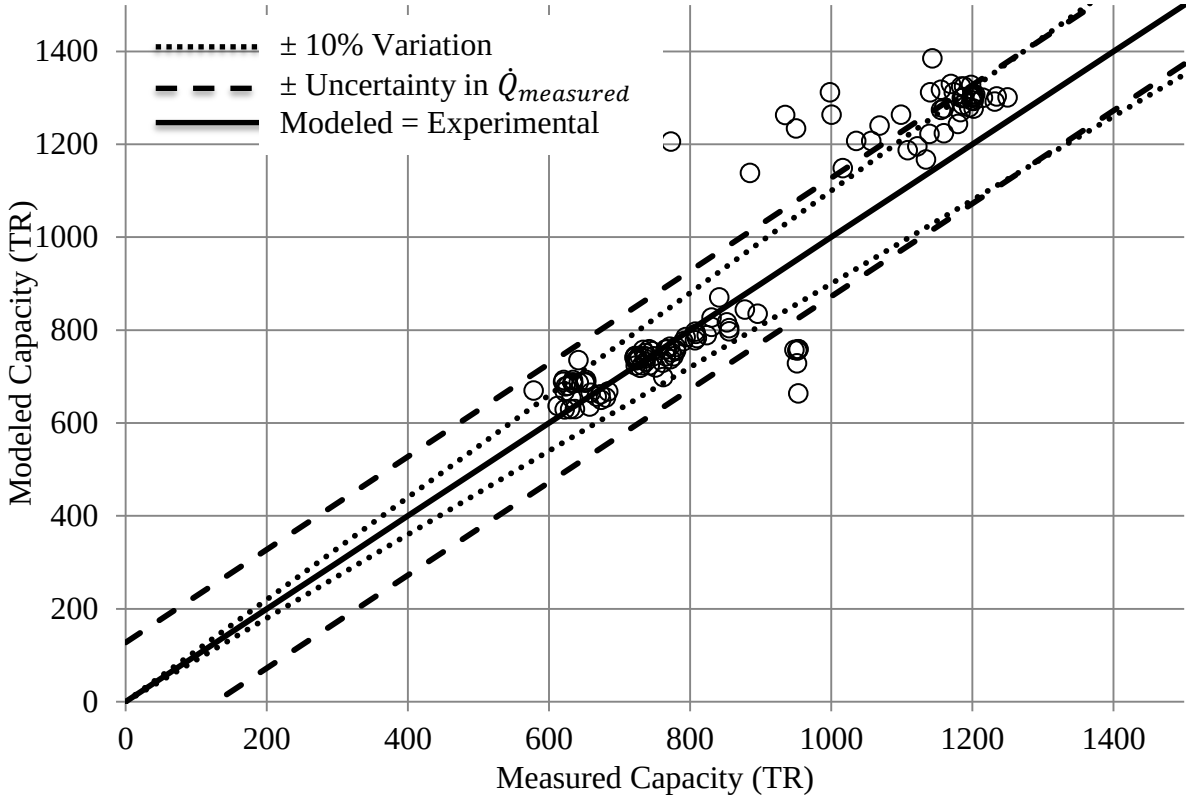

Figure 5-12 Comparison of Modeled Refrigeration Plant Capacity with Measured Capacity

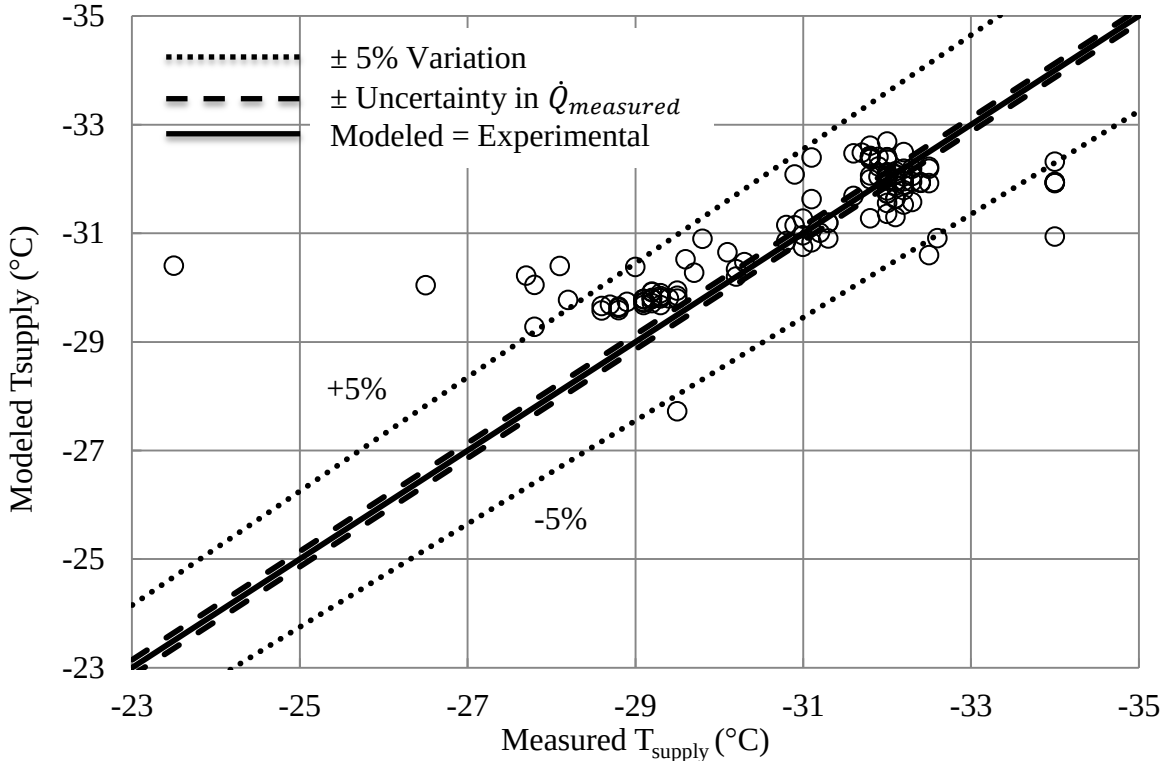

Figure 5-13 Comparison of Measured and Modeled Plant Brine Exit Temperature

The primary goal of this research was to develop a model capable of calculating the capacity of an industrial refrigeration plant under different operating conditions using only basic plant specifications. In this chapter the results of simulations which determine the capacity of the refrigeration modules and the refrigeration plant as a whole are presented. A sensitivity analysis is also presented that demonstrates which parameters have the greatest effect on refrigeration capacity.

6.1 Simulation Results and Discussion

The capacity of the refrigeration plant, and individual refrigeration modules, is calculated using the models developed in Chapter Four. Figure 6-1 presents a family of curves giving the capacity of the refrigeration modules as a function of the evaporator brine inlet temperature ($T_{\text{brine,return.M}}$). The curves in Figure 6-1 are based on a brine flow rate through the evaporator $\dot{V}_{\text{brine,evap}}$ of 250 m^3/hr.

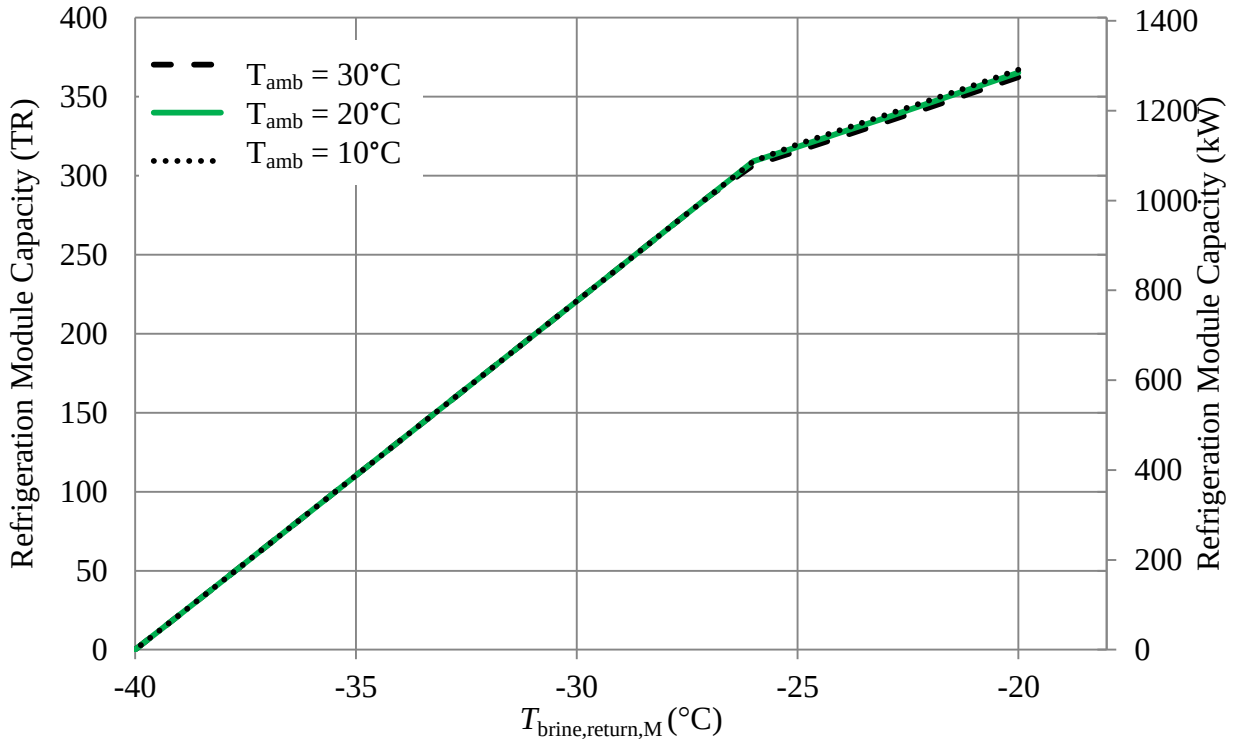

Figure 6-1 Refrigeration Module Capacity as a Function of Brine Inlet Temperature

The simulation results show that the refrigeration plant's capacity is highly dependent on the temperature of the brine entering the evaporator. The simulation also demonstrates that the elevated ambient air temperatures weakly affect the refrigeration module capacity as previously discussed in Section 2.5.4. Although the model is considered to be validated by the results presented in Chapter Five, a further validation of the model's results is obtained by comparing Figure 6-1 to Figure 6-2, which provides chiller capacity as a function of the water temperature leaving the chiller for a York YCAV0207S/P chiller package. The York chiller utilizes twin screw compressors and air-cooled condensers. York rated the chiller using the AHRI 550/590 standard (York, 2013). As Figure 6-2 illustrates, the capacity of both the Cigar Lake plant and the York chiller depend on the secondary coolant temperature and the ambient air temperature. This comparison shows that, although the York system is different in size and design from the Cigar Lake refrigeration plants, it shares the same general characteristics. This serves as a verification that the relationship between plant capacity and brine temperature the model produces is realistic.

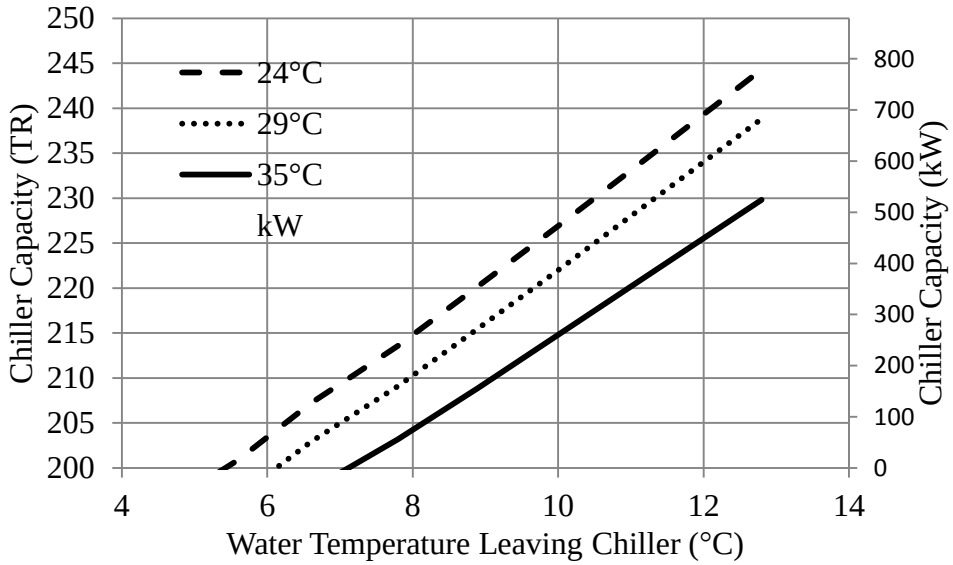

Figure 6-2 York Chiller Capacity as a Function of Water Temperature

The capacity of the refrigeration plant as a function of the brine temperature returning from the freeze pipes is shown in Figure 6-3. Figure 6-3 is based on an ambient temperature of 20°C, a field brine flow rate of 583 m^3/hr, and a module brine flow rate of 250 m^3/hr. Again the plant capacity is dependent on the brine temperature returning to the plant, although the inflection point that occurs in Figure 6-1 at -26°C is delayed until approximately -21°C in Figure 6-3. The

shift in the inflection point implies the brine is being cooled off in the brine tank by the underflow before it returns to the plant.

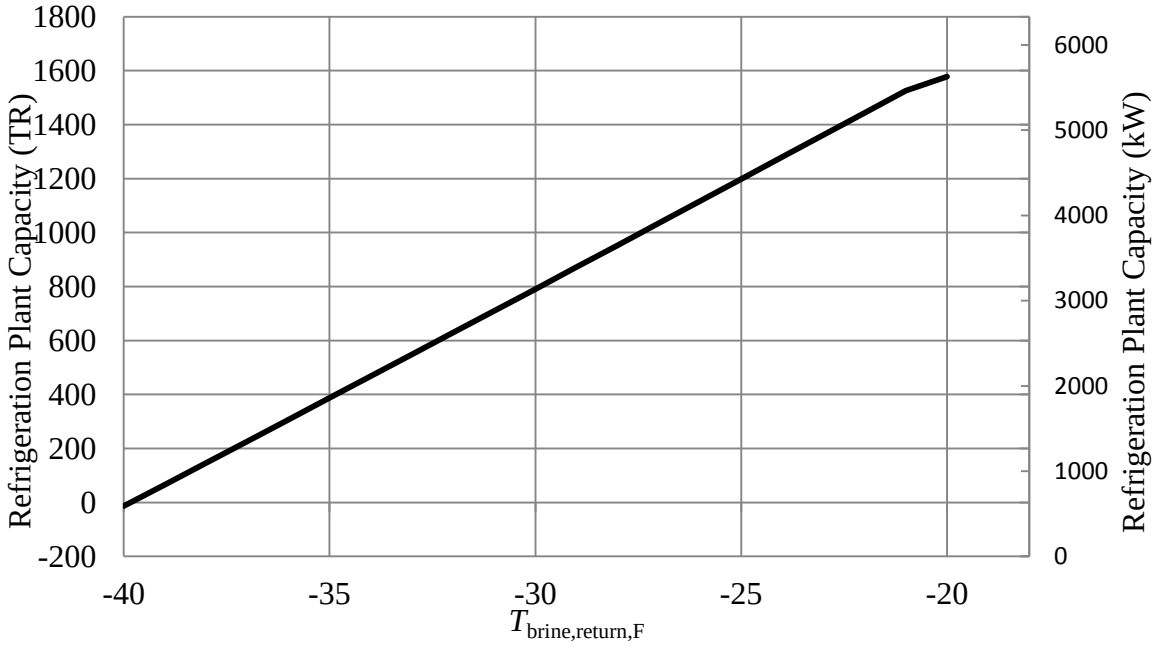

Figure 6-3 Refrigeration Plant Capacity as a Function of Brine Return Temperature

The refrigeration plant model can be coupled with existing models of the artificial ground freezing process by calculating the brine supply temperature to the freeze pipes given the brine temperature returning from the freeze pipes (Figure 6-4).

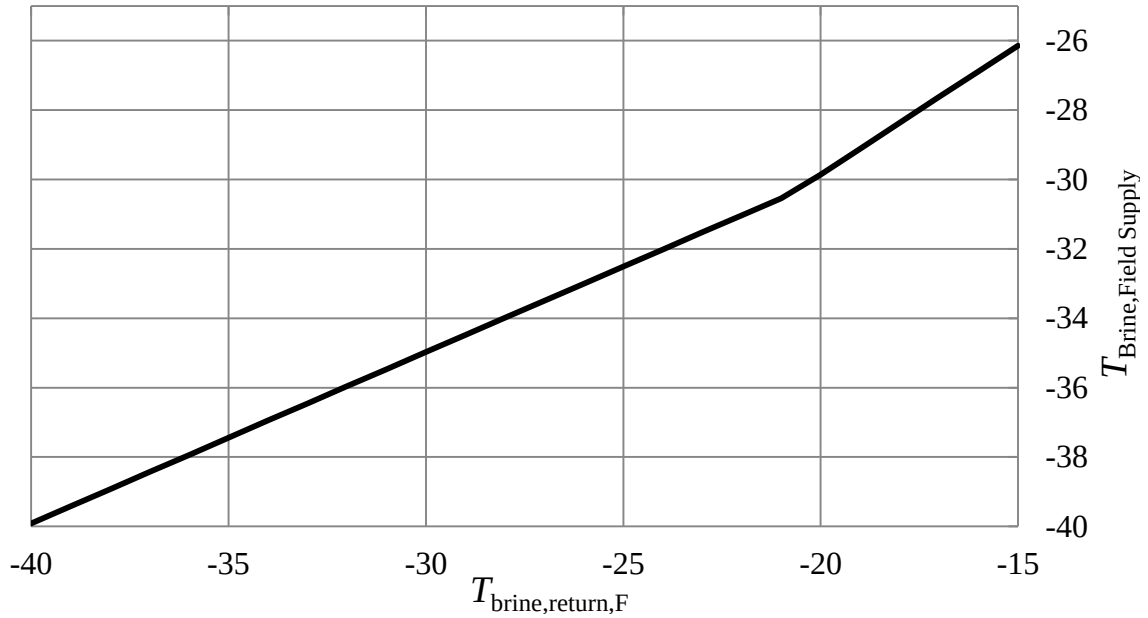

Figure 6-4 Brine Field Supply Temperature as a Function of Brine Return Temperature

Again Figures 6-3 and 6-4 show an inflection point, which represents the point at which the compressor capacity instead of the evaporator capacity limits the system capacity. In the case of the refrigeration plant as a whole, the inflection point is at a warmer brine temperature (-21°C) than for the individual refrigeration modules. This shift results from the brine tank effectively cooling the brine returning from the freeze pipes before it is pumped to the refrigeration modules.

6.2 Sensitivity Analysis

The performance of the refrigeration plant is dependent upon many different parameters. To determine which parameters are significant, multiple simulations were carried out and analyzed. Many of the parameters affect refrigeration capacity simultaneously. Therefore, simultaneous changes in at least two parameters must be considered for many of the parameters. For example the effect of ambient temperature on capacity depends on the brine return temperature. Table 6-1 summarizes the results of the simulations that were carried out for the refrigeration modules. Unless otherwise noted, the sensitivity analysis for the modules uses a module brine flow rate of 250 m^3/hr, an ambient air temperature of 20°C, a brine concentration of 29% $CaCl_2$, and a brine temperature entering the modules ($T_{return,M}$) of -20°C.

Table 6-1 Refrigeration Module Sensitivity Analysis Summary

Studied Variable	Variation		Base Capacity kW (TR)	Total Variation kW (TR)	Total Variation (%)
$T_{return,M}$ (°C)	-20	±10%	1284 (365)	137 (39)	11%
$\dot{V}_{brine,M}$ (m^3/hr)	250	±10%	1284 (365)	67 (19)	5.2%
Brine Concentration (%)	29	±1%	1284 (365)	18 (5)	1.4%
P_{int} (kPa (psi))	414 (60)	±10%	1284 (365)	14 (4)	1%
T_{amb} (°C)	30	±10%	1273 (362)	4 (1)	0.3%

The performance of the refrigeration modules is very sensitive to the brine temperature. A ±10% (20% total change) change in brine temperature creates a total change in module capacity of 11%. Lower brine temperatures result in lower plant capacities because the reduced temperature difference between the brine and the refrigerant in the evaporator reduces the evaporator capacity. The brine flow rate through the evaporator has the second largest impact on the performance of the refrigeration plant with a ±10% change in flow rate causing a total change in module capacity of 5.2%. Unlike the brine temperature, the flow rates through the evaporator are relatively constant during plant operation. Therefore, they do not have a large effect on plant performance during normal operation. In addition, evaporator brine flow rates cannot be increased much more than 250m^3/hr without risking evaporator tube erosion and a reduced evaporator service life. Brine concentration has a small impact on the performance with a change from 28% $CaCl_2$ to 30% $CaCl_2$ causing a 1.4% change in the capacity of the refrigeration modules. Brine concentration must also remain relatively constant during the operation of the refrigeration plant, because too much of a decrease in concentration may cause the brine to freeze and too much of an increase in concentration will cause brine crystallization. The intermediate pressure selected by the operator affects capacity by ±1% when the intermediate pressure is changed by ±10%. Finally, the ambient air temperature has very little effect on plant performance at warm brine temperatures. Further analysis shows that the ambient air temperature should have no effect on plant performance when the brine return temperature is below -26°C, because the evaporator capacity limits the overall refrigeration module capacity (Figure 6-1).

The results of the sensitivity analysis performed for the refrigeration plant are summarized in Table 6-2. Again unless otherwise noted, the simulations use an ambient air temperature of 20°C, a brine field return temperature of -22°C, a brine field flow rate of 583 m^3/hr, and a module brine flow rate of 250 m^3/hr.

The sensitivity analysis for the refrigeration plant demonstrates that the plant as a whole has much the same characteristics as the individual refrigeration modules. In response to the brine temperature returning from the field changing by ±10% the overall plant capacity changes by ±22%, which is double the change for individual refrigeration modules. A change in the field brine flow rate of ±10% changes the refrigeration capacity by 10.1%, which is significant

because the field flow rate constantly changes as more freeze pipes are connected to the refrigeration plant.

A 10% change in brine concentration changes the plant capacity by 0.1%, and a ±10% change in ambient air temperature changes the plant capacity by 0.5%.

Table 6-2 Refrigeration Plant Sensitivity Analysis Summary

Studied Variable	Variation		Fixed Variable	Value	Base Capacity kW (TR)	Total Variation kW (TR)	Total Variation (%)
$T_{return,M}$ (°C)	-22	±10%	T_{amb} (°C)	20	5079 (1444)	1111 (316)	22%
$\dot{V}_{brine,F}$ (m^3/hr)	583	±10%	$T_{return,F}$ (°C)	-22	5079 (1444)	470 (146)	10.1%
$\dot{V}_{brine,M}$ (m^3/hr)	250	±10%	$T_{return,F}$ (°C)	-22	5079 (1444)	116 (33)	2.3%
Brine Concentration (%)	29	±1%	$T_{return,M}$ (°C)	-22	5079 (1444)	7 (2)	0.1%
T_{amb} (°C)	30	±10%	$T_{return,M}$ (°C)	-15	6222 (1769)	28 (8)	0.5%

The results of the simulations carried out in Chapter Six are used in this chapter to determine how to optimize the performance of the refrigeration plant. The optimization goal of this study is to maximize the refrigeration capacity of the plant in a practical manner. Further simulations are used to determine if upgrading system components, such as the evaporator, will result in a significant capacity increase.

7.1 Optimizing Plant Operation

There are few refrigeration plant parameters that can be changed without replacing refrigeration plant components. The easiest parameters to adjust are the intermediate pressure set point and suction pressure set point. Figure 7-1 compares the module capacity for suction pressure set points of corresponding to evaporation temperatures of -38°C and -40°C. Using a higher suction temperature set point reduces the capacity of the plant when the evaporator capacity is the plant bottleneck. Therefore, to maximize the capacity of the refrigeration plant the suction temperature should be set as low as practical without causing the brine to freeze or crystalize in the evaporator.

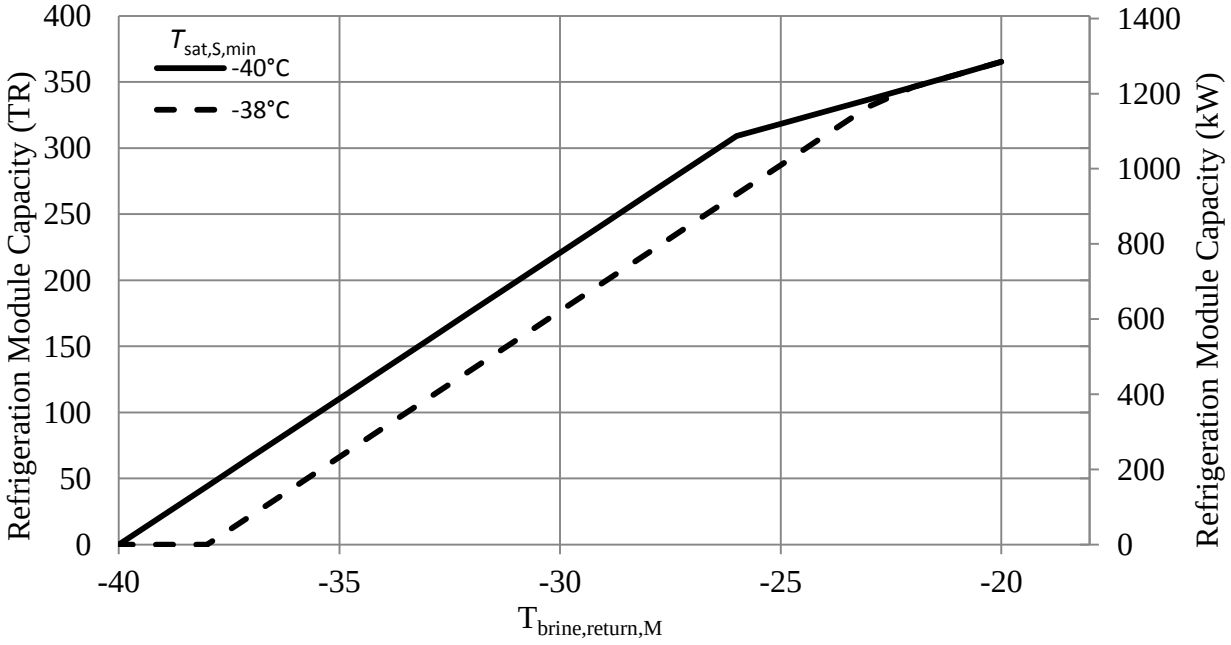

Figure 7-1 Refrigeration Module Suction Temperature Set Point Comparison

In Chapter Two it was established that the optimum intermediate pressure can be calculated by adding 5°C to the saturation temperature corresponding to the geometric mean intermediate pressure. According to the small amount of data available from the Cigar Lake plant, the intermediate pressure is typically held constant at 238.6 kPa (34.6 psi), which corresponds to a saturation temperature of -14.8°C. Comparing the module capacity curves in Figure 7-2 it is evident that this technique of setting the intermediate temperature lower than the optimum intermediate temperature established in Chapter two, which varies with the evaporation and discharge temperatures, results in greater refrigeration module capacities.

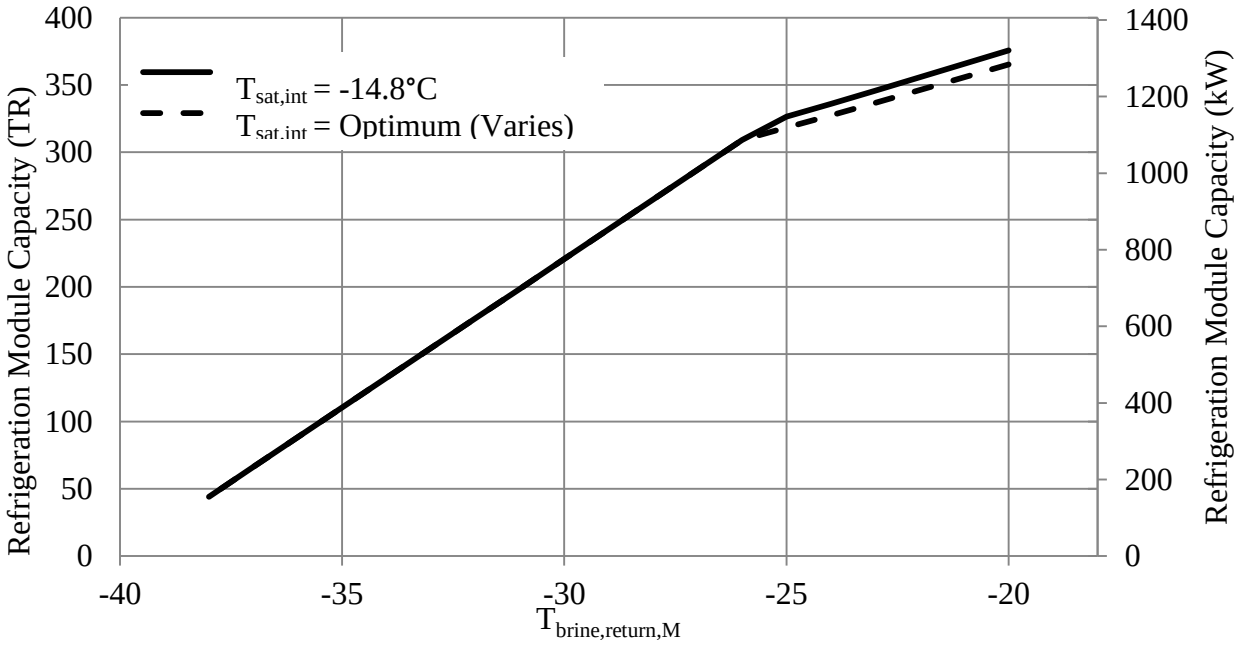

Figure 7-2 Refrigeration Module Capacity at High and Low Intermediate Temperatures

Figure 7-3 and 7-4 show that as the intermediate temperature decreases the capacity of the refrigeration module increases and the coefficient of performance decreases. Figures 7-3 and 7-4 are based on a brine flow rate through the modules of 250m^3/hr, an ambient air temperature of 20°C, and a brine return temperature of -20°C. The intermediate temperature established as the optimum in Chapter Two is illustrated by the vertical bar on the right. As Figure 7-4 illustrates the optimum intermediate temperature from Chapter Two maximizes the coefficient of performance for the refrigeration plant but it does not maximize refrigeration capacity. Therefore, the intermediate temperature should be kept as low as practical to maximize the performance of the refrigeration plant. The intermediate temperature used at Cigar Lake is close to the intermediate temperature that maximizes capacity. It results in a refrigeration capacity

increase of 4% over the optimum intermediate temperature that maximizes the coefficient of performance. Further simulation shows that even at elevated ambient temperatures as high as 30°C a lower intermediate temperature improves the refrigeration plant's capacity.

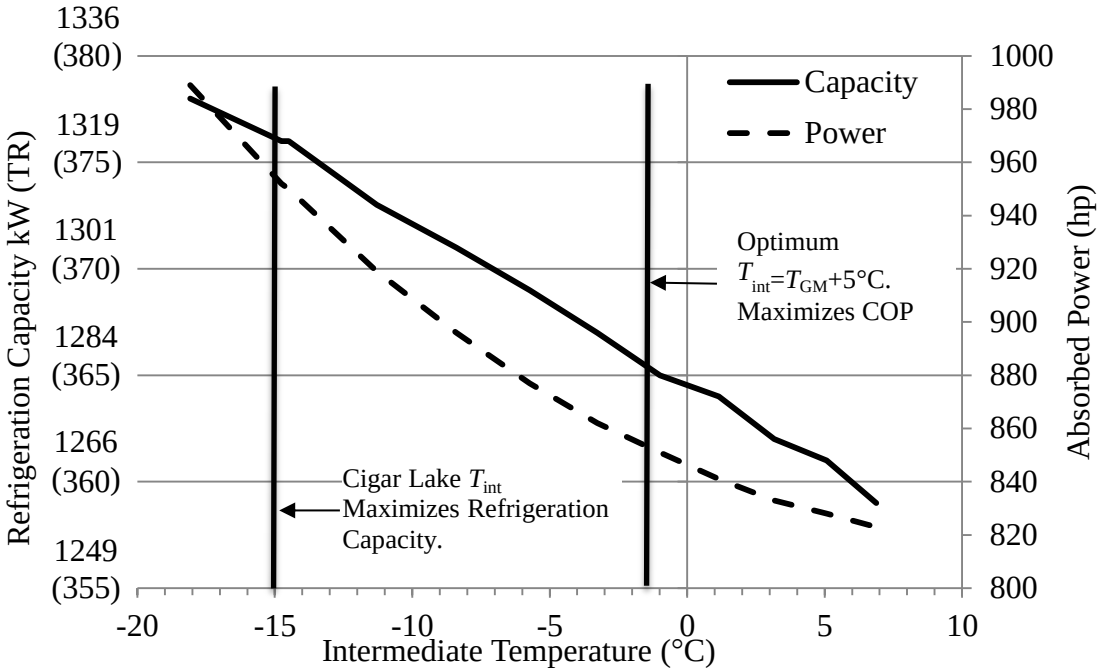

Figure 7-3 Effect of Intermediate Temperature on Module Capacity and Absorbed Power

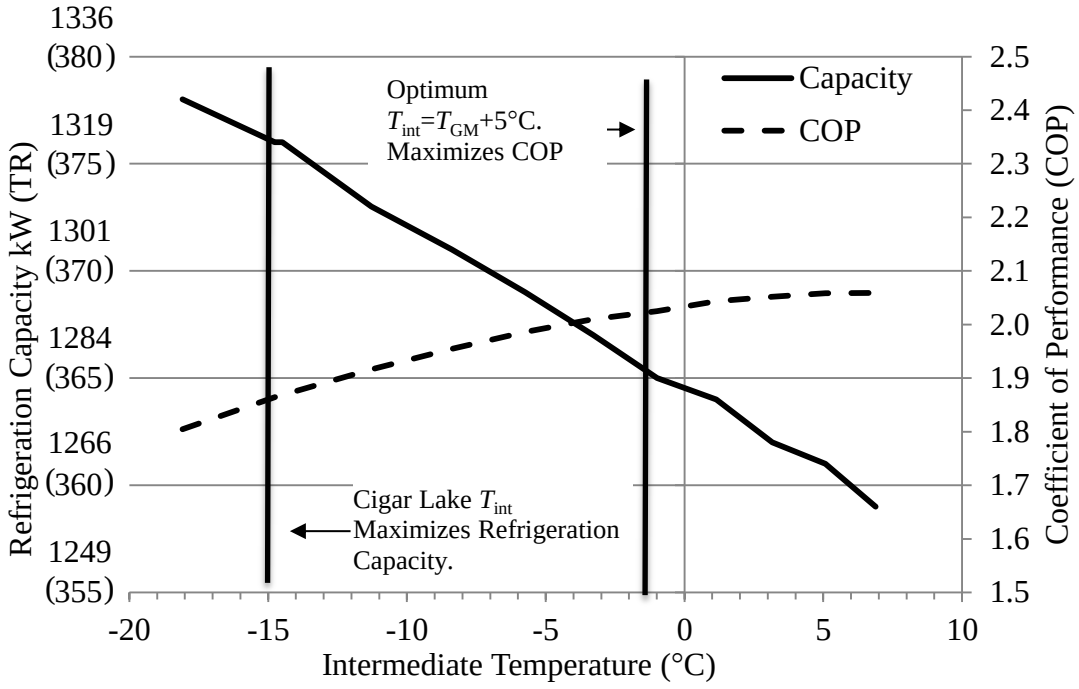

Figure 7-4 Effect of Intermediate Temperature Module Capacity and Coefficient of Performance

7.2 Optimization of Plant Arrangement

The sensitivity analysis in Chapter Six demonstrates that the capacity of the refrigeration plant as a whole is sensitive to the field brine flow rate. In addition, the capacity of the refrigeration modules depends heavily on the brine temperature with higher brine temperatures leading to higher refrigeration capacities. Further investigation demonstrates that with increasing brine field flow rates, substantial capacity gains can be achieved (Figure 7-5).

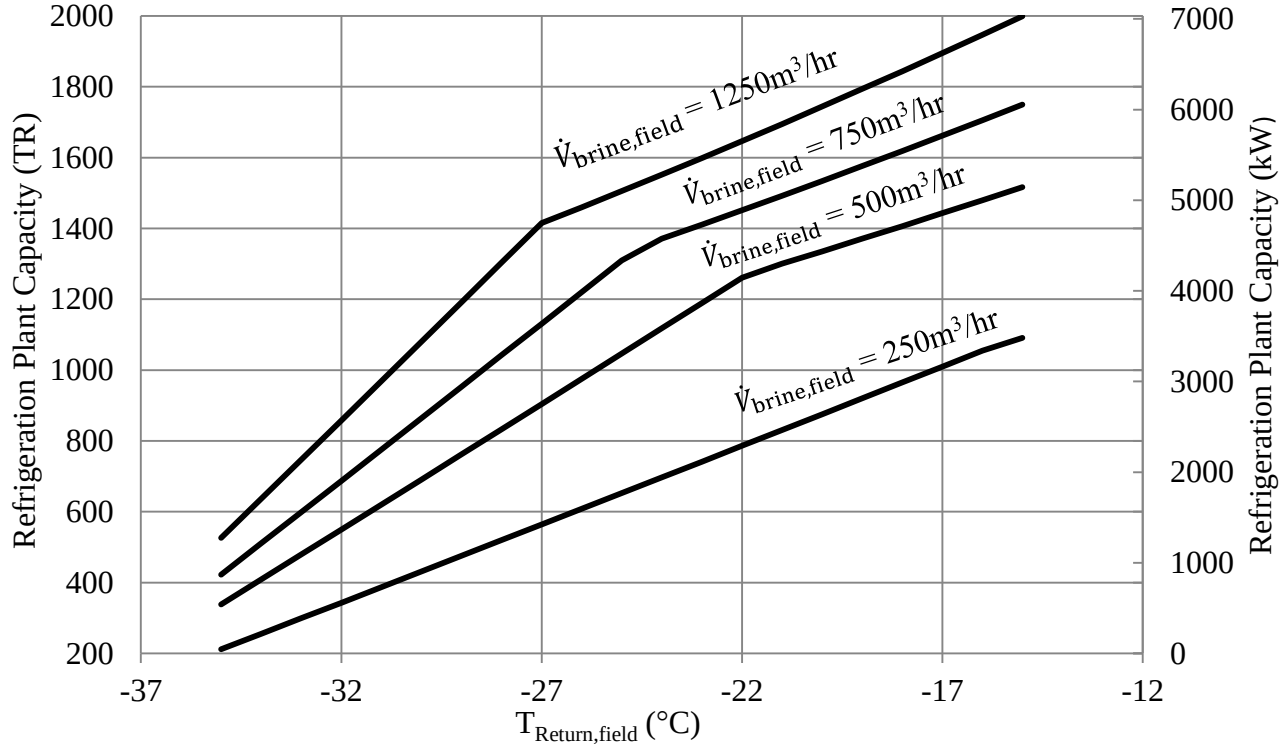

Figure 7-5 Refrigeration Plant Capacity for Different Brine Field Flow Rates

As the field brine flow rate approaches the total module flow rate of $1250m^3/hr$ the flow rate through the tank baffle approaches zero. This prevents the brine from being cooled before it reaches the plant. Therefore, increasing the field brine flow rate takes advantage of the higher plant capacities at warmer brine temperatures. The field brine flow rate is governed by the number of freeze pipes connected to the refrigeration plant. Therefore, it is not always possible to change the field flow rate to optimize the plant capacity. Removing the brine tank entirely and re-designing the brine system would solve this problem and at the same time eliminate the losses from heat transfer across the tank baffle. Figure 7-6 shows an alternate plant arrangement with all of the modules in parallel. Using such an arrangement would require replacing the

evaporators and brine circulation pumps with evaporators and pumps appropriately sized to handle lower brine flow rates of approximately 116.6 m^3/hr.

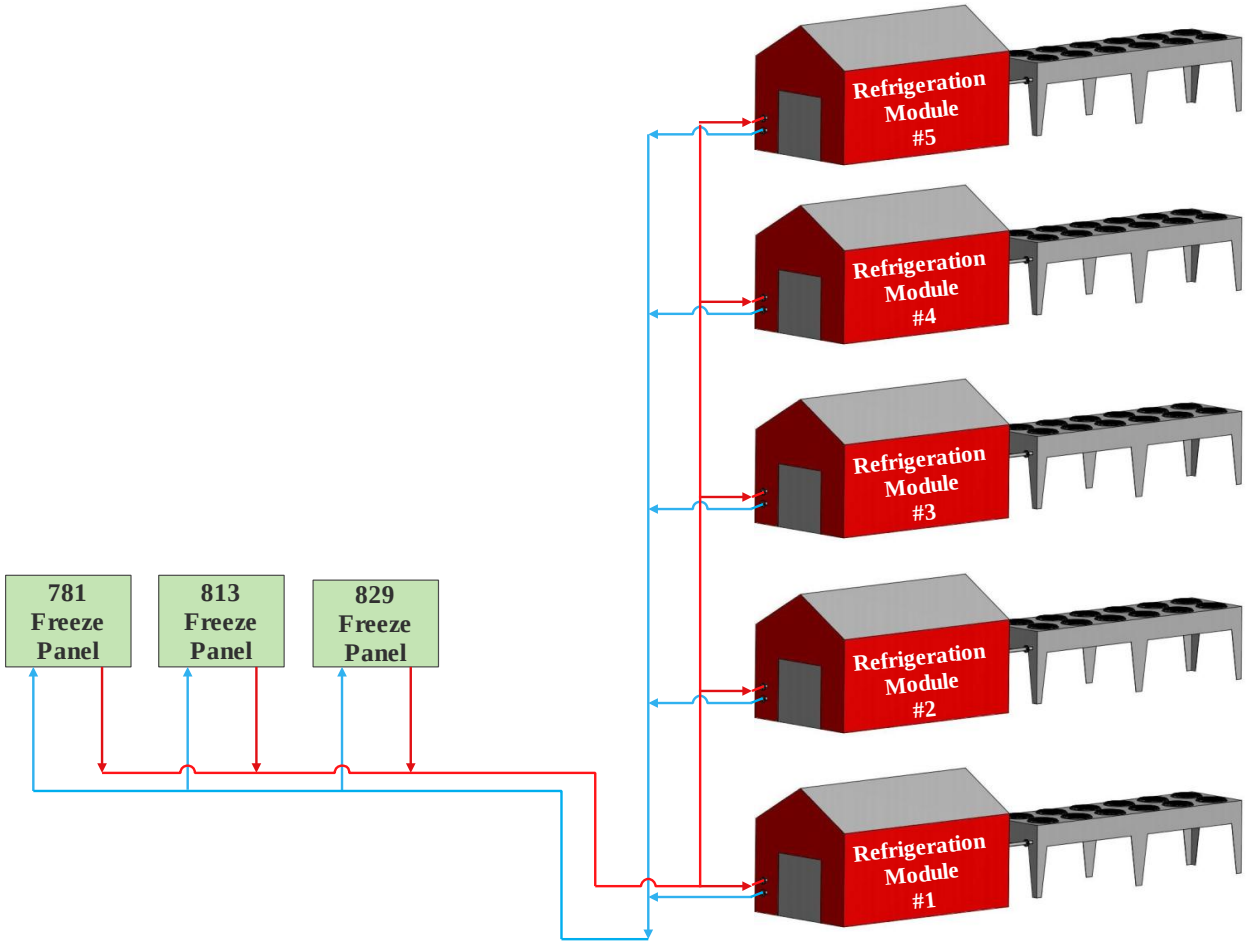

Figure 7-6 Refrigeration Plant with Modules in Parallel

Assuming appropriately sized evaporators are used with identical operating conditions, including an ambient temperature of 20°C, a brine field return temperature of -20°C, and a brine field flow rate of 583m^3/hr, the arrangement shown in Figure 7-6 increases the capacity of the refrigeration plant by 17.6% and decreases the field supply temperature by 6%.

7.3 Component Upgrades

The simulation results presented in Figure 6-1 show that the capacity of the refrigeration modules is limited by the capacity of the evaporator for brine return temperatures between -40°C and -26°C. Increasing the size of the evaporators improves the performance of the refrigeration

plant over the entire range of brine return temperatures (Figure 7-7). The evaporator upgrade shifts the inflection point in the capacity charts to a lower brine temperature, which represents the point at which the compressor limits the capacity instead of the evaporator. In addition the upgrade introduces an additional inflection point at brine temperatures of approximately -25°C where the compressor is forced to unload to keep its power consumption at or below 746 kW (1000 hp). The upgrade also increases the capacity of the plant where the compressor is the limiting factor. The larger evaporator increases the evaporation temperature over the entire operating range which leads to increased compressor capacity.

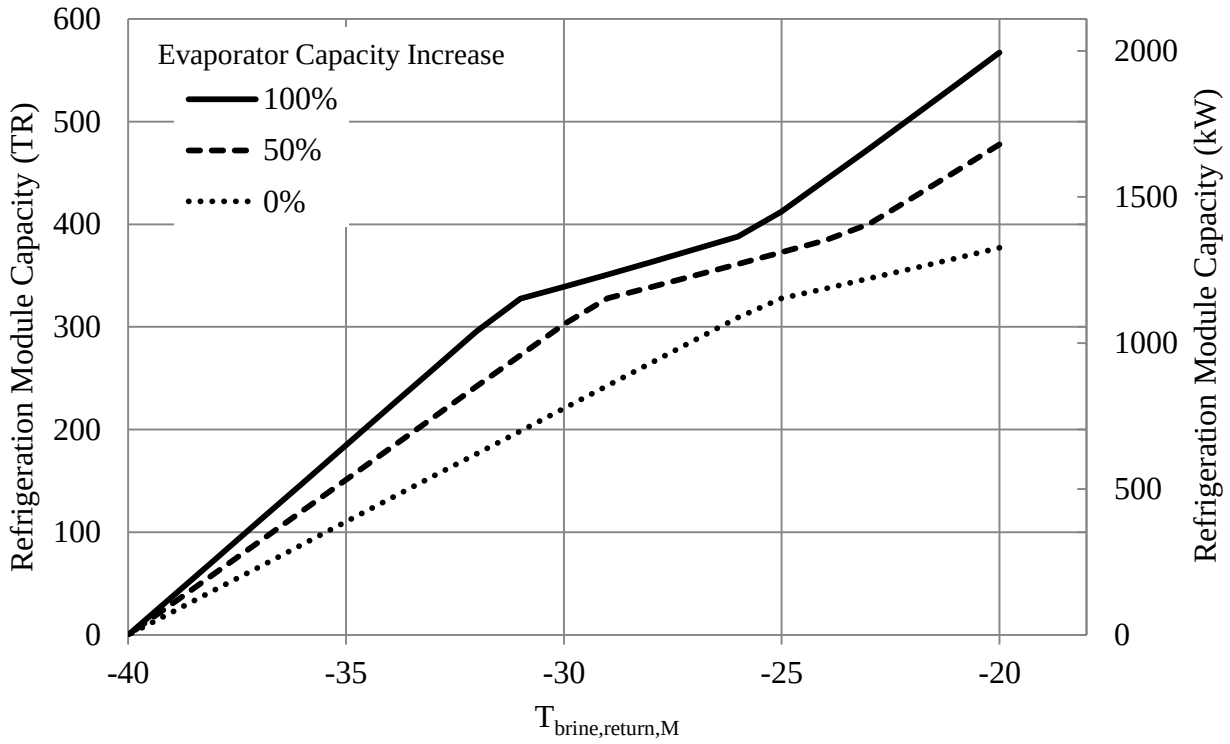

Figure 7-7 Effect of Evaporator Upgrade on Refrigeration Plant Capacity

CHAPTER 8: CONCLUSIONS AND RECOMMENDATIONS

The primary goal of this research is to develop a model capable of calculating the performance of an existing refrigeration system used for artificial ground freezing. The model has to be capable of calculating the performance of the refrigeration plant over a wide range of operating conditions. A model of the modular refrigeration plant at Cameco's Cigar Lake mine based on first principle thermodynamics is presented. The model is validated using operating data collected over a period of eight months by the plant's operators. The development of the model was an excellent learning experience, and several conclusions can be drawn from the lessons learned through the development and use of the model.

8.1 Conclusions

- Models developed to optimize the efficiency of refrigeration systems are not directly applicable for optimizing the capacity of a refrigeration system because they do not simulate the capacity limiting system controls.
- The thermodynamic model developed for the Cigar Lake refrigeration plant successfully represented the performance of the actual refrigeration plant. When the model`s predictions are compared with actual operating data, predicted capacities match measured capacities within ±14%. The capacity predictions all fall within the uncertainty in the measured data.
- Predicted brine temperatures match the measured brine temperatures leaving the plant within ±5%.
- The evaporator model predicts a capacity 30% greater on average than the measured performance; therefore, a calibration factor of 0.7 was applied to the evaporator model.
- The actions of the compressor controller, which ensures the compressor operates within machine limits, ultimately determine the capacity of the refrigeration plant when it is fully loaded.
- Set points selected by the plant operator, which are used by the compressor controller, impact the performance of the refrigeration plant.
    - Setting the evaporation temperature just above the brine crystallization temperatures (-40°C) will help maximize plant performance.

    - To maximize the plant's refrigeration capacity, the intermediate pressure must be set as low as practical.
    - To maximize the plant's coefficient of performance (COP) the optimum intermediate pressure can be calculated from the saturation temperature corresponding to the geometric mean intermediate pressure plus 5°C.
- The capacity of the refrigeration plant is highly dependent on the temperature of the brine entering the evaporator. A ±10% change in brine temperature creates a 22% overall change in the refrigeration plant capacity.
    - Data for commercial chillers rated using the existing standards show a very similar dependence on the temperature of the fluid that is being chilled.
    - Ensuring the warmest brine available from the freeze pipes is pumped to the evaporators will help maximize plant performance. The existing design using a brine tank to balance the brine flow between the field and refrigeration modules reduces the overall plant capacity. Cool brine from the plants is mixed in the tank with warm brine returning from the field and recirculated to the refrigeration modules. In addition the tank allows heat to be transferred between the warm brine to the cold brine further reducing plant capacity. By eliminating the tank, plumbing the refrigeration modules in parallel, and installing evaporators sized appropriately for the new flow rates, the performance of the refrigeration plant can be improved by approximately 17%.
- The performance of the refrigeration plant can be improved through an evaporator upgrade. The existing evaporator capacity is lower than the compressor capacity for brine temperatures between -40°C and -26°C. The capacity of the new evaporator should meet or exceed the compressor capacity for a wide range of brine temperatures.

8.2 Recommendations

Further research into modeling industrial refrigeration plants is still required. Future research should expand the model developed for this research to include both shell and coil, and flash chamber economizers. The model's capabilities could be further expanded by including an evaporative condenser model. The air cooled condenser model could also be expanded to account for the capacity limitations of the condenser and thereby allow the model to be used for

optimizing the condenser capacity. More research should also be performed to gain a better understanding of how the refrigeration plant's control system behaves. This would allow research to be done into optimizing the algorithms used by the compressor control system.

Further work is also required to couple the refrigeration system model to existing ground heat transfer models. Coupling the models would improve the accuracy of existing ground heat transfer models by providing more accurate brine temperatures to the ground heat transfer models.

Instrumentation is important for measuring refrigeration plant performance, and is helpful for assessing the impact of changes in operating philosophy and plant diagnostics. Installing flow meters to measure the brine flow into each evaporator would be helpful at Cigar Lake. Alternatively, liquid ammonia flow meters installed before each evaporator could be used for the same purpose, and would provide insight into the performance of the compressor.

REFERENCES

Acromag Inc. (2011). *Criteria for Temperature Sensor Selection of T/C and RTD Sensor Types - The Basics of Temperature Measurement Using RTDs part 2 of 3*. Retrieved December 15th, 2014, from http://www.acromag.com/sites/default/files/RTD_Temperature_Measurement_917A.pdf

AHRI. (2011). *Performance Rating Of Water-Chilling and Heat Pump Water-Heating Packages Using the Vapor Compression Cycle*. (Standard 550/590).Arlington, VA: Air-Conditioning, Heating, &Refrigeration Institute

Andersland, O. B., & Ladanyi, B. (2004). *Frozen ground engineering, 2nd Edition*. Hoboken, N.J: John Wiley & Sons, Inc.

ANSI. (2010). *Effects of Liquid Viscosity on Rotodynamic (Centrifugal and Vertical)Pump Performance*. (ANSI/HI 9.6.7-2010).Parsippany, NJ: Hydraulic Institute

ASHRAE. (1995). *Method for Testing Liquid-Chilling Packages*.(ASHRAE Standard 30). Atlanta, GA: American Society of Heating, Refrigerating and Air-Conditioning Engineers, Inc.

ASHRAE. (2010). *ASHRAE Handbook: Refrigeration*. Atlanta: American Society of Heating, Refrigerating and Air-Conditioning Engineers, Inc.

ASHRAE. (2012). *ASHRAE Handbook: Systems and Equipment*. Atlanta: American Society of Heating, Refrigerating and Air-Conditioning Engineers, Inc.

ASHRAE. (2013). *ASHRAE Handbook: Fundamentals*. Atlanta, GA: American Society of Heating, Refrigerating and Air-Conditioning Engineers, Inc.

Beasley, D. E., & Figliola, R. S. (2011). *Theory and Design for Mechanical Measurements 5th*. Hoboken, N.J: John Wiley & Sons, Inc.

Bell, I. H. (2015a). *Ammonia*. Retrieved January 9, 2015, from http://www.coolprop.org/fluid_properties/fluids/Ammonia.html#fluid-ammonia

Bell, I. H. (2015b). *Incompressible Fluids*. Retrieved January 9, 2015, from http://www.coolprop.org/fluid_properties/Incompressibles.html#massmix

Bell, I. H., Wronski, J., Quoilin, S., & Lemort, V. (2014). Pure and Pseudo-pure Fluid Thermophysical Property Evaluation and the Open-Source Thermophysical Property Library CoolProp. *Industrial & Engineering Chemistry Research*, *53*(6), 2498–2508.

Bergman, T. L., Lavine, A. S., Incropera, F. P., & DeWitt, D. P. (2011). *Fundamentals of Heat and Mass Transfer, 7th Edition*. Hoboken, N.J: John Wiley & Sons, Inc.

Bloch, H. P. (2006). *A practical Guide to Compressor Technology*. Hoboken, NJ: Wiley-Interscience.

Chapman, D., Harbicht, T., Newman, G., & Newman, L. (2011). Artificial Ground Freezing: An Environmental Best Practice at Cameco's Uranium Mining Operations in Northern Saskatchewan, Canada. *Conference proceedings of the 11th international mine water association congress: mine water - managing the challenges, IMWA 2011. Aachen, Germany*.

Cigar Lake Mining Corporation. (1995). *The Cigar Lake project environmental impact statement: main document*.

COLMAC COIL Manufacturing. (N.D.). *Installation, Operation, and Maintenance Manual ENG0018622 - Air Cooled Condenser*. Retrieved December 4,2014,from http://www.colmaccoil.com/Literature/IOMs/ENG00018622.pdf

Cuevas, C., Lebrun, J., Lemort, V., & Ngendakumana, P. (2009). Development and validation of a condenser three zones model. *Applied Thermal Engineering*, *29*(17–18), 3542–3551.

Ding, G. (2007). Recent developments in simulation techniques for vapour-compression refrigeration systems. *International Journal of Refrigeration*, *30*(7), 1119–1133.

DOW Chemical Corporation. (2003). *Calcium Chloride Handbook - A Guide to Properties, Forms, Storage, and Handling*. Retrieved December 4, 2014, from http://www.prog-univers.com/IMG/pdf/CalciumChloridHandbook-2.pdf

Endress + Hauser. (2012). *Technical Information for Levelflex M FMP40*. Retrieved December 5,2014, from https://portal.endress.com/wa001/dla/5000557/6439/000/10/TI00358FEN_1512.pdf

Eslami-nejad, P., & Bernier, M. (2012). Freezing of geothermal borehole surroundings: A numerical and experimental assessment with applications. *Applied Energy*, *98*, 333–345.

Ge, Y. T., & Cropper, R. (2005). Performance evaluations of air-cooled condensers using pure and mixture refrigerants by four-section lumped modelling methods. *Applied Thermal Engineering*, *25*(10), 1549–1564.

GEO-SLOPE International. (2015). TEMP/W 2012 Thermal Analysis. Retrieved March 21, 2015, from http://www.geo-slope.com/products/tempw.aspx

Gosney, W.B. (1982) *Principles of Refrigeration*. New York: Cambridge University Press.

Invensys Systems, Inc. (2013). *FoxBoro Measurements & Instruments Product Catalog. Invensys Systems*, Inc. Retrieved December 11, 2014, from http://iom.invensys.com/EN/pdfLibrary/Catalog_Foxboro_MeasurementsAndInstruments_01-13.pdf

Johnson Controls. (2014). *P499 Series Electronic Pressure Transducers - Product / Technical Bulletin*. Retrieved December 18, 2014, from http://cgproducts.johnsoncontrols.com/met_pdf/12011190.pdf

Mayekawa MFG. CO., LTD. (2011). *Instruction Manual For Screw Compressor Unit Controller Mypro CPIV*. Retrieved December 11,2014, from http://www.mayekawa.ca/techdata/pdf/CP4_manual.pdf

Mayekawa MFG. CO., LTD. (2014). *MYCOMW2014B Compressor Capacity Calculation Software*.

Moran, M. J., Shapiro, H. N., Boettner, D. D., & Bailey, M. (2011). *Fundamentals of Engineering Thermodynamics 7th edition*.Hoboken NJ: John Wiley & Sons.

NIST. (2010). *NIST Standard Reference Database 23*. Retrieved January 30, 2015, from http://www.nist.gov/srd/nist23.cfm

Sanger, F. J., & Sayles, F. H. (1979). Thermal and rheological computations for artificially frozen ground construction. *Engineering Geology*, *13*(1–4), 311–337.

Scott, D. (2014). Comparing Evaporative and Air Cooled Condensing for Ammonia Systems. *2014 IIAR Technical Papers*. Retrieved December 15, 2015 from http://www.iiar.org/iiar/WCM/IIAR_Publications/IIAR_Technical_Papers/2014_Technical_Papers.aspx

Seshaiah, N., Ghosh, S. K., Sahoo, R. K., & Sarangi, S. K. (2007). Mathematical modeling of the working cycle of oil injected rotary twin screw compressor. *Applied Thermal Engineering*, *27*(1), 145–155.

Solati, B., Zmeureanu, R., & Haghighat, F. (2003). Correlation based models for the simulation of energy performance of screw chillers. *Energy Conversion and Management*, *44*(12), 1903–1920.

Stroud, K. A., & Booth, D. J. (2003). *Advanced engineering mathematics* (Vol. 175). Hoboken N.J: John Wiley & Sons, Inc.

The Government of Canada (Environment Canada). (2014). Cigar Lake Saskatchewan - Daily Temperature Data. Retrieved December 1, 2014, from http://climate.weather.gc.ca/climateData/dailydata_e.html?timeframe=2&Prov=&StationID=3359&dlyRange=1987-06-01|2014-10-08&Year=2014&Month=1&Day=10

The Heating, Refrigeration, and Air Conditioning Institute of Canada. (N.D.). *R-410A Information*. Retrieved December 17, 2014, from http://www.hrai.ca/r-410a.html

TRNSYS. (2010). *TRNSYS 17 - Standard Component Library Overview*. Retrieved December 20, 2014, from http://www.trnsys.com/assets/docs/03-ComponentLibraryOverview.pdf

Vera-García, F., García-Cascales, J. R., Gonzálvez-Maciá, J., Cabello, R., Llopis, R., Sanchez, D., & Torrella, E. (2010). A simplified model for shell-and-tubes heat exchangers: Practical application. *Applied Thermal Engineering*, *30*(10), 1231–1241.

Webb, R. L., Choi, K.-D., & Apparao, T. R. (1989). A theoretical model for prediction of the heat load in flooded refrigerant evaporators. In *ASHRAE transactions* (Vol. 95, pp. 326–338). American Society of Heating, Refrigerating and Air-conditioning Engineers.

Wika Corporation. (N.D.). *TR10 Industrial RTD Assembly*. Retrieved December 11, 2014,from http://www.wika.ca/upload/BR_TR10_en_us_18425.pdf

Wika Instrument Corporation. (2011). *Intrinsically Safe Hazardous Area Transmitters Type IS-20, IS-20F, IS-21F*. Retrieved December 11, 2014, from http://www.wika.ca/upload/DS_PE_IS_20_en_us_16603.pdf

York. (2013). York Model YCAV Air-Cooled Screw Compressor Liquid Chillers Style A. Retrieved December 18, 2014, from http://cgproducts.johnsoncontrols.com/YorkDoc/201.21-EG1.pdf

Zhang, W.-J., Zhang, C.-L., & Ding, G.-L. (2009). Transient modeling of an air-cooled chiller with economized compressor. Part I: Model development and validation. *Applied Thermal Engineering*, *29*(11–12), 2396–2402.

APPENDIX A: MYCOM SAMPLE COMPRESSOR RUN SHEET

Table A-1 provides a sample of the data which is available for the Cigar Lake twin screw compressors from the manufacturer (Mayekawa). This data was used to determine the compressor's swept volume rates, as well as its isentropic and volumetric efficiencies.

Table A-1 Mycom Compressor Specifications for a Single Operating Point (Mayekawa MFG. CO., LTD., 2014)

DATE :		**08-20-2014**
MODEL :		N3225LSC-MBM-*1
ROTOR & PORT 2ND :		250S M
ROTOR & PORT 1ST :		320L MB
REFRIGERANT :		AMMONIA
CAPACITY :	[KW]	1088.7
CAPACITY :	[TR]	309.6
ABSORBED POWER :	[kW]	705.2
ABSORBED POWER 2ND :	[kW]	407
ABSORBED POWER 1ST :	[kW]	298.2
DRIVE SHAFT SPEED :	[min-1]	3550
COMPRESSOR SPEED :	[min-1]	3550
INDICATOR POSITION 2ND :	[%]	100
INDICATOR POSITION 1ST :	[%]	100
SWEPT VOLUME RATIO (2ND/1ST) :	[-]	3
CONDENSING TEMP. :	[degC]	43.2
EVAPORATIVE TEMP. :	[degC]	-40
SUCTION SUPERHEAT :	[degC]	1.6
INTERMED. SUPERHEAT :	[degC]	0
LIQUID APPROACH TEMP. :	[degC]	5
LIQUID SUBCOOLING :	[degC]	0
SUCTION TEMP. 1ST :	[degC]	-38.4

OIL SUPPLY TEMP. :	[degC]	50
SUCTION PRESS. :	[PSIA]	10.4
DISCHARGE PRESS. :	[PSIA]	246
OIL SUPPLY PRESS. :	[PSIA]	275
SUCTION PRES. DROP :	[PSIA]	0
DISCHARGE PRES. DROP :	[PSIA]	0
SWEPT VOLUME 2ND :	[m3/h]	1900
SWEPT VOLUME 1ST :	[m3/h]	5700
LOAD(VOL. FLOW RATE) 2ND :	[%]	100
LOAD(VOL. FLOW RATE) 1ST :	[%]	100
INTERMED. TEMP. :	[degC]	-3.73
SUCTION TEMP. 2ND :	[degC]	60.1
DISCHARGE TEMP. 2ND :	[degC]	90.3
DISCHARGE TEMP. 1ST :	[degC]	62.5
INTERMED. PRESS. :	[PSIA]	53.9
REFRIG. FLOW RATE 2ND :	[m3/h]	370
REFRIG. FLOW RATE INT. :	[m3/h]	266
REFRIG. FLOW RATE 1ST :	[m3/h]	5110
REFRIG. FLOW RATE 2ND :	[kgf/h]	3894
REFRIG. FLOW RATE INT. :	[kgf/h]	620
REFRIG. FLOW RATE 1ST :	[kgf/h]	3263
INJECT. OIL FLOW RATE 1ST :	[L/min]	119
LUB. OIL FLOW RATE 2ND :	[L/min]	96
LUB. OIL FLOW RATE 1ST :	[L/min]	204
TOTAL OIL FLOW RATE 2ND :	[L/min]	96
TOTAL OIL FLOW RATE 1ST :	[L/min]	323
TOTAL OIL FLOW RATE :	[L/min]	419
OIL HEAT REJECTION :	[kW]	476.4
OIL SPEC HT :	[J/kgK]	1930
OIL DENSITY :	[kg/m3]	880

COP :	[-]		1.54
--- SUPER HEAT is NOT counted in refrigeration capacity ---			
--- WITH WATER COOLED OIL COOLER ---			
--- WITH LIQUID SUBCOOLER ---			
REFRIG. FLOW RATE :	[m3/h]	266	
REFRIG. FLOW RATE :	[kgf/h]		620
HEAT REJECTION :	[kW]		181
--- Refrigeration oil is not soluble with refrigerant (mineral oil) ---			
--- When choosing the motor set a safety factor of more than 10% for the brake power ---			
! All data herein is for reference only.			
! Content is subject to change without notice.			
*** MYCOMW2014B compressor performance table is valid until the end of December, 2014. ***			

APPENDIX B: CENTRIFUGAL PUMP HEAT GAIN EQUATION DERIVATION

Centrifugal pumps are used in the modular refrigeration plants to pump brine from the brine tank through each module heat exchanger, and from the brine tank to the freeze panels. There is one centrifugal pump installed in each refrigeration module, and there are three distribution pumps installed in parallel. Pumps can often add a significant amount of heat to the fluid which they are pumping, which is counterproductive for a refrigeration system. Therefore, the pump heat gain is a parameter of interest for the refrigeration plant model. This appendix details the derivation of the pump heat gain equation used in the plant model.

The pump heat gain model assumes that the heat transfer between the pump / process fluid and its surroundings is negligible; therefore any pump power which does not increase the head or velocity of the process fluid heats the fluid. The work done on the process fluid by a pump is defined as (ASHRAE, 2012)

$$\dot{W}_{\text{fluid}} = \frac{\dot{m}_{\text{fluid}} \Delta P}{\rho} \tag{B.1}$$

where $\dot{m}_{\text{fluid}}$ is the fluid mass flow rate through the pump in kg/s, ρ is the fluid density in kg/m^3, ΔP is the change in fluid pressure across the pump in Pa which can be calculated as

$$\Delta P = \rho g \Delta H \tag{B.2}$$

where ΔH is the change in total head across the pump in metres.

The efficiency of the pump is defined as

$$\eta_{\text{pump}} = \frac{\dot{W}_{\text{fluid}}}{\dot{W}_{\text{pump,in}}}. \tag{B.3}$$

Using the definition of efficiency, and the assumption that any pump power that is not converted to fluid power becomes heat, the change in temperature of the working fluid resulting from a heat addition is

$$\Delta T_{\text{fluid}} = \frac{\left(1 - \eta_{\text{pump}}\right) \dot{W}_{\text{in}}}{\dot{m}_{\text{fluid}} Cp_{\text{fluid}}}. \tag{B.4}$$

Combining Equations B.1, through B.4 the fluid heat addition by each pump can be calculated as

$$\Delta T_{\text{brine}} = \frac{(1 - \eta_{\text{pump}})}{\eta_{\text{pump}}} \frac{g \Delta H}{Cp_{\text{brine}}}. \tag{B.5}$$

APPENDIX C: UNCERTANTY IN MEASURED CAPACITY DERIVATION

The measured capacity, or rate of heat removal, for the evaporator, refrigeration modules, or refrigeration plant is determined using experimental data and Equation C.1.

$$\dot{Q} = \rho \dot{V}_{\text{brine}} c_P \left(T_{\text{brine,in}} - T_{\text{brine,out}}\right) \tag{C.1}$$

where the brine flow rate ($\dot{V}_{\text{brine}}$) and the brine temperatures ($T_{\text{brine,in}}$), and ($T_{\text{brine,out}}$) are obtained from the Cigar Lake data sets.

The uncertainty in a function $\bar{y} = f(\bar{x}_1, \bar{x}_2, \ldots\ldots, \bar{x}_{\text{n}})$ based on the uncertainty in the independent variables $\bar{x}_1, \bar{x}_2, \ldots\ldots, \bar{x}_{\text{n}}$ can be calculated using the relationship

$$u_{\bar{y}} = \left(\sum_{i=1}^{n} (\theta_{\text{i}} u_{\bar{x}i})^2\right)^{1/2} \tag{C.2}$$

where $u_{\bar{x}i}$ is the uncertainty in the mean value of the independent variables within the sample space for that variable, and θ_i is the sensitivity of the function to changes in the each independent variable, which can be calculated by taking the partial derivative of the function with respect to each independent variable (Beasley & Figliola, 2011)

$$\theta_i = \left(\frac{\delta y}{\delta x_i}\right)_{x=\bar{x}}. \tag{C.2}$$

Taking the partial derivatives with respect to the measured quantities in Equation C.1 gives:

$$\left(\frac{\delta \dot{Q}}{\delta \dot{V}}\right)_{\dot{V}_{\text{brine}}=\bar{\dot{V}}_{\text{brine}}} = \rho c_P \left(T_{\text{brine,in}} - T_{\text{brine,out}}\right), \tag{C.3}$$

$$\left(\frac{\delta \dot{Q}}{\delta T_{\text{brine,in}}}\right)_{T_{\text{brine,in}}=\bar{T}_{\text{brine,in}}} = \rho c_P \dot{V}_{\text{brine}}, \text{and} \tag{C.4}$$

$$\left(\frac{\delta \dot{Q}}{\delta T_{\text{brine,out}}}\right)_{T_{\text{brine,out}}=\bar{T}_{\text{brine,out}}} = \rho c_P \dot{V}_{\text{brine}}. \tag{C.5}$$

Combining Equations C.3, C.4, and C.5 using Equation C.2 gives the overall uncertainty in capacity as

$$u_{\dot{Q}} = \pm \left(\left(\rho c_P \left(T_{\text{brine,in}} - T_{\text{brine,out}}\right) u_{\dot{V}}\right)^2 + \left(\rho c_P \dot{V}_{\text{brine}} u_{T_{\text{out}}}\right)^2 + \left(\rho c_P \dot{V}_{\text{brine}} u_{T_{\text{in}}}\right)^2\right)^{1/2}. \tag{C.6}$$

The uncertainty in the measured temperatures is a combination of the uncertainty for the Resistance Temperature Detectors (RTDs) used to measure the brine temperature, which is given in Table 3-2 as

$$u_{\mathrm{T}} = \pm(0.15 + 0.002|T|)℃ \tag{C.7}$$

and the measurement resolution uncertainty u_{res}. The resolution uncertainty is the error introduced by instrument or display resolution in repeated measurements of the same quantity (Beasley & Figliola, 2011). For the temperature measurements the resolution uncertainty is estimated as ±0.1℃. The total uncertainty in any quantity can be calculated as

$$u_{\mathrm{Tot}} = \pm\sqrt{{u_1}^2 + {u_1}^2 \ldots\ldots {u_n}^2}. \tag{C.8}$$

Therefore, the total uncertainty in the temperature measurements can be calculated as

$$u_{\mathrm{T,Tot}} = \pm\sqrt{{u_{\mathrm{T}}}^2 + {u_{\mathrm{T,res}}}^2}. \tag{C.9}$$

The uncertainty in the brine flow rate depends on the method used to determine the brine flow rate. In the first data set the brine flow rate was calculated using the brine pump model described in Appendix B, and the uncertainty in the brine flow rate is calculated using Figure 5-7, Figure 5-8, and Equation C.8. In the second data set the brine flow rate on the field side was determined by summing the brine flow rates to the 781, 813, and 829 freeze panels which were measured using the magnetic flow meters listed in Table 3-2. Therefore, Equation C.2 the uncertainty in the total field flow rate can be calculated as

$$u_{\mathrm{brine,Tot}} = \pm\sqrt{{u_{\dot{V}_{\mathrm{brine,F}}}}^2 + {u_{\mathrm{brine,res}}}^2} \tag{C.10}$$

where the uncertainty in the flow rates due to instrumentation accuracy, $u_{\dot{V}}$ is calculated as

$$U_{\dot{V}_{\mathrm{brine,F}}} = \pm\left(\left(u_{\dot{V}_{781}}\right)^2 + \left(u_{\dot{V}_{813}}\right)^2 + \left(u_{\dot{V}_{829}}\right)^2\right) \tag{C.11}$$

and the flow meter accuracy is given in table 3-2 as ±.25%. The resolution error in the flow measurements is estimated as ±0.1° m^3/hr.P